Acta morphologica et anthropologica 27 (1–2)

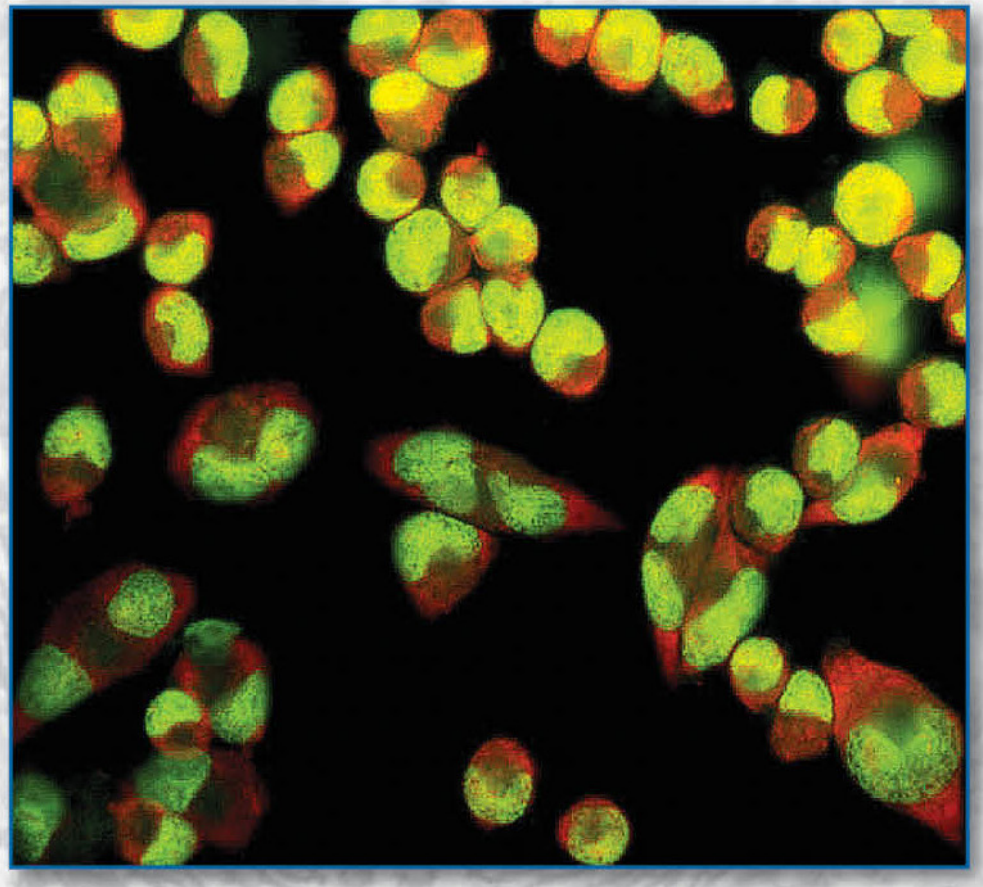

Prof. Marin Drinov Publishing House
of Bulgarian Academy of Sciences

Acta morphologica et anthropologica

is the continuation of Acta cytobiologica et morphologica

Editor-in-Chief: Prof. Nina Atanassova
e-mail: ninaatanassova@yahoo.com
+359 2 979 2342

Deputy Editor-in-Chief: Prof. Dimitar Kadiysky
e-mail: dkadiysky@yahoo.com
+359 2 979 2340

Managing Editor: Assoc. Prof. Y. Gluhcheva
e-mail: ygluhcheva@hotmail.com
+359 2 979 2344

Editorial Correspondence

Institute of Experimental Morphology, Pathology and Anthropology with Museum
Bulgarian Academy of Sciences
Acta morphologica et anthropologica
Acad. Georgi Bonchev Str., Bl. 25
1113 Sofia, Bulgaria
E-mail: ygluhcheva@hotmail.com, iempam@bas.bg
Tel.: +359 2 979 2344

Издаването на настоящия том 27, книжки 1 и 2 е осъществено с финансовата подкрепа на Фонд „Научни изследвания“

Prof. Marin Drinov Publishing House of Bulgarian Academy of Sciences
Bulgaria, 1113 Sofia, Acad. Georgi Bonchev Str., Bl. 6

Graphic designer Veronika Tomcheva
Format 70×100/16 Printed sheets 6,63

Printing Office of Prof. Marin Drinov Publishing House of Bulgarian Academy of Sciences
Bulgaria, 1113 Sofia, Acad. Georgi Bonchev Str., Bl. 5

ISSN 1311-8773 (print)
ISSN 2535-0811 (online)

Acta morphologica et anthropologica

27 (1-2)

27 (1-2) ● Sofia ● 2020
Institute of Experimental Morphology, Pathology and Anthropology with Museum
Bulgarian Anatomical Society

Contents

MORPHOLOGY 27 (1)

Original Articles

Review Articles

Original Articles

Institute of Experimental Morphology, Pathology and Anthropology with Museum
Bulgarian Anatomical Society

Acta morphologica et anthropologica, 27 (1-2)
Sofia ● 2020

MORPHOLOGY 27 (1)

Original Articles

Effects of the TYR-MIF-1 Peptides on the Expression of CB1 Cannabinoid Receptors in the Rat Mesencephalic Trigeminal Nucleus Following Thermal Stress

Angel Dandov[1], Dimitrinka Atanasova[2,3], Nikolai Lazarov[1,3]*

[1] Department of Anatomy and Histology, Medical University of Sofia, Sofia, Bulgaria
[2] Department of Anatomy, Faculty of Medicine, Trakia University, Stara Zagora, Bulgaria
[3] Institute of Neurobiology, Bulgarian Academy of Sciences, Sofia 1113, Bulgaria

* Corresponding author e-mail: didiatan@bio.bas.bg; didiatanasova7@gmail.com

The present study aims at elucidating the role of TYR-MIF-1 peptides in the expression patterns of cannabinoid type 1 (CB1) receptors in the mesencephalic nucleus of the trigeminal nerve (Me5) in rats after mild thermal stress. Immunohistochemistry revealed that in rats subjected to short-term heat stress the application of the CB1 agonist arachidonoylethanolamide (AEA) induces the intense expression of CB1 receptors in the Me5. Moreover, treatment with the peptides of the Tyr-MIF-1 family results in a distinct alteration in the CB1 expression. Specifically, the administration of MIF-1 and Tyr-K-MIF-1 increases CB1 expression levels, while Tyr-MIF-1 and Tyr-W-MIF-1 decrease them. It is likely that the first two members directly influence the CB1 expression in the rat Me5, while the other two probably interact via second messengers or another neutotransmitter. The exact mechanism of the interaction is yet to be clarified.

Key words: CB1 cannabinoid receptor, mesencephalic trigeminal nucleus, Tyr-MIF-1 peptides, endocannabinoid system, thermal stress

Introduction

The mesencephalic nucleus of the trigeminal nerve (Me5) is a unique brain structure with an unusual central location and a noticeable ability for adequate adaptive morphological and neurochemical responses to changes in the environment [1]. The Me5 is made up of

two distinct subpopulations of neurons, most of which are large-sized pseudounipolar while a few are small in size and of spherical or ovoid shape [1]. These form a band extending from the lateral border of the periaqueductal gray (PAG) to the trigeminal motor nucleus. The structure also receives input from the mechanoreceptors of the periodontal ligaments and innervates the jaw-closing muscles [3, 14]. Me5 neurons are located in the brainstem and are influenced by various brain regions regulating feeding behavior [4].

The endocannabinoid system (ECS) is proposed to be involved in the regulation of a variety of physiological processes. It is composed of lipid-derived neurotransmitters, called endocannabinoids, that bind to two G-protein-coupled receptors, the cannabinoid type 1 (CB1) and type 2 (CB2), and cannabinoid receptor proteins [2, 7, 9, 12]. CB1 is a pre-synaptic G protein-coupled heteroreceptor that is expressed in the central and peripheral nervous system of rats [13, 15]. Moreover, it is highly expressed in rat brain areas that are involved in pain modulation [11, 12, 16] and is activated by endocannabinoids that include N-arachidonoylethanolamide (anandamide, AEA). Our previous study has revealed that the application of AEA evokes a strong expression of CB1 in the Me5 in rats exposed to short-term thermal stress [6].

The Tyr-MIF-1 family consists of four peptides, i.e. MIF-1 (Pro-Leu-Gly-NH_2), Tyr-MIF-1 (Tyr-Pro-Leu-Gly-NH_2), Tyr-W-MIF-1 (Tyr-Pro-Trp-Gly-NH_2), and Tyr-K-MIF-1 (Tyr-Pro-Lys -Gly-NH_2). MIF-1 does not bind to opioid receptors, while Tyr-K-MIF-1 binds only to its own non-opioid receptor. The other two peptides, Tyr-MIF-1 and Tyr-W-MIF-1, possess both opioid and non-opioid binding sites [10].

Since the ECS modulates stress reaction, it would be intriguing to find out the possible interactions between the above-mentioned peptides and the ECS after heat stress exposure. Therefore, we set it as a goal of this study to investigate the effects of the Tyr-MIF-1 peptides on the expression of CB1 cannabinoid receptors in the rat Me5 following thermal stress.

Materials and Methods

Animals

The experiments were carried out on 25 male Wistar rats, weighing 180-200 g, kept at an optimal room temperature of 22°C and under normal conditions. The animals were divided into 4 experimental and 1 control groups, each including 5 animals (n=5). The study was approved by the Institutional Ethics Committee at the Institute of Neurobiology of the Bulgarian Academy of Sciences. All experimental procedures were performed in agreement with the European Communities Council Directive 2010/63/EU for the protection of animals used for scientific purposes.

Acute experimental model of heat stress

The animals were kept for 1 hour at a high ambient temperature of 38°C. The rats moved freely in the thermal chamber but were not supplied with food or water during the heat exposure.

Administered drugs and treatments

CB1 receptor agonist AEA at a dose 1mg/kg b.w, dissolved in dimethyl sulfoxide (DMSO), was injected intraperitoneally. The peptides of the Tyr-MIF-1 family at a

dose 1mg/kg b.w. were dissolved in sterile saline solution (0.9% NaCl) and introduced intraperitoneally. The administered drugs used in this study were purchased from Sigma (Sigma Chem. Co., St. Louis, MO, USA).

Experimental design

The animals were divided into 5 groups and were subjected to heat stress for one hour. AEA was injected immediately after the stress. In the four experimental groups (1h HS+AEA+MIF-1; 1h HS+AEA+Tyr-MIF-1; 1h HS+AEA+Tyr-W-MIF-1; 1h HS+AEA+Tyr-K-MIF-1) the peptides of the Tyr-MIF-1-family were administered 10 min after the AEA application. On the other hand, the control group underwent only 1h HS+AEA treatment.

Immunohistochemical procedure

The rats were deeply anesthetized with ketamine-xylazine at the appropriate dosage for rats and perfused first with 0.05 M phosphate-buffered saline (PBS), pH 7.4, followed by 4% paraformaldehyde (PFA) in 0.01 M phosphate buffer (PB), pH 7.4. The brain was dissected out and postfixed in the same fixative overnight at 4ºC. Thereafter, the tissues were embedded in paraffin and cut into 5 µm thick sections. The samples were then deparaffinized and subsequently processed for immunohistochemistry using an ImmunoCruz™ goat ABC Staining System (Santa Cruz Biotechnology, Inc., Santa Cruz, CA, USA). In brief, the sections were treated with 1% hydrogen peroxide in methanol for 30 min to inactivate endogenous peroxidase. The background staining was blocked with 5% normal goat serum in PBS for 1 hour. Subsequently, they were incubated with a polyclonal goat anti-CB1 receptor antibody (1:500, Santa Cruz Biotechnology) overnight at 4°C in a humid chamber, followed by donkey anti-goat IgG (1:500, Santa Cruz Biotechnology) for 2 h at room temperature, and lastly the AB enzyme reagent was applied for 30 min at room temperature. The peroxidase activity was visualized by diaminobenzidine as a chromogen. Finally, the sections were dehydrated, cleared in xylene and coverslipped with Entellan (Merck, Darmstadt, Germany).

The specificity of the immunostaining was controlled by the replacement of the primary antibody with PBS.

Photodocumentation and image processing

The immunostained sections for the CB1 receptor were digitalized using a Nikon DXM1200c research microscope (Nikon Inc., Tokyo, Japan) equipped with a DMX 1200 digital camera. The digitized images were captured with an objective lens 40x and a total magnification 400x. Prior to use, the system underwent an accurate calibration to correct the captured images. For every single image, the camera settings and light source were kept the same. The digital images were saved in TIF format.

Densitometric analysis and statistics

The CB1 immunostaining intensity was assessed on binary converted images using the semi-automated densitometric evaluation after a threshold was set via the program ImageJ 1.48v (NIH, Bethesda, MD, USA). Staining intensities were semi-quantified and were presented as percentage areas. Two blinded researchers performed the evaluations and the obtained results were averaged.

The statistical analyses were performed using the GraphPad Prism (GraphPad Software Inc., San Diego, CA, USA). The data were presented as means±standard error of the mean (SEM). An unpaired *t*-test for Gaussian distributed data and Mann-Whitney *U*-test for non-Gaussian distributed data were accomplished. The results were considered statistically significant when $p<0.05$.

Results

The immunohistochemical experiments revealed immunostaining intensity for CB1 in two distinct subpopulations of pseudounipolar neurons in the Me5. The immunopositive reaction was localized mainly in the cytoplasm of the cells while their nuclei remained negative. The perikarya and proximal processes of the neurons were differently immunostained in the examined experimental groups (**Fig. 1**). Specifically, following a 1-hour heat exposure with AEA (1h HS+AEA), intensely stained large and small ovoid pseudounipolar neurons were observed in the Me5 (**Fig. 1A, B**).

The results of the statistical analysis showed an increased CB1 expression in 1h HS+AEA+MIF-1-animals (**Fig. 1C; Fig. 2**) compared to 1h HS+AEA controls (**Fig. 1A, B; Fig. 2**) (69.7826±2.14 vs 53.4636±3.67; p=0.0001). However, we found a decreased CB1 expression in the groups that were also treated with Tyr-MIF-1 (**Fig. 1D; Fig. 2**) and Tyr-W-MIF-1 (**Fig. 1E; Fig. 2**), (34.3982±4.77 vs 53.4636±3.67; p=0.0057) and (19.2488±4.97 vs 53.4636±3.67; p=0.0003), respectively when compared to the control group of 1h HS+AEA-animals (**Fig. 1A, B; Fig. 2**). The administration of Tyr-K-MIF-1 (**Fig. 1F; Fig. 2**) significantly altered the expression

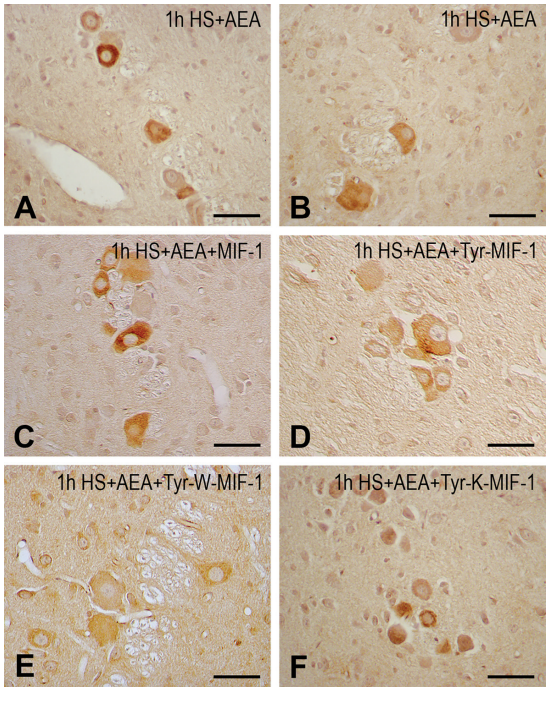

Fig. 1. Immunohistochemical expression of CB1 receptors in some large and small ovoid pseudounipolar neurons located in the mesencephalic trigeminal nucleus of rats. The cell bodies of these neurons are differently immunostained in the examined 5 groups. **(A, B)** Light photomicrographs showing CB1 receptor immunoreactivity in control group in which the animals are subjected to 1-hour of heat stress followed by CB1-receptor agonist anandamide (AEA). In the remaining groups four different peptides from the Tyr-MIF-1 family are administered, i.e. MIF-1 **(C)**, Tyr-MIF-1 **(D)**, Tyr-W-MIF-1 **(E)** and Tyr-K-MIF-1 **(F)**, respectively. Note that the administration of both MIF-1 **(C)** and Tyr-K-MIF-1 **(F)** enhances the expression of CB1 receptors in the examined area while the peptides Tyr-MIF-1 **(D)** and Tyr-W-MIF-1 **(E)** cause decreased CB-1 receptor expression. Scale bars = 50 μm.

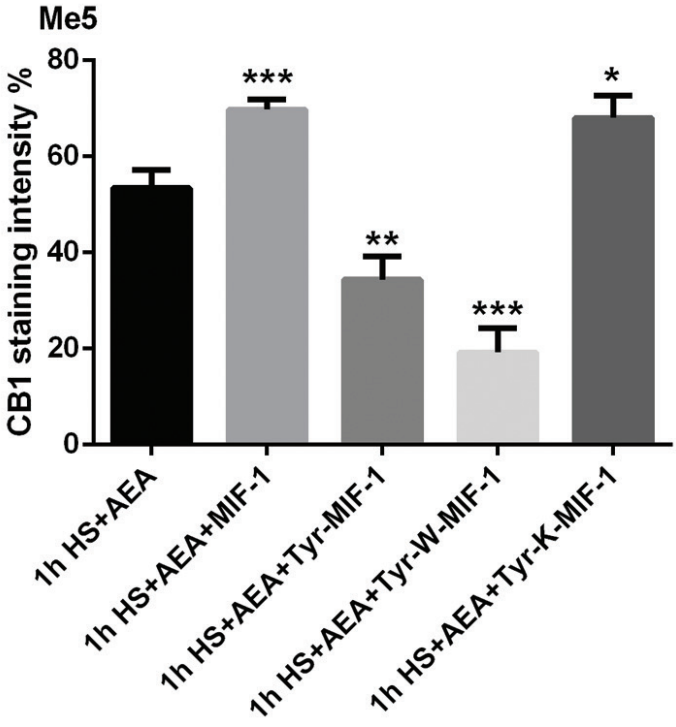

Fig. 2. Densitometric analysis of CB1 staining intensity in 1 control and 4 examined experimental groups in the rat mesencephalic trigeminal nucleus (Me5). The prominent statistically significant increase in the CB1 immunostaining was observed in groups 1h HS+AEA+MIF1 and 1h HS+AEA+Tyr-K-MIF1 compared to the control group. The data are presented as Mean+S.E.M. The level of significance: * $p < 0.05$, ** $p < 0.01$, *** $p < 0.001$.

of the CB1 receptor when compared to the non-peptide treated control group 1h HS+AEA (68.0626±4.63 vs 53.4636±3.67; p=0.0299).

Discussion

The results of this study show that the peptides of the Tyr-MIF-1 family interact differently with the ECS after an acute heat stress. The administration of each member of the family results in a distinct alteration in the expression of the CB1 receptor in the Me5. In particular, the administration of MIF-1 and Tyr-K-MIF-1 increases the CB1 expression under these conditions, while Tyr-MIF-1 and Tyr-W-MIF-1 decrease it.

Previous reports mainly focus on the distribution of the CB1 receptor in rat brainstem regions such as the PAG which is traditionally associated with pain transmission related to opioids [5, 16]. Data also show that under normal conditions this type of cannabinoid receptor is expressed only in the gray matter of the fourth ventricle in rats [13, 15]. Here we provide further evidence that the thermal stress induces such an expression in the rat

Me5 and that the administration of its agonist AEA at the end of the stress leads to some decrease in heat-induced analgesia.

The most important concept of the "gate control" theory of pain is that the pain sensation is subject to modulation, both by inputs from the periphery and by signals that come from the brain itself [8]. The rostroventromedial medulla and the PAG are thought to be areas that modulate pain and receive significant projections from the brainstem trigeminal nuclear complex [11]. This modulation is exerted by a presynaptic inhibition of primary afferent nociceptors and by post-synaptic inhibition of second-order trigeminal neurons via inhibitory interneurons [11].

In conclusion, it can be inferred that Tyr-MIF-1 and Tyr-W-MIF-1 have a direct impact on CB1 expression in the Me5, while MIF-1 and Tyr-K-MIF-1 probably interact via second messengers or through the activation of additional neurotransmitter system(s). Further research would clarify the nature of this input mechanism and could favor the development of new therapeutic strategies of pain management.

References

1. **Dandov, A., D. Atanasova, N. Lazarov.** Morphological and neurochemical plasticity of rat mesencephalic trigeminal neurons. – *Biomed. Rev*., **30**, 2019, 63-81.
2. **Devane, W. A., F. A. Dysarz, M. R. Johnson, L. S. Melvin, A. C. Howlett.** Determination and characterization of a cannabinoid receptor in rat brain. – *Mol. Pharmacol.,* **34**, 1988, 605-613.
3. **Goodwin, G. M., E. S. Luschei.** Effects of destroying spindle afferents from jaw muscles on mastication in monkeys. – *J. Neurophysiol*., **37**, 1974, 967-981.
4. **Lazarov, N. E.** Neurobiology of orofacial proprioception. – *Brain Res. Rev.,* **56**, 2007, 362-383.
5. **Lazarov, N., D. Atanasova, A. Ivanov.** Thermal stress-induced expression of CB1 cannabinoid receptors in the rat rostral pons. – *Acta morphol. anthropol.*, **21**, 2015, 75-79.
6. **Lazarov, N. E., D. Y. Atanasova, A. D. Dandov, N. D. Dimitrov.** Anandamine-induced expression of CB1 cannabinoid receptors in the rat mesencephalic trigeminal nucleus after short-term thermal stress. – *Comp. Rend. Acad. Bulg. Sci.*, **71**, 2018, 1272-1278.
7. **Matsuda, L. A., S. J. Lolait, M. Brownstein, A. C. Young, T. I. Bonner.** Structure of a cannabinoid receptor and functional expression of the cloned cDNA. – *Nature*, **346**, 1990, 561-564.
8. **Melzack, R., P. D. Wall.** Pain mechanisms: a new theory. – *Science*, **150**, 1965, 971-979.
9. **Munro, S., K. L. Thomas, M. Abu-Shaar.** Molecular characterization of a peripheral receptor for cannabinoids. – *Nature*, **365**, 1993, 61-65.
10. **Pan, W., A. J. Kastin.** From MIF-1 to endomorphin: The Tyr-MIF-1 family of peptides. – *Peptides*, **28**, 2007, 2411-2434.
11. **Sessle, B. J.** Acute and chronic craniofacial pain: Brainstem mechanisms of nociceptive transmission and neuroplasticity, and their clinical correlates. – *Critical Reviews in Oral Biology & Medicine*, **11**, 2000, 57–91.
12. **Starowicz, K., N. Malek, B. Przewlocka.** Cannabinoid receptors and pain – *WIREs Membrane Transport and Signaling*, **2**, 2013, 121-132.
13. **Svíženská, I., P. Dubový, A. Šulcová.** Cannabinoid receptors 1 and 2 (CB1 and CB2), their distribution, ligands and functional involvement in nervous system structures – A short review. – *Pharmacology Biochemistry and Behavior*, **90**, 2008, 501-511.
14. **Taylor, A., M. R. Davey.** Behaviour of jaw muscle stretch receptors during active and passive movements in the cat. – *Nature,* **220**, 1968, 301-302.
15. **Tsou, K., S. Brown, M.C. Sañudo-Peña, K. Mackie, J.M. Walker.** Immunohistochemical distribution of cannabinoid CB1 receptors in the rat central nervous system. – *Neuroscience*, **83**, 1998, 393-411
16. **Wilson-Poe, A. R., M. M. Morgan, S. A. Aicher, D. M. Hegarty.** Distribution of CB1 cannabinoid receptors and their relationship with mu-opioid receptors in the rat periaqueductal gray. – *Neuroscience*, **213**, 2012, 191-200.

Institute of Experimental Morphology, Pathology and Anthropology with Museum
Bulgarian Anatomical Society

Acta morphologica et anthropologica, 27 (1-2)
Sofia ● 2020

Alterations in Myonuclear Number and BDNF Expression in Soleus Muscle Fibres Following Endurance Training are Androgen-Dependent

Slavi Delchev[1], Fanka Gerginska[1], Katerina Georgieva[2], Michaela Shishmanova-Doseva[3]*

[1] Department of Anatomy, Histology and Embryology, Faculty of Medicine, Medical University, Plovdiv Bulgaria;
[2] Department of Physiology, Faculty of Medicine, Medical University, Plovdiv, Bulgaria;
[3] Department of Pharmacology and Drug Toxicology, Faculty of Pharmacy, Medical University, Plovdiv, Bulgaria

* Corresponding author e-mail: Slavi.Delchev@mu-plovdiv.bg

The aim was to determine the changes in myonuclear number, cross-sectional area (CSA) and the expression of brain–derived neurotrophic factor (BDNF) in soleus muscle of endurance trained rats treated with androgen receptorblockers (ARB). Male Wistar rats were divided into 3 groups: non-trained (NT), trained (T) and trained receiving Flutamide (T+F). The two trained groups were exercised on a treadmill for 8 weeks. Hematoxylin-eosin, Azan staining and immunohistochemical reaction for BDNF were applied. The nuclear number per fibre on cross-sections of the T+F group was lower compared to T ($P<0.001$) and higher compared to NT ($P<0.05$). No significant effects of training and ARB treatment on CSA were found ($P>0.05$). Strongest BDNF immunoexpression in muscle fibres and myoblasts of soleus was detected in the T group. The results suggest that androgens are involved in the process of submaximal training adaptation in slow-twitch muscle fibres of male rats via AR.

Key words: soleus, cross-sectional area, BDNF, Flutamide, endurance training

Introduction

Adaptation of skeletal muscles to exercise training occurs by change in their function and structure. This response is fully dependent on the type of training applied [25]. For instance, in resistance training muscle mass and myofibre cross-sectional area (CSA) are mainly increased. In regular endurance training alterations also involve metabolic adaptation combined with increase in fatigue resistance. Adaptation mechanisms include interaction between a multitude of organs, tissues, cells, subcellular structures and various signalling pathways [10, 13].

Traditionally, aerobic training is not associated with muscular hypertrophy; however, evidence in the accessible literature is controversial. A number of studies have demonstrated

an increase in the myofibre cross section size [11]. The increase in muscle mass is due to an increased protein synthesis in the muscles [22] and the formation of new myofibres with the participation of satellite cells (SCs) [25]. Under the influence of various stimuli (in muscle injury or exercise training) SCs are activated and give rise to daughter myogenic cells. Following several proliferation stages these myogenic cells participate in the formation of new muscle fibres [19, 21]. These adaptation alterations are associated with an increase in myonuclear number [24]. The mechanisms of hypertrophy and SCs activation in the growing myofibres are modulated by endocrine anabolic factors and locally expressed auto/paracrine growth factors [5], sensitive to exercise training [16]. A number of neurotrophic factors play a role in the activation of quiescent SCs [15, 18, 23].

Neurotrophins in skeletal muscles act as potential regulators of growth, maintenance, function and regeneration of muscle fibres. These neurotrophic factors modulate myoblast and myofibre differentiation [4]. The expression of BDNF in skeletal muscles is associated with SCs differentiation and is influenced by exercise [18]. There is evidence of an increased BDNF expression in homogenates from soleus muscle after 5-day treadmill training at a rate of 20 $m \cdot min^{-1}$ [20]. The molecular mechanisms responsible for these processes during endurance training and the role of androgens in these processes are still unclear [8, 9].

The aim of the present study was to investigate the changes in myocyte cross section and myonuclear number as signs of muscular hypertrophy, as well as the BDNF expression in soleus muscle of endurance trained rats receiving an androgen receptor blocker (ARB).

Materials and Methods

Male adult Wistar rats (baseline weight 180-200 g) were divided into two main groups – a non-trained one (NT, n=6) and a trained one (T, n=12). The trained rats were exercised on an EXER-3R-Treadmill (Columbus Instruments, Columbus, OHIO, USA) under conditions of submaximal training (70-75% VO_{2max}) 5 days a week for 8 weeks. Training duration was gradually increased during the first week, reaching 40 min per day in the second week and this duration was maintained until the end of the experiment. Half of the trained rats were treated with 15 $mg \cdot kg^{-1}$. Flutamide dissolved in sesame oil and administered subcutaneously (T+F), whereas the other half of the trained (T) and non-trained (NT) rats were treated with sesame oil for the same period of time. The experimental protocol was approved by the Ethical Committee on Human and Animal Experimentation of the Medical University - Plovdiv, and the Commission for Ethical Treatment of Animals at the Bulgarian Food Safety Agency. The rats were reared and all experimental procedures were performed according to the recommendations of the European Commission for the protection and humane treatment of laboratory animals.

Two days following the last exercise training the rats were decapitated under anaesthesia with Thiopental 30 $mg.kg^{-1}$, after which the soleus muscles of the animals were severed, fixed in Bouin's solution for 24 hours at room temperature and embedded in paraffin. Immunohistochemical reaction was applied to the paraffin-embedded sections (5 μm). Primary BDNF antibody (Santa Cruz Biotechnology, USA) and ImmunoCruz ABC Staining System (Santa Cruz Biotechnology, USA) were used. Some of the sections were investigated by hematoxylin-eosin staining and the Azan method.

Using the DP-Soft specialized software (Olympus, Japan) installed on a Microphot microscope (Nikon, Japan), the intensity of BDNF expression in the soleus muscle was recorded, as well as the cross sectional myonuclear number (in a sample of 50 fibres per animal) and the CSA (μm^2). The cross sections were investigated using one and the same magnification (x200). Data were analysed with one-way ANOVA and in cases

of significance of the F-criterion, Tuckey or Games-Howell *post hoc* test was applied, depending on the homogeneity of dispersions. Difference at $P<0.05$ was accepted as statistically significant. The results were presented as a mean ± standard error of the mean (x±SEM).

Results

Largest nuclear number per fibre on cross-sections was observed in the animals from the T group (7.52±0.21). In the T+F group myonuclear number was lower as compared to T ($P<0.001$), but higher as compared to NT ($P<0.05$) (**Fig. 1; Fig. 2**).

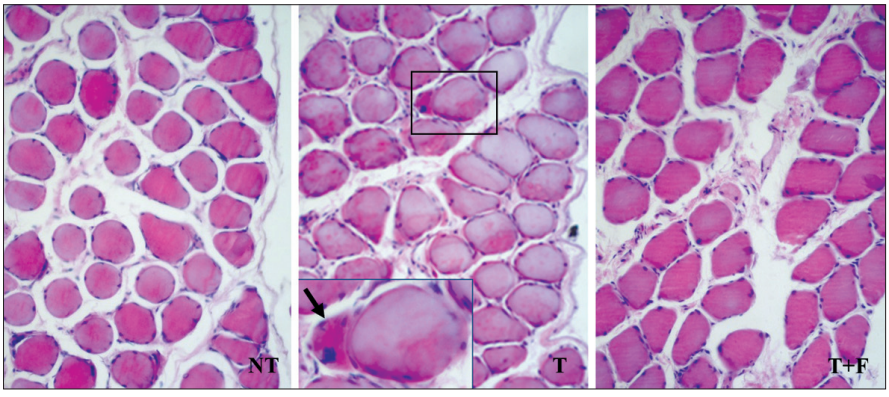

Fig. 1. H&E staining (*Magn. x 200*). Cross section of soleus muscle myofibres. **NT**. Non-trained control. **T**. Endurance-trained rats. Peripherally located myoblast (enlarged). **T+F**. Endurance-trained rats receiving ARB.

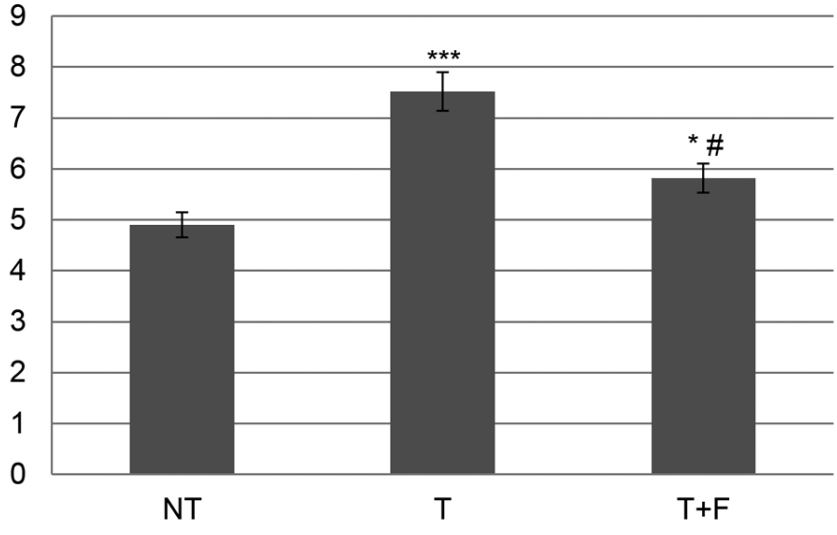

Fig. 2. Mean myonuclear number per fibre on cross section of soleus muscle. ***$P<0.001$ as compared to NT, *$P<0.05$ as compared to NT, $^{\#}P<0.001$ as compared to T.

The statistical analysis of the data obtained from the soleus muscle showed that trained rats had a larger cross section of the muscle fibres as compared to the non-trained controls ($P<0.05$). ARB administration reduced the CSA in the T+F group as compared to T, but a significant difference was not reached. As compared to the NT group, the CSA values in the T+F group were higher ($P<0.01$) (**Fig. 3; Fig. 4**).

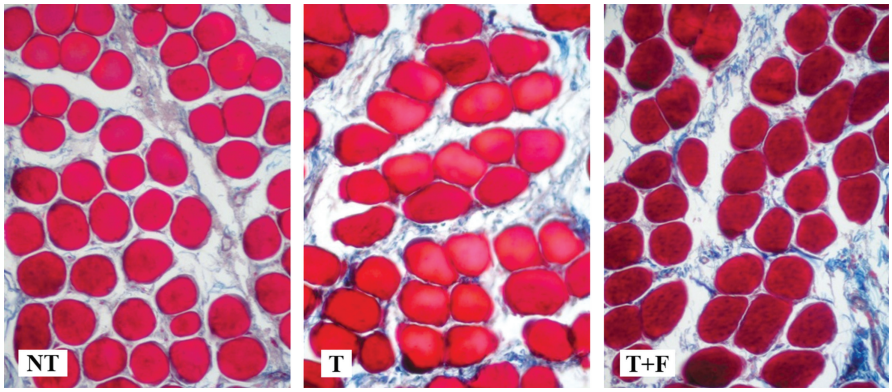

Fig. 3. Azan staining (*Magn. x 200*). Cross sections of soleus muscle of the animals from the experimental groups. **NT**. Non-trained control. **T**. Endurance-trained rats. **T+F**. Endurance-trained rats receiving ARB.

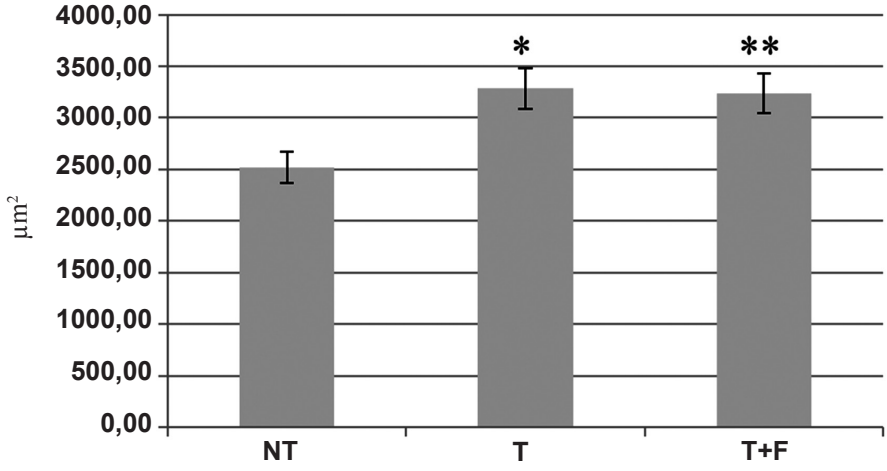

Fig. 4. Cross-sectional area (μm^2) of soleus muscle myofibres. *P<0.05, **P<0.01 as compared to NT

Immunoreactivity for BDNF in the soleus muscle fibres of the animals from the T group was significantly higher as compared to the NT group ($P=0.001$). Flutamide administration did not alter the intensity of the reaction for BDNF ($P>0.05$) in the muscle fibres.

Greatest intensity of immunoexpression was recorded in the newly formed myoblasts of the trained animals not receiving ARB, and the differences observed were significant not only in comparison to the non-trained animals (P<0.001), but also to the trained ones receiving ARB (P<0.01) (**Fig. 5; Fig. 6**).

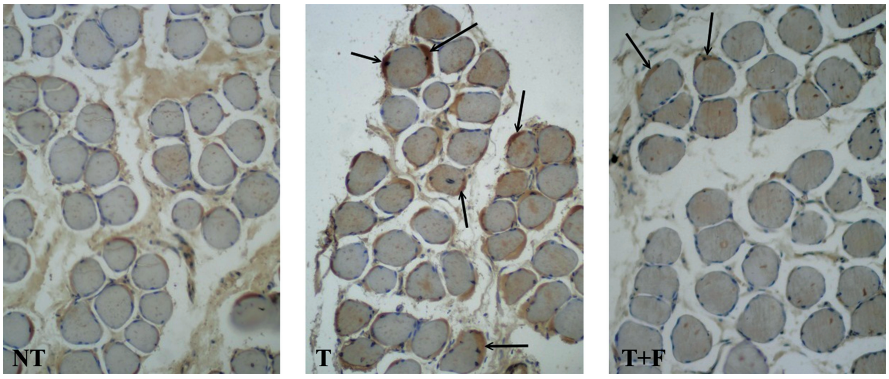

Fig. 5. BDNF immunoreactivity in soleus muscle on cross section (*Magn. x 200*). **NT**. Non-trained control. **T**. Endurance-trained rats. **T+F**. Endurance-trained rats receiving ARB. *Arrows* - expression in myoblasts located peripherally to myocytes.

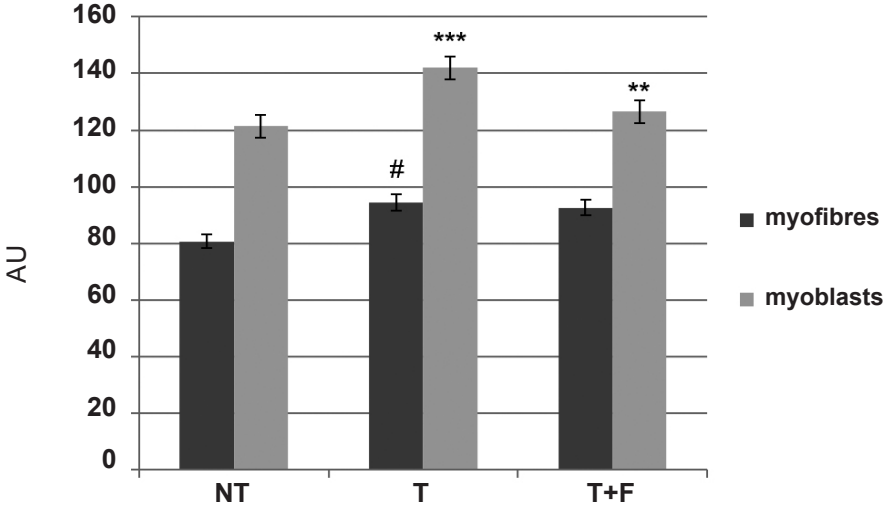

Fig. 6. Intensity of BDNF expression (AU) in myofibres of soleus muscle on cross section. #P<0.01 as compared to NT, ***P<0.001 as compared to NT, **P<0.01 as compared to T.

Discussion

Our results showed that endurance training increased the number of myonuclei and the myofibre cross-sectional area of soleus muscle. They are consistent with the results of other studies [7] that have also found a CSA increase in type I fibres of soleus and

EDL muscles of rats following a 10-week treadmill exercise under similar training conditions. In people, it has also been found that a 12-week aerobic training results in an increase in the mean cross section of type I and type II muscle fibres, accompanied by an increase in the number of SCs associated with type I fibres. A higher myonuclear number in type I fibres was observed as well [10].

These data support the hypothesis discussed lately concerning one of the mechanisms underlying the response of muscles to exercise training - formation of new myofibres [3, 21]. It has been found that in resistance training the increase in SCs is type-specific and occurs in type II myofibres, which are associated to a greatest degree with the development of muscular hypertrophy [26]. In aerobic training muscles made up of predominantly type I and type IIa fibres are involved, such as the soleus muscle (85% type I), [6]. We observed the largest myonuclear number per fibre on cross section in this muscle. Our results support the concept that new myonuclei are added to these muscle fibres, so that the latter can respond to the increased requirements resulting from regular aerobic training, expanding the so-called myonuclear domain [1]. This process occurs with the participation of stimulated SCs that proliferate and differentiate, since the nuclei in the mature myofibres are post-mitotic [24]. The so-formed myoblasts converge with the existing myofibres, providing nuclei as an additional source of protein synthesis.

The administration of ARB reduced the myonuclear number of soleus in the trained animals, as compared to the trained control. This fact can be explained with the absence of a testosterone (Ts) effect due to blocked androgen receptors (ARs). The latter are most likely localised in the muscle fibres and SCs [9, 14]. This alteration demonstrates the participation of androgens in the processes of adaptation of muscles made up mainly of type I fibres to aerobic training, an example of which is the soleus muscle.

The results obtained showed that regular submaximal training led to a significant increase in the CSA of soleus. Skeletal muscles are very plastic tissues capable of adapting to the increased motor and metabolic needs during training. A number of signalling pathways and myogenic regulatory factors are triggered, which activate protein synthesis (myofibrillar, sarcoplasmic, mitochondrial). These different types of protein synthesis in the muscles underlie the adaptation response to exercise training [2]. The enhanced protein production results in an increased myofibre bulk, which can be seen on cross section of the muscle. A number of studies have found an increase in myoglobin concentrations resulting from training or electric stimulation, which has been associated with the improved oxidative capacity of muscle fibres [17]. ARB administration in the trained animals reduced the myofibre CSA of soleus; however, the difference was not significant. These results can be explained with the different sensitivity of the fibre types to Ts and, to be more precise, of the ARs localised in them. Many authors share the opinion that type II myofibres are more sensitive to the action of Ts and its derivatives [12].

The type of exercise training determines to a greatest extent the presence of muscular hypertrophy [10]. This explains why some experimental models involving aerobic training have not found significant increase in myofibre bulk [13]. Prolonged training enhances proteolytic activity in the muscles mostly owing to the raised glucocorticoid levels. The exercise training applied in our experiment was submaximal, about 70-75% of VO_{2max}, which is more intensive than pure aerobic training (60-65% of VO_{2max}).

The increased BDNF expression that we found not only in the muscle fibres, but to a greater extent in the newly formed myoblasts of soleus, proves the participation of this

neurotrophin in the control and occurrence of part of the adaptation processes observed in skeletal muscles during training. McKay and colleagues report about cells of identical location (peripheral to the muscle fibres), which are BDNF-positive [18]. The authors emphasize the key role of BDNF in the late proliferation and early differentiation of SCs in vivo in humans.

AR blockade by Flutamide reduced BDNF expression in the myoblasts but did not influence its expression in the muscle fibres, which shows that androgens influence the synthesis of this neurotrophin mainly in the newly formed myofibres during training. Having auto/paracrine effects, BDNF is likely to participate in the mechanisms through which new muscle fibres are formed under conditions of submaximal training.

In conclusion, our results show that androgens participate in the adaptation to endurance training by means of their own ARs. This genomic mechanism is likely to be the one through which the increase in myonuclear number is influenced, as well as BDNF expression in the myofibres and the newly formed myoblasts of skeletal muscles made up mainly of type I fibres, an example of which is the soleus muscle.

References

1. **Allen, D. L., R. R. Roy, V. R. Edgerton**. Myonuclear domains in muscle adaptation and disease. – *Muscle Nerve*, **22**, 1999, 1350-1360.
2. **Atherton, P. J., K. Smith**. Muscle protein synthesis in response to nutrition and exercise. – *J. Physiol.*, **590**, 2012, 1049–1057.
3. **Bellamy, L. M., S. Joanisse, A. Grubb,C. J. Mitchell, B. R. McKay, S. M. Phillips, S. Baker, G. Parise**. The acute satellite cell response and skeletal muscle hypertrophy following resistance training. – *PLoS ONE*, **9**(10), 2014, e109739.
4. **Chevrel, G., R. Hohlfeld, M. Sendtner**. The role of neurotrophins in muscle under physiological and pathological conditions. – *Muscle Nerve*, **33**(4), 2006, 462-476.
5. **Conboy, I. M., M. J. Conboy, A. J. Wagers, E. R. Girma, I. L. Weissman, T. A. Rando**. Rejuvenation of aged progenitor cells by exposure to a young systemic environment. – *Nature*, **433**, 2005, 760-764.
6. **Delp, M. D., C. Duan**. Composition and size of type I, IIA, IID/X, and IIB fibers and citrate synthase activity of rat muscle. – *J. Appl. Physiol*., **80**, 1996, 261-270.
7. **Demirel, H. A., S. K. Powers, H. Naito, M. Hughes, J. S. Coombes**. Exercise-induced alterations in skeletal muscle myosin heavy chain phenotype: dose-response relationship. – *J. Appl. Phyiol*., **86**(3), 1999, 1002-1008.
8. **Dubois, V., M. Laurent, S. Boonen, D. Vanderschueren, F. Claessens**. Androgens and skeletal muscle: cellular and molecular action mechanisms underlying the anabolic actions. – *Cell. Mol. Life. Sci.*, **69**, 2012, 1651-1667.
9. **Dubois, V., M. Laurent, M. Sinnesael, N. Cielen, C. Helsen, L. Clinckemalie, L. Spans, G. Gayan-Ramirez, L. Deldicque, P. Hespel, G. Carmeliet, D. Vanderschueren, F. Claessens**. A satellite cell-specific knockout of the androgen receptor reveals myostatin as a direct androgen target in skeletal muscle. – *FASEB J*., **28**(7), 2014, 2979-2994.
10. **Fry, C. S., B. Noehren, J. Mula,M. F. Ubele, P. M. Westgate, P. A. Kern, C. A. Peterson**. Fibre type-specific satellite cell response to aerobic training in sedentary adults. – *J. Physiol.*, **5**(12), 2014, 2625-2635.
11. **Harber, M. P., A. R. Konopka, M. K. Undem, J. M. Hinkley, K. Minchev, L. A. Kaminsky, T. A. Trappe, S. Trappe**. Aerobic exercise training induces skeletal muscle hypertrophy and age-dependent adaptations in myofiber function in young and older men. – *J. Appl. Physiol*., **113**(9), 2012, 1495-504.
12. **Hartgens, F., H. Kuipers**. Effects of androgenic-anabolic steroids in athletes. – *Sports Med*., **34**, 2004, 513-554.
13. **Joanisse, S., J. B. Gillen, L. M. Bellamy,B. R. McKay, M. A. Tarnopolsky, M. J. Gibala, G. Parise**. Evidence for the contribution of muscle stem cells to nonhypertrophic skeletal muscle remodeling in humans. – *FASEB J.*, **27**(11), 2013, 4596-4605.

14. **Kadi, F**. Cellular and molecular mechanisms responsible for the action of testosterone on human skeletal muscle. A basis for illegal performance enhancement. – *Br. J. Pharmacol.*, **154**, 2008, 522–528.
15. **Knaepen, K., M. Goekint, E. M. Heyman, R. Meeusen**. Neuroplasticity – exercise-induced response of peripheral brain-derived neurotrophic factor. – *Sports Med*., **40**(9), 2010, 765-801.
16. **Liu, W., G. Chen, F. Li, C. Tang, D. Yin**. Calcineurin-NFAT signaling and neurotrophins control transformation of myosin heavy chain isoforms in rat soleus muscle in response to aerobic treadmill training. – *J. Sport. Sci. Med.*, **13**, 2014, 934-944.
17. **Mänttäri, S., K. Anttila, M. Järvilehto**. Testosterone stimulates myoglobin expression in different muscles of the mouse. – *J. Comp. Physiol. B.*, **178**, 2008, 899-907.
18. **McKay, B. R., J. P. Nederveen, S. A. Fortino, T. Snijders, S. Joanisse, D. A. Kumbhare, G. Parise**. Brain-derived neurotrophic factor is associated with human muscle satellite cell differentiation in response to muscle damaging exercise. – *Appl. Physiol. Nutr. Metab.*, 2019,doi: 10.1139/apnm-2019-0501.
19. **Motohashi, N., A. Asakura**. Muscle satellite cell heterogeneity and self-renewal. – *Front. Cell. Dev. Biol.*, **2**, 2014, 1.
20. **Ogborn, D. I., P. F. Gardiner**. Effects of exercise and muscle type on BDNF, NT-4/5, and TrKB expression in skeletal muscle. – *Muscle Nerve.*, **41**(3), 2010, 385-91.
21. **Petrella, J. K., J. Kim, J. M. Cross, D. J. Kosek, M. M. Bamman**. Efficacy of myonuclear addition may explain differential myofiber growth among resistance-trained young and older men and women. – *Am. J. Physiol. Endocrinol. Metab.*, **291**, 2006, E937–E946.
22. **Robinson, M. M., C. Bell, F. F. Peelor, B. F. Miller**. β-Adrenergic receptor blockade blunts postexercise skeletal muscle mitochondrial protein synthesis rates in humans. – *Am. J. Physiol. Regul. Integr. Comp. Physiol.*, **301**(2), 2011, R327-R334.
23. **Sakuma, K., A. Yamaguchi**. The recent understanding of the neurotrophin's role in skeletal muscle adaptation. – *J. Biomed. Biotechnol*., 2011; 201696.
24. **Sinha-Hikim, I., S. M. Roth, M. I. Lee, S. Bhasin**. Testosterone-induced muscle hypertrophy is associated with an increase in satellite cell number in healthy, young men. – *Am. J. Physiol. Endocrinol. Metab*., **285**, 2003, E197–E205.
25. **Snijders, T., J. P. Nederveen, B. R. McKay,S. Joanisse, L. B. Verdijk, L. J. van Loon, G. Parise**. Satellite cells in human skeletal muscle plasticity. – *Front. Physiol.*, **6**, 2015, 283.
26. **Verdijk, L. B., B. G. Gleeson, R. A. Jonkers, K. Meijer, H. H. Savelberg, P. Dendale, L. J. van Loon**. Skeletal muscle hypertrophy following resistance training is accompanied by a fiber type – specific increase in satellite cell content in elderly men. – *J. Gerontol. A. Biol. Sci. Med. Sci.*, **64**(3), 2009, 332–339.

Institute of Experimental Morphology, Pathology and Anthropology with Museum
Bulgarian Anatomical Society

Acta morphologica et anthropologica, 27 (1-2)
Sofia ● 2020

Accessory Thymic Tissue in the Neck – an Incidental Finding during Anatomical Dissection

Albert Gradev[1], Julide Kasaboglu[1], Vesela Ivanova[2], Tihomir Dikov[2], Nikolai Krastev[1], Lina Malinova[1], Lazar Jelev[1]*

[1] Department of Anatomy, Histology and Embryology, Medical University, Sofia, Bulgaria
[2] Department of General and Clinical Pathology, Medical University, Sofia, Bulgaria

* Corresponding author e-mail: ljelev@abv.bg

Herewith, we report a rare case of an accessory thymic remnant in the infrahyoid region. During routine anatomical dissection of the neck muscles of a 65-year-old Caucasian male cadaver, we discovered four small aberrant oval bodies. Histologically, the two lower bodies were composed of thyroid gland tissue. The upper left body was composed of uni- and multilocular adipocytes. The routine histology of the upper right aberrant structure showed adipose tissue and hypercellular areas of small cells with fine chromatin texture, arranged in nests. In some parts, they showed gradual transition into spindle-shaped elements resembling immature squamous epithelium. Further examination was provided by automated immunohistochemistry. CD45 was found to be expressed on all small cells, corresponding to lymphocytes, while Cytokeratin 5/6 decorated the Hassall's bodies-like structures, confirming their squamous nature. The final histological diagnosis was thymic tissue with immature Hassall's corpuscles.

Key words: accessory thymus, neck, immunohistochemistry, clinical significance, human

Introduction

The thymus is usually composed of two loosely connected lobes of variable shape, situated just behind the manubrium and body of the sternum and occupying parts of the superior and anterior mediastina [7]. Not infrequently, the upper parts of the thymic lobes extend into the base of the neck just behind the infrahyoid (strap) muscles and even higher reaching the thyroid gland [7]. This cervical location can be explained by migration downwards of the thymic epithelial cords during the development [4], remnants of which can persist in the neck as either accessory or ectopic thymus [10]. The aberrant thymic tissue may suffer from the same pathological conditions as the usual thymus, and has a clinical importance in thymoma and myasthenia gravis surgery [2, 13].

Materials and Methods

The gross anatomy observations were done in a formalin-fixed adult male cadaver. For routine histological observations, the tissue samples were paraffin embedded, cut into 7µm thin slices and stained with H&E according to a standard laboratory protocol. The immunohistochemistry was performed on paraffin embedded tissue slices by using Autostainer Link 48 (Dako, Agilent, USA) after antigen retrieval in PTLink in low pH buffer. EnVision Flex protocol was followed with 20 min incubation with pre-diluted primary antibodies: CD45 (LCA, clones 2B11+PD7/26), Cytokeratin 5/6 (CK 5/6) (clone D5/16 B4), CD56 (clone 123C3; Dako, Agilent).

Results

Herewith, we report a rare case of an aberrant thymic tissue found in the anterior cervical region of a 65-year-old Caucasian male cadaver. Upon dissecting the infrahyoid muscles, we discovered four small oval bodies (long diameter about 10-15 mm), quite flattened (thickness about 4-5 mm), that were grouped in two pairs - upper and lower.The two lower bodies were found under the layer of the sternothyroid muscle at the level of the C6 vertebral body (**Fig. 1a**). They were closely related but separated from the capsule covering the lower parts of the thyroid gland lobes. The two upper bodies were identified at the level of the C4 vertebral body between the sternohyoid and thyrohyoid muscles (**Fig. 1b**), covering the lower half of thyroid cartilage. In gross anatomy inspection, the four bodies looked similar. Hence, we proceed with their microscopic examination.

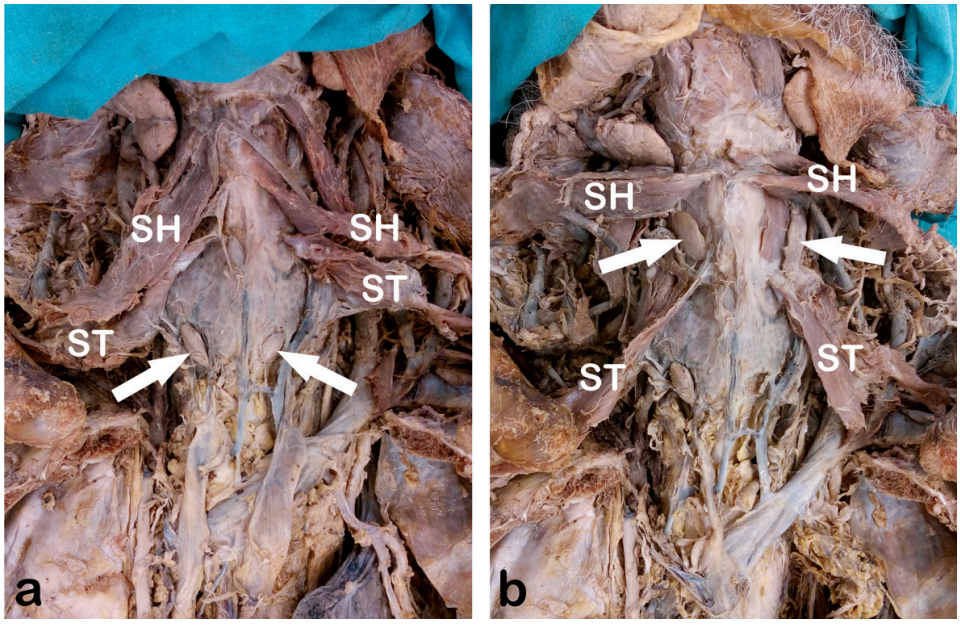

Fig. 1. Photograph of the neck dissection. White arrows showing the lower (a) and upper (b) aberrant bodies. Muscles: SH – sternohyoid; ST – sternothyroid.

The paraffin embedded tissue slices stained routinely with H&E revealed quite a different histology. The two lower structures were composed of thyroid gland tissue (**Fig. 2a**). Adipose tissue was identified in the upper left oval body, containing unilocular and small number of multilocular adipocytes (**Fig. 2b**).

The histological structure of the upper right oval body, however, was more demanding. Based on the first look observations, we were vacillating between thymic tissue and parathyroid gland. Detailed observations on routine histology revealed mature fatty tissue with unevenly distributed hypercellular areas, composed of small cells with fine chromatin texture, pale cytoplasmic rim and well-defined cellular borders (**Fig. 3a, b**). These cells were arranged in small nests, lacking apparent vessels and harbor gradual transition into spindle-shaped elements with incipient formation of structures, resembling immature squamous epithelium (Hassall's corpuscles).This finding was consistent with descriptions of Zielinsky et al. [13], who also did not find Hassall's bodies in 34,4% of accessory thymic tissue examined.

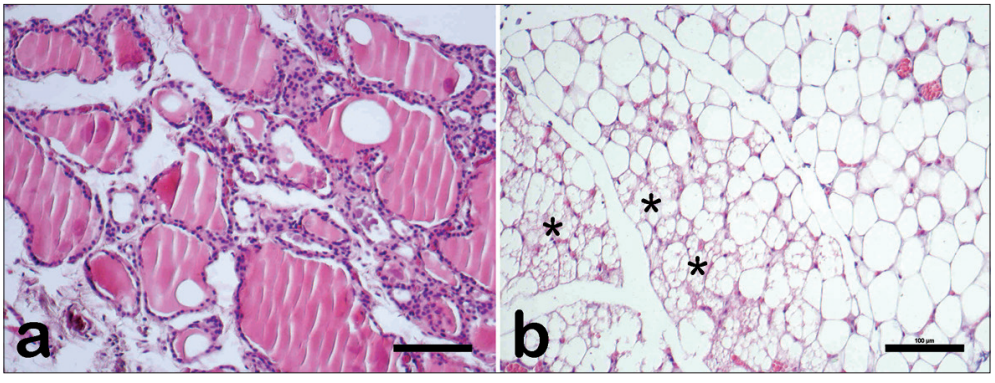

Fig. 2. Photomicrographs of the routine stained slides (H&E) from the lower (a) and upper left (b) aberrant neck structures. In (b), the asterisks indicate small groups of multilocular adipocytes, surrounded by unilocular adipocytes. Objective x20. Scale bar – 100 µm.

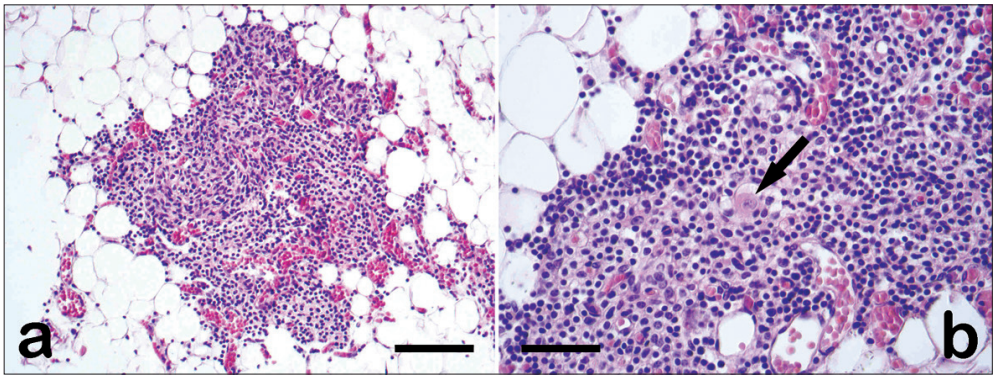

Fig. 3. Photomicrographs of the routine stained slides (H&E) from the upper right aberrant structure. In (a) adipose tissue mixes with hypercellular areas, composed of small cells with fine chromatin texture. Objective x20. Scale bar – 100 µm. In (b) arrow indicates spindle-shaped elements resembling immature Hassall's corpuscle. Objective x40. Scale bar – 50 µm.

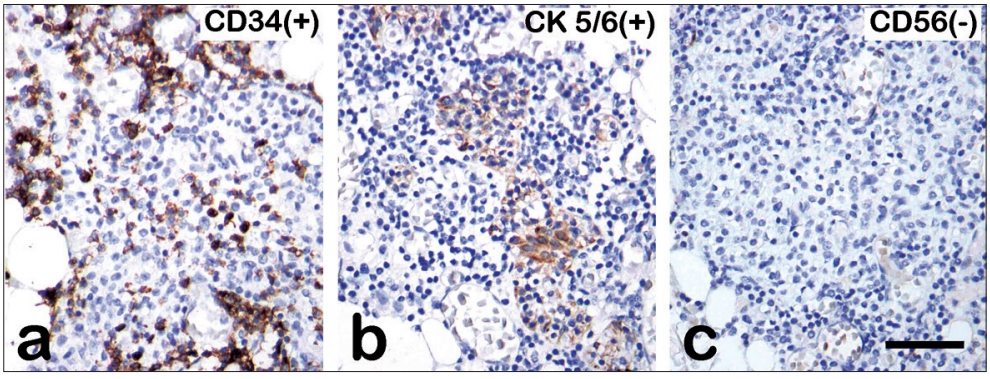

Fig. 4. Immunohistochemistry of upper right aberrant structure, showing CD34 positive reaction of the lymphocytes (a), CK 5/6 positive reaction of the epithelioreticular cells (b) and negative CD56 marker, excluding neuroendocrine cells (c). Objective x40. Scale bar – 50 μm.

For further examination, immunohistochemistry for was performed with pre-diluted primary antibodies: CD45 (LCA, clones 2B11+PD7/26), Cytokeratin 5/6 (CK 5/6)(clone D5/16 B4), CD56 (clone 123C3; Dako, Agilent).CD45 (leukocyte common antigen) was found to be expressed on all small cells, corresponding to lymphocytes (**Fig. 4a**), while CK 5/6 decorated the Hassall's bodies-like structures, confirming their squamous nature (**Fig. 4b**). The neuroendocrine cell marker CD56 was found negative (**Fig. 4c**). The final histological diagnosis was thymic tissue with immature Hassall's corpuscles.

Discussion

In the present literature, there are many reports of aberrant thymic tissue that might be classified as either accessory or ectopic [3, 6, 8, 12]. An "accessory" thymic tissue exists additionally to the normal mediastinal thymus, while the "ectopic" thymus basically means the whole organ in unusual location [10]. In our case, the small thymic remnant was classified as accessory because it was located between the sternohyoid and thyrohyoid and was existing together with the involuted thymus in the superior mediastinum.

Despite different theories proposed, the recent studies suggested the "endoderm-centric" ("endoderm-only") model of thymic development [1]. During 5th-7th week of human development, the thymic epithelial cells, deriving from the endoderm of the paired third pharyngeal pouch, descend along the neck to reach the superior mediastinum and later become populated with lymphoid stem cells [4, 5]. This descensus defines the possible places of ectopic or accessory thymic tissue.

The incidence of cervical accessory thymic tissue in general adult population is not known, because it might remain asymptomatic. In the patient groups, treated for myasthenia gravis with extended thymectomy, an accessory thymus was variably reported from 12.1% [13] to 22% [2]. Another group examined is thyroidectomied patients, who present some accessory thymic tissue in 4.45% of the cases [8]. Additionally, in nearly

50% of the cases of ectopic thymoma, an origin from the accessory cervical thymic tissues might be expected [11].

The reported here accessory thymic tissue should be considered in differential diagnosis of neck tumors, including cervical lymphadenomegaly [3, 11]. The thymic remnants can be found accidentally during different surgical interventions in anterior neck region [9]. The surgeons must be well aware of these possible aberrant thymic focci in order not the miss them during thymectomy for myasthenia gravis thus preventing any reoperations [2, 13].

R e f e r e n c e s:

1. **Gordon, J., N. R. Manley.** Mechanisms of thymus organogenesis and morphogenesis. – *Development*, **138**, 2011, 3865-3878.
2. **Jaretzki 3rd, A.** Thymectomy for myasthenia gravis: analysis of controversies-patient management. – *Neurologist*, **9**, 2003, 77-92.
3. **Martin, J. M., G. Randhawa, W. J. Temple.** Cervical thymoma. – *Arch. Pathol. Lab. Med.*, **110**, 1986, 354-357.
4. **Moore, K. L., T. V. N. Persaud, M. G. Torchia.** *The Developing human: Clinically oriented embryology*, 9th Ed, Philadelphia, Saunders, 2013, 166-168.
5. **Palumbo, C**. Embryology and anatomy of the thymus gland. – In: *Thymus gland pathology: clinical, diagnostic and therapeutic features* (Eds. C. Lavini, C. A. Moran, U. Morandi, R. Schoenhuber), Milan, Springer, 2008, 13-18.
6. **Saggese, D., G. Ceroni Compadretti, C. Cartaroni.** Cervical ectopic thymus: a case report and review of the literature. – *Int. J .Pediatr. Otorhinolaryngol.*, **66**, 202, 77-80.
7. **Standring, S.** *Gray's anatomy – The Anatomical basis of clinical practice*, 41th Ed, London, Elsevier, 2016, 983-986.
8. **Tabatabaie, S. A., S. M. Hashemi, B. Sanei, M. H. Sanei.** The frequency of ectopic thymic tissue in the necks of patients without any thymic disease. **–** *Med. Sci. Monit.*, **13**, 2007, 283-285.
9. **Talmon, G. A., J. E. Lewis.** Lymphocyte-depleted thymic remnants: a potential diagnostic pitfall in the evaluation of central neck dissections. – *Am. J. Clin. Pathol.*, **132**, 2009, 707-712.
10. **Tubbs, R. S., M. M. Shoja, M. Loukas**. *Bergman's comprehensive encyclopedia of human anatomic variation*, Hoboken, New Jersey, John Wiley & Sons, Inc., 2016, 914-917.
11. **Weissferdt, A., C. A. Moran.** The spectrum of ectopic thymomas. – *Virchows Arch.*, **469**, 2016, 245-254.
12. **Yamashita, H., N. Murakami, S. Noguchi, A. Noguchi, S. Yokoyama, A. Moriuchi, I. Nakayama.** Cervical thymoma and incidence of cervical thymus. **–** *Acta Pathol. Jap.*, **33**, 1983, 189-194.
13. **Zieliński, M., J. Kuzdzal, A. Szlubowski, J. Soja.** Comparison of late results of basic transsternal and extended transsternal thymectomies in the treatment of myasthenia gravis. **–** *Ann. Thorac. Surg.*, **78**, 2004, 253-258.

Institute of Experimental Morphology, Pathology and Anthropology with Museum
Bulgarian Anatomical Society

Acta morphologica et anthropologica, 27 (1-2)
Sofia ● 2020

Morphology of NADPH-Diaphorase Reactive Neurons in the Human Thalamic Reticular Nucleus

Lina Malinova, Todor Kirov, Angel Dandov*

Department of Anatomy, Histology and Embryology, Medical University, Sofia, Bulgaria

* Corresponding author e-mail: lmalinova@abv.bg

Nitric oxide (NO) has recently emerged as an important factor in neural signaling and synaptic plasticity. By using the histochemical procedure for NADPH-diaphorase (NADPH-d) the morphology of neurons and fibers containing NADPH-diaphorase activity in the human thalamic reticular nucleus (TRN) was examined. The morphological differences in the TRN neurons could contribute to the better understanding of the different functions in these cells associated with psychiatric disorders, epileptic seizures, and also the regulation of thalamocortical and corticothalamic inputs or outputs.

Key words: thalamic reticular nucleus, morphology, NADPH-diaphorase, nitric oxide (NO).

Introduction

The thalamic reticular nucleus (TRN) is a slender sheet of GABAergic cells, with colocalization of parvalbumin, situated around the external medullar lamina of the thalamus and medially to the internal capsule. This nucleus is considered as a pacemaker, indirectly regulating the activity of the cerebral cortex by thalamocortical and corticothalamic collaterals. On the other hand, it has direct connections with different subcortical regions and the other thalamic nuclei. The dendrites of its neurons form a local inhibitory network [1]. The TRN has been subdivided into specific sectors containing somatotopically organized projections of different parts of the body and head [1, 21].

Nitric oxide (NO) has the unconventional characteristics of being a gaseous neurotransmitter [2]. Nitric oxide synthase (NOS), the enzyme required for NO production, is localized within the GABAergic TRN neurons [3]. There is a big interest to identify the neurons producing nitric oxide (NO) with the involvement of NADPH-diaphorase (NADPH-d) [4, 5].

The structural features of NADPH-d-positive neurons in the rat [6, 7] and human brain have been well described in cortical cells [8, 9]. There is a small number of studies on them in other human brain areas. NADPH-d positive cells have been observed in the amygdaloid nucleus, the putamen [9, 10] and besides, we were only able to find few studies on NADPH-d-positive cells in the nuclei of the dorsal thalamus and the

adjacent reticular nucleus in the human brain [11, 12]. The aim of the present study was to determine the morphology and distribution of NADPH-diaphorase positive neurons in the TRN of the human brain.

Material and Methods

TRN samples were obtained from the brains of two females (40 and 45 years of age) and two males (43 and 52 years of age) at autopsy. The brains did not show any overt signs of pathology or trauma. The time from death until fixation was up to 12 hours. The brains were cut into slabs with a thickness of 1-2 cm in the coronal plane. The blocks were fixed for two days under gentle agitation in a mixture of 4% paraformaldehyde, 1% picric acid and 10 % glucose. Thereafter, the blocks were sectioned in the coronal plane and washed repeatedly in 0.1 M phosphate buffer, pH 7.4. Serial coronal sections of 40 µm were cut on a freezing microtome and collected in the same phosphate buffer. In brief, all slices, prepared as described above, were treated with sodium borohydride for 45 min followed by three consecutive rinses in 0,01 M PBS, each for 2 min. The sections were stained with the NADPHd-technique using 0.1-0.2 mg/ml nitro blue tetrazolium and 1 mg/ml b-NADPH and 0.3-0.5% Triton X100 in 0.1 M TRIS-HC1 buffer (pH 7.4) at 37°C for 30-60 min in a thermostat. Afterwards, the sections were rinsed for 5 min, 3 times in the same phosphate buffer and mounted on gelatin-coated glass slides. The slides were air dried for 24 hours, then washed in distilled water for 5 min, 3 times, air dried again and cover-slipped with Entellan (Merck, Germany) and examined using a light microscope (Olympus, Tokyo, Japan).

Results

Each of the 4 human brains showed numerous intensely or moderately stained NADPH-d positive cells in the TRN. The light-microscopic analysis of the TRN showed that the nucleus contained islets of neurons or scattered single NADPH-d-positive cells with different shape along the rostro-caudal and dorso-ventral axis and a different arrangement of their outgrowths. The staining of some of the cells was so intense that it resembled Golgi-impregnated neurons. The reaction product diffusely filled the cytoplasm of the positive neurons and their branches. At times, the non-stained nuclei of the neurons were distinguishable. The NADPH-d positive neurons were found in all sections from rostral to caudal extension of the human TRN, but their distribution and density were irregular. A high number of stained cells were observed first in the anterior portion, i.e. limbic and motor sector of the TRN. In shape, the NADPH-d positive neurons varied from fusiform, oval, or triangular to multipolar (**Fig.1**). Two to

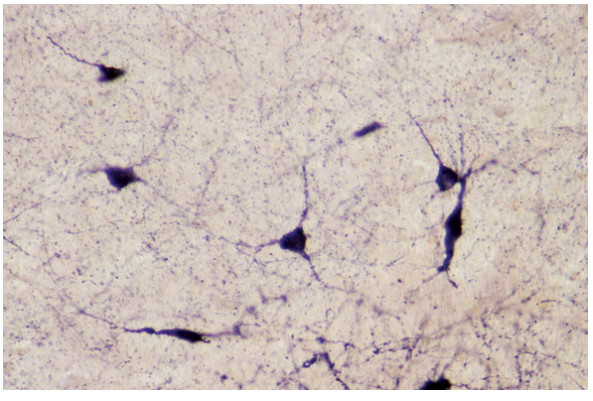

Fig. 1. Histochemical demonstration of NADPH-d reactive group of cells with fusiform, triangular and multipolar shape from the anterior part of the human TRN. The branches of these cells are short and can be followed in different directions (×400).

several outgrowths arose from each perikaryon, and then they branched dichotomically or threechotomically to secondary ones. Some of them had sparse branches that were covered with few spines. The axons of the cells could not be followed thoroughly although some of them were fork-bifurcated.

We observed clusters of positive cells only in the anterior part of the sagittal section of the TRN. In the intermediate part, a large number of neurons were typically fusiform in shape on the lateral and medial borders of the nucleus (**Fig. 2**). Others were oval and triangular in the central subdivision of the intermediate part of the TRN (**Fig. 3**) with almost straight, sparse, and very long, branched dendrites. Some of the dendrites could be followed from the cell bodies (**Fig. 4; Fig. 5**). The perikarya and dendrites of NADPH-d-positive cells of the TRN usually extended parallel to the internal capsule.

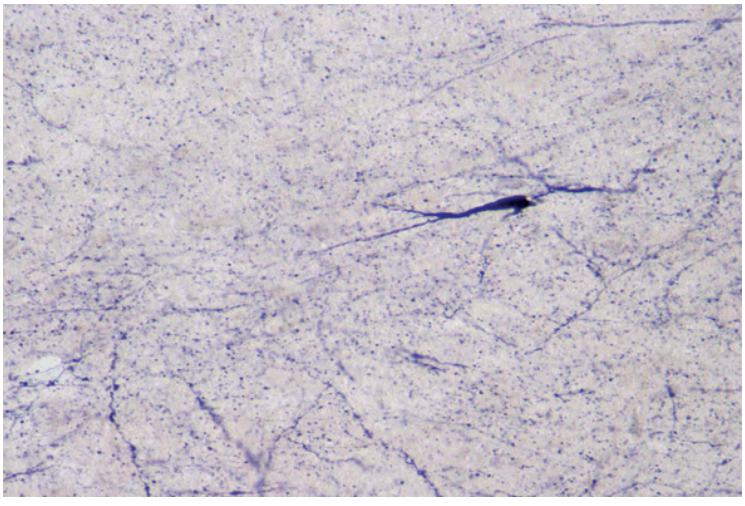

Fig. 2. NADPH-d reactive fusiform neuron from the dorsal portion of TRN with long dendrites with beads along their length (× 400).

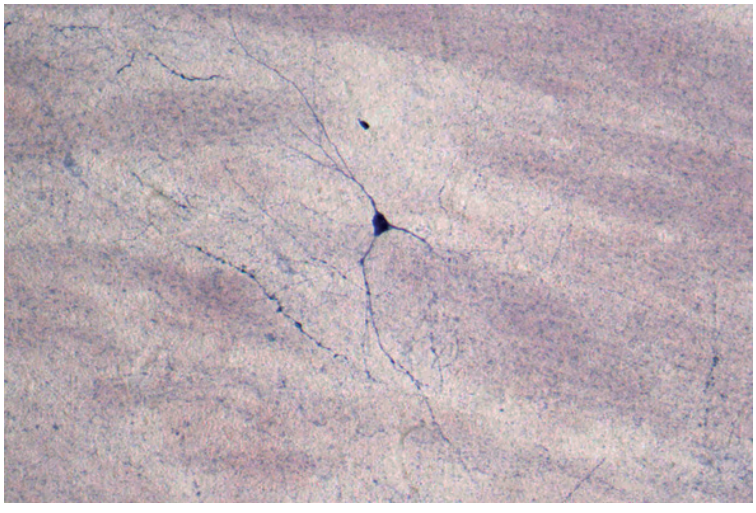

Fig. 3. A typical NADPH-d reactive triangular neuron from the dorsal part of the TRN with long, thin, straight and smooth fork-like branches (× 400).

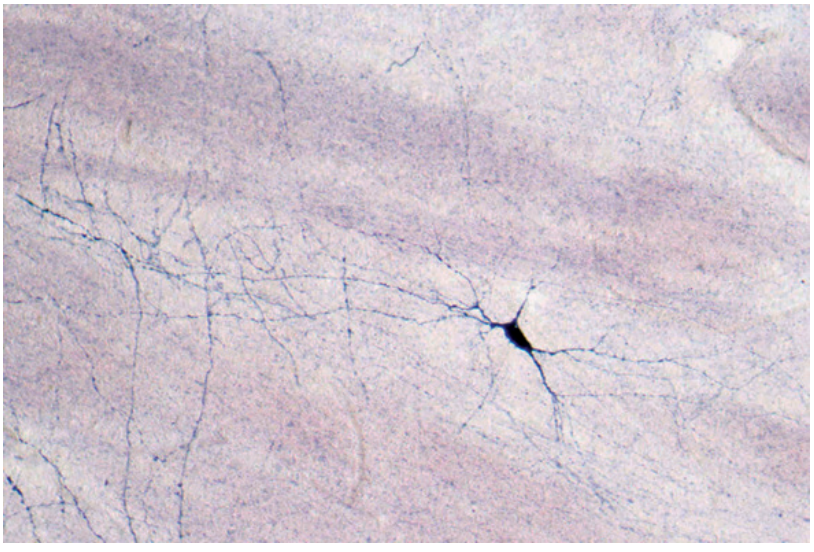

Fig. 4. NADPH-d reactive large, sparsely-branched, long-dendrite neuron of the TRN in the human (× 400).

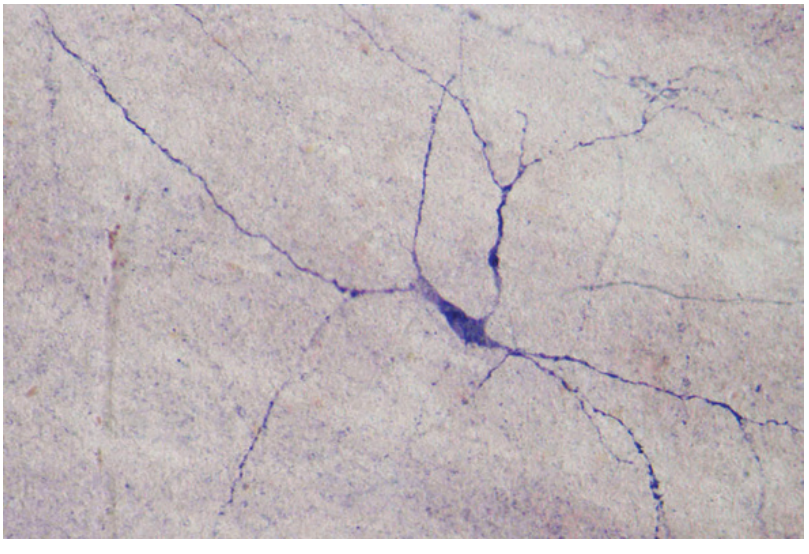

Fig. 5. A large neuron of the human TRN stained with NADPH-d with long dendrites significantly, extending from the cell body (× 400).

The posterior portion consisted of single, predominantly fusiform cells with forked dendrites parallel to the internal capsule with a lot of well visible varicosites (**Fig. 6**).

It should be noted that the neuropil everywhere in the nucleus contained a lot of unidentified NADPH-d- positive fibers with a different course and they contained beads with irregular shape and size.

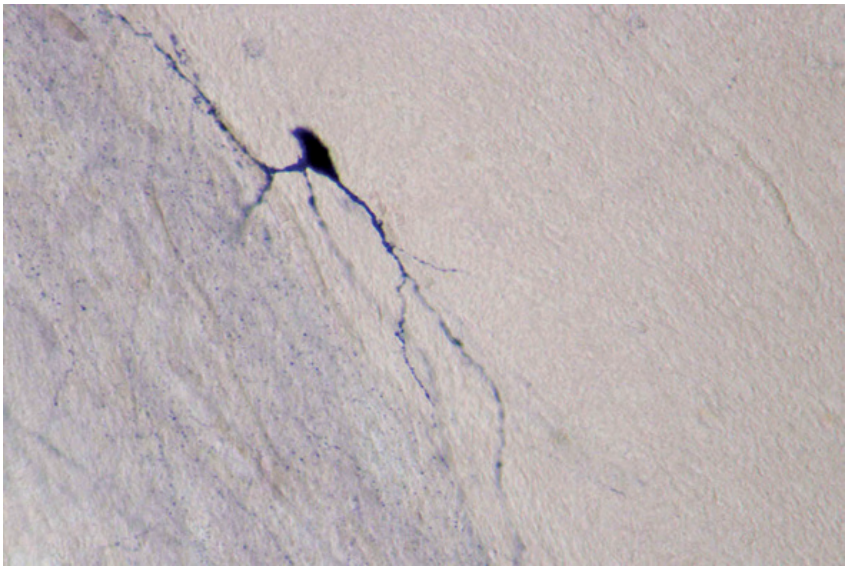

Fig. 6. An oval NADPH-d reactive neuron close to the internal capsule with thick bulbous dendrites, extending longitudinally (× 400).

Discussion

Studies on TRN in the human brain demonstrate the presence of NADPH-d-positive cells. This method also allows visualization of the structural details of neurons, which shows them to be reticular and short-axonal [12]. Our results indicate the existence of NADPH-d positive neurons in all the subdivisions of the TRN. In some cases the staining is so intense that it resembles Golgi impregnation with its axonal and dendritic arborizations [13]. We find a higher number of positive neurons in the rostral part of the nucleus and they are of a different shape. The neurons of the TRN are classified according to their perikaryal size into large, medium and small [11, 13-15]. They are not only isolated [11], but are also organized in groups or clusters, though only in the rostral part.

Previous data have shown that in the TRN there are two types of neurons. The first type is characterized by fusiform or angular neuronal profiles of large and intermediate size, with almost straight, sparse, and very long, rarely branched dendrites located on the margins of the nucleus [11]. Long collaterals with beads along their length make small-area contacts with two or three diagonal vessels. Besides, NADPH-d-positive cells of the second type possess short smooth dendrites. The bodies of these neurons vary from small to intermediate in size. The proximal parts of the cell dendrites tend to be rather thicker than the distal parts. The dendrite stems are straight or slightly tortuous [11]. Our data indicate the existence of NADPH-d positive neurons in all the subdivisions of the TRN. Recent studies have indicated that the increase in the NO levels potentiates inhibitory activity, presumably increasing the GABA release from presynaptic terminals by a cGMP-dependent process. Such an action is further

potentiated by the depolarization of the TRN neurons, thereby increasing the inhibitory tone in thalamocortical neurons [16]. NO is involved in different functions of the central nervous system, i.e. neurotransmitter release, regulation of neuronal electrical activity, and synaptic plasticity [17]. It plays a significant role in the normal aging and neurodegenerative processes in the CNS [18]. The TRN is particularly prone to oxidative stress [19] and also acts as a key player in the local sleep control [20], as well as in the temporal epileptic seizures [22].

Conclusion

Our results enlarge the existing data concerning the morphology and distribution of NADPH-d positive neurons in the human TRN. Moreover, NADPH-d positive neurons have both toxic and protective effects on the different parts of the CNS.

References

1. **Pinault, D.** The thalamic reticular nucleus: structure, function and concept. – *Brain Res. Rev*., **46**(1), 2004, 1, 1-31.
2. **Boehning, D., S. H. Snyder.** Novel neural modulators. – *Annu. Rev. Neurosci*., **26**, 2003, 105-131.
3. **McCauley, A. K., G. A. Meyer, D. W. Godwin.** Developmental regulation of brainnitric oxide synthase expression in the ferret thalamic reticular nucleus. – *Neurosci. Lett.,* **320**(3), 2002, 151-155.
4. **Hope, B., G. Michael, K. Knigge, S. Vincent.** Neuronal NADPH- diaphorase is a nitric oxide synthase. - *Proc. Natl. Acad. Sci.,* **88**(7), 1991, 2811-2814.
5. **Bredt, D. S., S. H. Snyder.** Nitric oxide, a novel neuronal messenger. – *Neuron*, **8**(1), 1992, 3-11.
6. **Malinova, L., B. Landzhov, A. Bozhilova-Pastirova, W. Ovtscharoff.** Differentiation of tyrosine hydroxylase immunoreactivity and NADPH-d-reactivity neurons in the piriform cortex of prepubertal male and female rats quantitative double-staining study. – *Compt. Rend. Acad. Bulg. Sci.,* **64 (**11**)**, 2011, 1631-1636.
7. **Dzambazova, E., B. Landzhov, A. Bocheva, A. Bozhilova-Pastirova**. Effects of kyotorphin on NADPH-d reactive neurons in rat's Cerebral cortex after acute immobilization stress. – *Compt. Rend. Acad. Bulg. Sci*., **64(**12**)**, 2011, 1779-1784.
8. **Hashikawa, T., M. G. Leggio, R. Hattori, Y. Yui.** Nitric oxide synthase immunoreactivity colocalized with NADPH-diaphorase histochemistry in monkey cerebral cortex. – *Brain Res.,* **641**(2), 1994, 341-349.
9. **Unger, J. W., W. Lange.** NADPH-diaphorase-positive cell populations in the human amygdala and temporal cortex: neuroanatomy, peptidergic characteristics and aspects of aging and Alzheimer's disease. – *Acta Neuropathol*., **83**, 1992, 636-646.
10. **Leontovich, T. A., Yu. K. Mukhina, A. A. Fedorov.** Neurons of the human basal ganglia (striatum and basolateral amygdala) expressing the enzyme NADPH-d. - *Ros. Fiziol. Zh. im. I. M. Sechenova,* **88**(10), 2002, 1295–1308.
11. **Berezhnaya, L. A.** NADPH-diaphorase-positive cells in the thalamic nuclei and internal capsule in humans. – *Neurosci. Behav. Physiol.,* **35**(3), 2005, 273-279.
12. **Berezhnaya, L. A.** NADPH-diaphorase-positive nuclei in the thalamus and internal capsule in humans. – *Morfologiya,* **125**(1), 2004, 16-22.
13. **Berezhnaya, L. A.** Neuronal organization of the ventral anterior and ventral lateral nuclei of the human thalamus. – *Morfologiya,* **121**(1), 2002, 38-43.
14. **Scheibel, M. E., A. B. Scheibel.** The organization of the nucleus reticularis thalami: A Golgy study. – *Brain Res.,* **1**(3), 1966, 250-268.
15. **Leontovich, T. A., A. I. Khrenov, Iu. K. Mukhina, A. A. Fedorov, L. A. Berezhnaya.** A common system of sparsely-branched projection (reticular) NADPH-diaphorase neurons in formations of densely-branched cells in the human forebrain. – *Neurosci. Behav. Physiol.,* **36**(9), 2006, 929-940.

16. **Sunggu, Y., C. L. Cox.** Modulation of Inhibitory Activity by Nitric Oxide in the Thalamus. – *J. Neurophysiol.,* **97**(5)**,** 2007, 3386-3395.
17. **Zhuo, M., R. D. Hawkins.** Long-term depression: a learning - related type of synaptic plasticity in the mammalian central nervous system. – *Reviews in Neuroscience,* **6**(3), 1995, 259-277.
18. **Law, A., S. Gauthier, R. Quirion.** Say NO to Alzheimer s disease: the putative links between nitric oxide and dementia of the Alzheimer s type. – *Brain Res. Rev.,* **35**(1), 2001, 73-96.
19. **Kim, S. Y., B. M. Cohen, X. Chen, S. E. Lukas, A. K. Shinn, A. C. Yuksel, T. Li, F. Du, D. Öngür.** Redox dysregulation in schizophrenia revealed by in vivo NAD+/NADH measurement. – *Schizophr. Bull.,* **43**(1), 2017, 197–204.
20. **Vantomme, G., A. Osorio-Forero, A. Lüthi, L. M. J. Fernandez**. Regulation of local sleep by the thalamic reticular nucleus. – *Front Neurosci.,* **5**9(13), 2019, 576.
21. **Shosaku, A., Y. Kayama, I. Sumitomo**. Somatotopic organization in the rat thalamic reticular nucleus. – *Brain Res., **311***(1), 1984, 57-63.
22. **Jo, H. J., D. L. Kenny-Junga, I. Balzekasa, E. E. Benarrocha, D. T. Jonesa, B. H. Brinkmanna, S. M. Steada, J. J. Van Gompel, K. M. Welker, G. A. Worrella.** Nuclei-specific thalamic connectivity predicts seizure frequency in drugresistant medial temporal lobe epilepsy. – *NeuroImage: Clinical.,* **21**, 2019, 101671

Institute of Experimental Morphology, Pathology and Anthropology with Museum
Bulgarian Anatomical Society

Acta morphologica et anthropologica, 27 (1-2)
Sofia ● 2020

Meloxicam and Its Metal Complexes: Cytotoxic Activity and Ability to Induce Autophagy in Human Triple Negative Breast Cancer Cells

Tanya Zhivkova[1], Zdravka Petrova[1*], Lora Dyakova[2], Rossen Spasov[1,3], Chukwuemeka Obinna Ekeh[1,4], Abedulkadir Abudalleh[1], Daniela-Cristina Culita[5], Gabriela Marinescu[5], Radostina Alexanderova[1**]*

[1] *Institute of Experimental Morphology, Pathology and Anthropology with Museum, Bulgarian Academy of Sciences, Sofia, Bulgaria;*
[2] *Institute of Neurobiology, Bulgarian Academy of Sciences, Sofia, Bulgaria;*
[3] *Faculty of Medicine, Sofia University " St. Kliment Ohridski", Sofia, Bulgaria;*
[4] *Faculty of Biology, Sofia University " St. Kliment Ohridski", Sofia, Bulgaria;*
[5] *Institute of Physical Chemistry "Ilie Murgulescu", Romanian Academy, Bucharest, Romania*

* Both authors - T. Zh. and Z. P., contributed equally to this work
** Corresponding author e-mail: rialexandrova@hotmail.com

The study aimed to evaluate the influence of the selective non-steroidal anti-inflammatory agent meloxicam and its metal [Zn(II), Cu(II), Co(II), Ni(II)] complexes on viability and proliferation of cultured MDA-MB-231 human triple negative breast cancer cells as well as the ability of these compounds to induce autophagy. Thiazolyl blue tetrazolium bromide (MTT) test, double staining with acridine orange and propidium iodide (AO/PI) and immunocytochemical analysis were applied. Zn(II) complex of meloxicam (Zn-Mel) was found to be the most pronounced cytotoxic agent among the compounds examined with CC_{50} calculated to be 376.5 μg/ml (470.0 μM) and 298.7 μg/ml (372.9 μM) after 48 and 72 h of treatment, respectively. Apoptosis was observed in cells incubated for 72 h with 250 μg/ml Zn-Mel (late apoptosis) and Co-Mel (early apoptosis) after double staining with AO/PI. Autophagosomes were detected in MDA-MB-231 cells after treatment for 48 h with 100 μg/ml meloxicam, Co-Mel and Ni-Mel, but not in the case of Zn-Mel and Cu-Mel.

Key words: Non-steroidal anti-inflammatory drugs, meloxicam, human triple negative breast cancer cells, cytotoxic activity, autophagy

Introduction

Non-steroidal anti-inflammatory drugs (NSAIDs) are a chemically diverse class of more than 20 medications frequently prescribed in the world because of their anti-inflammatory, analgesic and antipyretic properties. The biological activity of these agents is based on their ability to suppress the enzyme cyclooxygenase (COX) that

converts arachidonic acid to prostaglandine H2 (PGH2) - the key first step in synthesis of biologically active molecules with significant physiological importance such as prostanoids, prostacyclins and thromboxanes. There are two isoforms of COX: COX-1 – constitutively expressed in most tissues playing a crucial role in homeostasis; and COX-2 – induced by inflammation signals (e.g. IL-1β, TNF-α, lipopolysaccharide), mitogenic or oncogenic stimuli (e.g. phybole esters, oncogene v-src) [1].

According to their capacity to inhibit both of COX isoforms or predominantly the COX-2 enzyme, NSAIDs are divided into two groups – nonselective and selective NSAIDs, respectively. In recent years, there has been an increasing interest in the antitumor activity of NSAIDs. COX-2 expression has been documented in various solid tumors including colorectal cancer, cancers of the prostate, mammary gland, pancreatic and lung cancer, which makes this molecule an attractive target for selective antitumor treatment. The antitumor activity of NSAIDs can be explained also by COX-independent mechanisms of action [1, 8, 11, 16].

The so-called triple negative breast cancer (TNBC) is one of the major challenges in modern clinical oncology, as TNBC cells do not express receptors for estrogen, progesterone, and epidermal growth factor (Her2/Neu), and currently available (targeted) therapeutic strategies are limited [11].

It has been found in our previous investigations that selective non-steroidal anti-inflammatory agent meloxicam and its metal [Zn(II), Cu(II), Co(II), Ni(II)] complexes decrease viability and proliferation of human (cervical carcinoma, glioblatoma multiforme) and animal (chicken hepatoma, rat sarcoma) tumor cells [4, 6]. The aim of the present study was to evaluate the cytotoxic/antitumor effect of these compounds in cultured human triple negative breast cancer cells as well as their ability to induce autophagy.

Materials and Methods

Materials

Dulbecco's modified Eagle's medium (D-MEM) and fetal bovine serum (FBS) were purchased from Gibco-Invitrogen (UK). Dimethyl sulfoxide (DMSO) and trypsin were obtained from AppliChem (Germany); thiazolyl blue tetrazolium bromide (MTT) was from Sigma-Aldrich Chemie GmbH (Germany). The antibiotics (penicillin and streptomycin) were from Lonza (Belgium). Immunocytochemistry detection system (Novolink Polymer Detection System) was purchased from Leica Biosystems, UK and Rabbit polyclonal antibody to LC3B protein (abcam 48394) is manufactured by Abcam, UK. The Bio-Mount DPX Medium viscosity covering for microscope slides and nuclear dye (Mayer's Haematoxylin) were delivered from Biognost, Croatia. All other chemicals of the highest purity commercially available were purchased from local agents and distributors. All sterile plastic ware was from Orange Scientific (Belgium).

Compounds

The metal complexes with meloxicam were obtained following the method reported in a previous work [4]. All complexes were characterized by various physicochemical methods. Their molecular formulae have been established by correlating the elemental analysis data with the spectral data (infrared, ultraviolet-visible) and magnetic measurements. All these data were presented and discussed in one of our previous papers [4].

The complexes were denoted Zn-Mel (molecular formula: $[Zn(HMel)_2(H_2O)_2]$), Cu-Mel (molecular formula: $[Cu(HMel)_2(H_2O)_2]$), Co-Mel (molecular formula: $[Co(HMel)_2(H_2O)_2]$), Ni-Mel (molecular formula: $[Ni(HMel)_2(H_2O)_2]\cdot H_2O$).

Cell lines and cultivation

The permanent cell line MDA-MB-231 established from human triple negative breast cancer and proved to express COX-2 was used as a model system [7]. The cells were routinely grown as monolayer cultures in a D-MEM medium, supplemented with 5-10% fetal bovine serum, 100 U/ml penicillin and 100 mg/ml streptomycin. The cultures were maintained at 37°C in a humidified CO_2 incubator (Thermo Scientific, HEPA Class 100). For routine passages the cells were detached using a mixture of 0.05% trypsin – 0.02% ethylendiaminotetraacetic acid.

Cytotoxicity assay

The cells were seeded in 96-well flat-bottomed microplates for cell culturing at a concentration of 1 x 10^4 cells/well. At the 24th hour the culture medium was removed and changed with media containing different concentrations of the compounds examined (10-500 μg/ml). Each concentration was applied in 6 to 8 wells. The concentration of the solvent DMSO in the working solutions containing 500, 250, 200, 100, 50 and 10 μg/ml of the investigated compounds (meloxicam and its metal complexes) was calculated to be 2.00, 1.00, 0.80, 0.40, 0.20 and 0.04%, respectively. Samples of cells grown in non-modified medium (Culture medium control) and in medium containing the corresponding amount of DMSO (DMSO-control) served as controls. The effect of the compounds on cell viability and proliferation was evaluated using thiazolyl blue tetrazolium bromide (MTT) test after 48 h and 72 h of incubation as it was earlier described [6].

Double staining with acridine orange (AO) and propidium iodide (PI)

The cells were grown on sterile cover glasses in 6-well plates (3 – 3.5 x 10^5 cells / well) in the presence of the compound tested. Culture-medium controls as well as DMSO-controls were included in the experiments. After 72h of incubation, the coverslips were removed and washed with phosphate buffered saline (PBS) for 2 min. Equal volumes of fluorescent dyes containing AO (10 μg/mL in PBS) and PI (10 μg/mL in bidistilled water) were added to the cells [6]. Fresh stained cells were placed on a glass slide and examined under fluorescence microscope (Leica DM 5000B, Leica Microsystems, Germany) within 30 min before the fluorescent color started to fade.

Autophagy detection

The intracellular expression of the autophagy marker - the LC3B protein – was identified by immunocytochemical method using a rabbit polyclonal antibody.

The cells were seeded in 6-well plates on sterile cover glasses, 2 x 10^5 cells / well. After culturing for 24 hours, negative control (untreated cells), positive control (cells treated with known autophagy inducer - Rapamycin), as well as cells treated with studied compounds – meloxicam and its Zn(II), Cu(II), Co(II) and Ni(II) complexes were incubated for 48 h under the same conditions. The cover glasses were then washed PBS and fixed with 10% neutral buffered formalin (10 minutes), washed three times with PBS and processed by immunocytochemical detection protocol. It includes blocking endogenous peroxidase (5 minutes), protein block (5 minutes), incubation with primary antibody against LC3B protein (60 minutes), incubation with secondary antibody (30 minutes), incubation with enzyme-conjugating polymer (30 minutes). DAB (3,3′-diaminobenzidine) - 50μl plus 1 ml Substrate buffer (5 minutes) was used as the chromogen. After each step, the slides were washed three times with PBS. As a result of the antigen site, brown colored precipitates were obtained. After staining, the

preparations were washed several times with distilled water and counterstained with hematoxylin for 3 minutes, then dehydrated with an ascending series of alcohols and incorporated onto slides using Bio-Mount DPX synthetic resin. The procedure was carried out at room temperature and the slides were incubated in a humidified chamber.

The prepared immunocytochemical samples were microscoped with a Leica DM 5000B, Leica Microsystems, Germany and documented with a Leica DFC 420 C camera, Leica Suite 3.1.0 software.

Statistical analysis was performed using one-way analysis of variance (ANOVA) followed by Dunnett post-hoc test and Origin 6.1™.

Results and Discussion

Information about cytotoxic activity of meloxicam and its Zn(II), Cu(II), Co(II) and Ni(II) complexes in cultured MDA-MB-231 human triple negative breast cancer cells is obtained by MTT assay – the gold standard for such type of investigations. Concentration response curves based on experimental data are presented in **Fig. 1**. Cytotoxic concentration 50 (CC_{50}) that reduces the amount of viable cells by 50% as compared to the DMSO control has been determined (where possible) from these curves. Zn(II) complex of meloxicam (Zn-Mel) has been found to be the most pronounced cytotoxic agent among the compounds examined with CC_{50} calculated to be 376.5 μg/ml (470.0 μM) and 298.7 μg/ml (372.9 μM) after 48 and 72 h of treatment, respectively. In the case of meloxicam and its Cu(II), Co(II) and Ni(II) complexes the viability of the treated cells has been determined to be >50% as compared to the DMSO control.

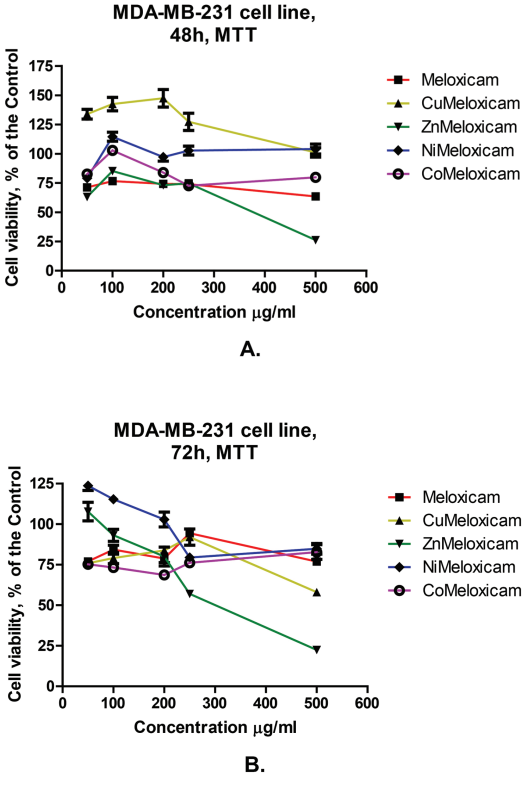

The experimental data obtained by double staining with acridine orange and propidium iodide are presented in **Fig. 2**. While untreated MDA-MB-231 cells (control) form dense and vital monolayer (**Fig. 2a**), MDA-MB-231 cells treated with meloxicam and its metal complexes show different (in type and degree) cytopathological changes. Cells treated with 500 μg / mL meloxicam for 72 hours have a 30% cell population reduction, as well as visible cellular and nuclear polymorphism (**Fig. 2b**). The cytoplasm is swollen and filled with vacuoles, the chromatin is roughly dispersed. Cells treated with 250 μg / mL Zn-Mel are non-vital, with signs of late apoptosis – highly reduced cytoplasm and apoptotic patches on the cell sur-

Fig. 1. Effect of meloxicam and its metal [Zn(II), Cu(II), Co(II), Ni(II)] complexes on viability / proliferation of MDA-MB-231 human triple negative breast cancer cells evaluated by MTT test after 48 (**A**) and 72 h (**B**) treatment periods.

face (**Fig. 2c**), while treated with 250 µg / mL Cu-Mel cells are non-vital, but their cytoplasm is highly inflated and the nuclei are stacked (**Fig. 2d**). Vital cells in early apoptosis were observed after 72 h treatment with 500 µg / mL Co-Mel (**Fig. 2e**). In the treated cells for 72 h with 500 µg / mL Ni-Mel, a pronounced cellular polymorphism - spindle-shaped vital cells were observed, along with rounded non-vital cells with vacuolated and strongly enlarged cytoplasmic volume (**Fig. 2f**).

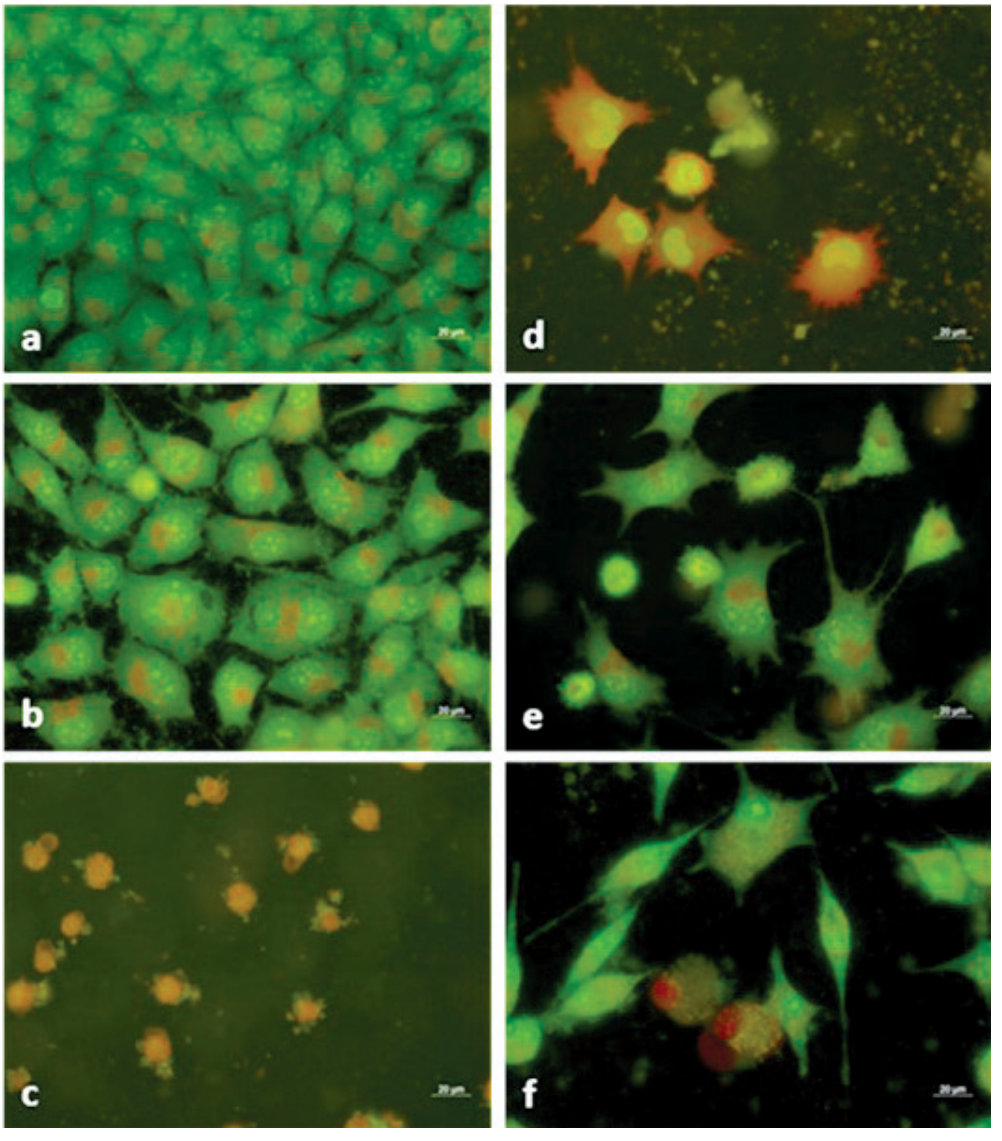

Fig. 2. Non-treated human triple negative breast cancer MDA-MB-231 cells (culture medium control – **a**) and MDA-MB-231 cells after 72 h treatment with 500 µg/mL meloxicam (**b**), 250 µg/mL Zn-Mel (**c**), 250 µg/mL Cu-Mel (**d**), 500 µg/mL Co-Mel (**e**), 500 µg/mL Ni-Mel (**f**). Double staining with acridine orange and propidium iodide. Bar = 20 µm (Leica DM 5000B, Leica Microsystems, Germany, 40x)

Immunocytochemical detection of autophagy in cell cultures and paraffin-embedded tissues has long been established as a reliable method for demonstrating this process [13]. The expression of autophagy marker - LC3B protein, was studied in MDA-MB-231 cells cultured in the presence of Rapamycin, known as autophagy inducer, as well as meloxicam and its metal [Zn(II), Cu(II), Co(II), Ni(II)] complexes. The results obtained are presented in **Fig. 3** and **4**. Untreated control MDA-MB-231 cells demonstrate diffuse cytoplasmic labeling of LC3B, the cells are monomorphic and formed a solid monolayer. In the presence of meloxicam (100 µg /ml, 48h) autophagosomes are observed only in individual cells. The cells treated with Cu-Mel and Zn-Mel (100 µg /ml, 48 h) show an intense cytoplasmic response without autophagosome formation with a well-pronounced cytotoxic effect. In cells cultured in

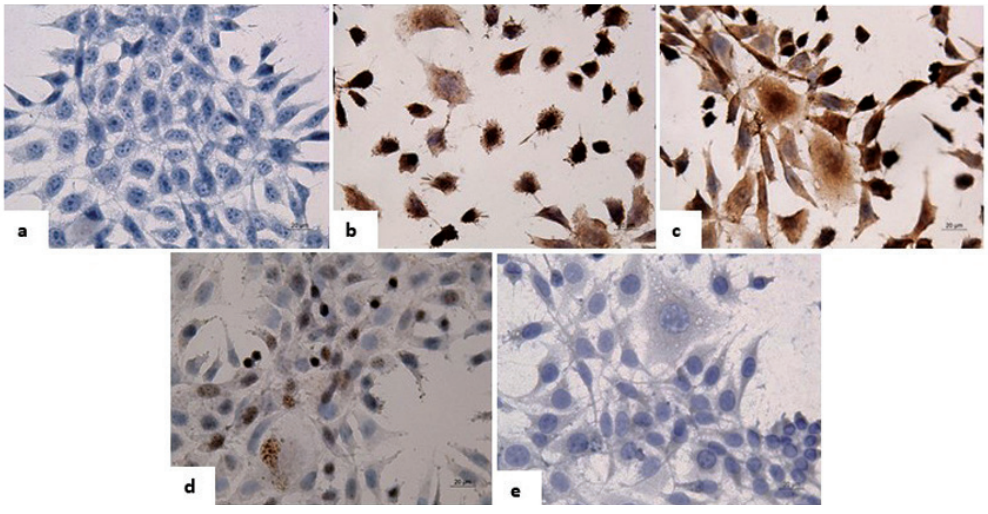

Fig. 3. Human triple negative breast cancer MDA-MB-231 cells. Negativ control – (**a**) and treated with an autophagy inducer Rapamycin applied at a concentyration of 500 nM for various time intervals: 3 hours (**b**), 6 hours (**c**), 24 hours (**d**) and 48hours (**e**). Immunocytochemical reaction with polyclonal antibody against LC3B protein, imaging with chromogen DAB (Diaminobenzidine), Leica DM 5000B, Leica Microsystems, Germany, x40.

the presence of Co-Mel and Ni-Mel (100 µg /ml, 48h) the cytoplasm is greatly increased in volume and a number of autophagosomes are visible near the nucleus, representing vesicular structures positively labeled by the LC3B protein. In the enlightenment of some of the autophagosomes, cellular organelles, which are integrated for the purpose of degradation, are seen (**Fig. 4**).

Because of their remarkable ability to treat pain, inflammation and fever, NSAIDs are among the most often prescribed medications all over the world. Increasing evidence suggests that these preparations also possess potential antitumor properties that are not surprising because of at least two reasons: i) chronic inflammation is well known to be involved in cancer development and progression by inducing proliferation, neoangiogenesis and metastasis as well as facilitating the escape from the immune system and drug resistance of tumor cells; ii) COX-2 is expressed in many types of cancer, including TNBC [1, 8, 11, 16]. Triple negative breast cancer affects younger

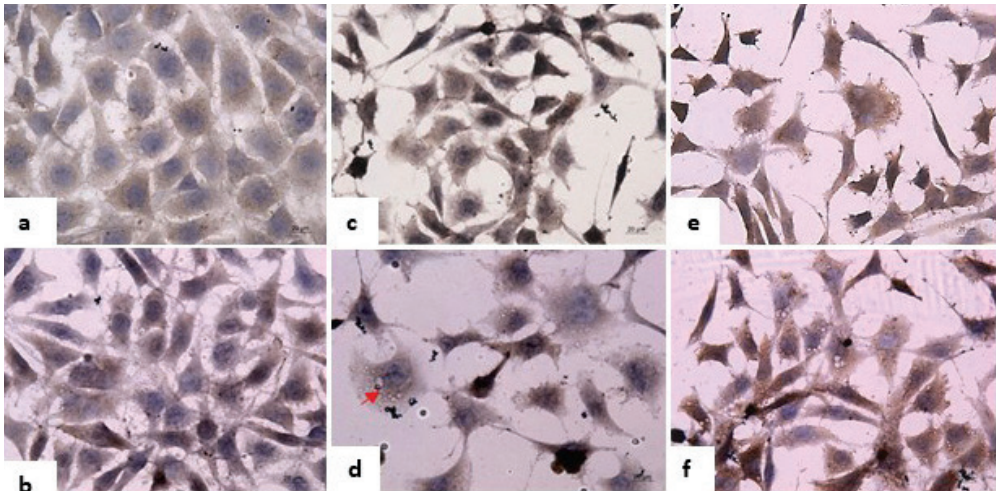

Fig. 4. Non-treated humah triple negative breast cancer MDA-MB-231 cells (culture medium control – **a**) and MDA-MB-231 cells after 48 h treatment with meloxicam **(b)** and its Cu(II) – **(c)**, Co(II) – **(d)**, Zn(II) – **(e)** and Ni(II) – **(f)** complexes at a concentration of 100 μg/ml for 48 hours. Immunocytochemical reaction with polyclonal antibody against LC3B protein, imaging with chromogen DAB (Diaminobenzidine), Leica DM 5000B, Leica Microsystems, Germany, x40. Autophagosomes with integrated cell organelles (CoMel, 100 μg/ml, arrow)

women, usually has an aggressive behavior and is associated with poor prognosis. The treatment of this tumor remains a problem in clinical oncology, as TNBC cells do not express estrogen and progesterone receptors and HER2/neu and therefore do not benefit from the available targeted therapies for breast cancer [11].

The selective non-steroidal anti-inflammatory agent meloxicam has been reported to exhibit antitumor activity alone or in combination with other therapeutic drugs and/or radiation using *in vitro* and *in vivo* experimental models of various human cancers such as osteosarcoma, ovarian cancer, hepatocellular carcinoma [2, 12, 14, 18]. Cardioprotective effect of meloxicam against doxorubicin has been demonstrated in a mouse model of breast cancer [9]. Meloxicam and its Zn(II), Cu(II), Co(II)) and Ni(II) complexes have been found to decrease viability and suppress 2D/3D growth of retrovirus-transformed avian hepatoma (expressing v-myc gene) and rat sarcoma (expressing v-src gene) cells as well as in cell lines established from human cervical carcinoma and glioblastoma multiforme [4, 6]. In this study we report for the first time data about cytotoxic activity of these compounds in MDA-MB-231 human triple negative breast cancer cells and their capacity to induce autophagy. The results obtained indicate that after exposure for 48 hours, the complexes of Co(II) and Ni(II) with meloxicam exhibit pro-autophagic activity in MDA-MB-231 cells, while the cell viability determined by the MTT test is relatively high (≥ 73% for Ni(II)Mel and ≥56% in the case of Co(II) complex with meloxicam), even when the compounds were applied at the maximal examined concentration – 500 μg / ml). Autophagy is not detected in cells incubated in the presence of the compound with the most pronounced cytotoxic activity – Zn-Mel.

The antitumor activity of meloxicam has been associated with its ability to affect apoptotic (i.e. by upregulating Bak and Fas-L, and downregulating survivin and Mcl- 1) and autophagic (PI3K/Akt/mTOR, MAPK/ERK1/2, P53/DRAM, etc.) pathways through COX-dependent and COX-independents mechanisms [5, 15, 18]. It

has been demonstrated that inhibition of autophagy can help to overcome the resistance to meloxicam-induced apoptosis in hepatocellular carcinoma cells [5]. There are data indicating that climacostol, natural compound produced by the ciliated protozoan Climacostomum virens induces apoptosis and impairs autophagy in human and murine melanoma and glioma cells [17].

Autophagy is an evolutionary conservative catabolic process that contributes to maintaining homeostasis in the cell, breaking down damaged and unnecessary macromolecules and organelles, as well as pathogens. Dysregulated autophagy is implicated in various pathological conditions including neoplastic diseases. That is why targeting autophagy is an attractive strategy for cancer treatment. At the same time this approach is very challenging because of the controversial role of autophagy in carcinogenesis – initially suppressing it but subsequently stimulating tumor progression. On one hand, autophagy is essential for a wide range of key biological processes including normal functioning of the immune system and stress response and can inhibit tumorigenesis and progression, therefore induction of autophagy may decrease viability, proliferation, invasiveness and dissemination of tumor cells. On the other hand, the cytoprotective function of autophagy may facilitate the survival and drug resistance of tumor cells [3, 10]. The "situation" becomes more complicated because of interactions between autophagy and apoptosis that are found to share many signaling molecules and pathways but their cross talk is not fully clarified yet.

Conclusion

The anticancer potential of NSAIDs is very attractive because these medications have been used for many years in clinical practice and their pharmacokinetics and pharmacodynamics as well as safety and side effects profiles are well understood. In this study we present for the first time data about cytotoxic activity of selective NSAID meloxicam and its metal [Zn(II), Cu(II), Co(II), Ni(II)] complexes as well as their ability to induce autophagy in MDA-MB-231 cells established from human triple negative breast cancer – an oncological disease whose successful treatment remains a challenge for modern biomedicine. The obtained results suggest that meloxicam and its Zn(II), Cu(II), Co(II) and Ni(II) can be recognized as promising candidates for further evaluation of their potential antitumor, including anti TNBC, properties. The complex role of autophagy in carcinogenesis as well as the relationship between apoptosis and autophagy indicate the need to investigate both the ability to induce apoptosis and autophagy of the potential new antitumor agents.

Acknowledgements: Supported by National Science Fund, Ministry of Education and Science, Bulgaria (Grant №ДКОСТ 01-19 from 08.12.2017 and Grant № ДКОСТ 01-16 from 17.08.2017) and a bilateral project between Bulgarian Academy of Sciences and Romanian Academy.

References

1. **Alexandrova, R., P. Beykov, O. Alexandrov, G. Marinescu, D. C. Culita, C. Podlipnik, C. O. Ekeh.** Nonsteroidal anti-inflammatory drugs – what do we (not) know about them. – *Merit Research Journal of Medicine and Medical Sciences*, **7**(10), 2019, 412-421.
2. **Ayakawa, S., Y. Shibamoto, C. Sugie, M. Ito, H. Ogino, N. Tomita, M. Kumagai, H. Murakami, H. Sawa.** Antitumor effects of a cyclooxygenase-2 inhibitor, meloxicam, alone and in combination with radiation and/or 5-fluorouracil in cultured tumor cells. – *Mol. Med. Rep.,* **2**(4), 2009, 621-625.

3. **Bishop, E., T.D. Bradshaw.** Autophagy modulation: a prudent approach in cancer treatment? – *Cancer Chemother. Pharmacol.,* **82**(6), 2018, 913-922.
4. **Culita, D. C., R. Alexandrova, L. Dyakova, G. Marinescu, L. Patron, R. Kalfin, M. Alexandrov.** Evaluation of Cytotoxic and Antiproliferative Activity of Co(II), Ni(II), Cu(II) and Zn(II) Complexes with Meloxicam on Virus – Transformed Tumor Cells. – *Revista de Chimie,* **63**(4), 2012, 384-389.
5. **Dong, X., R. Li, P. Xiu, X. Dong, Z. Xu, B. Zhai, F. Liu, H. Jiang, X. Sun, J. Li, H. Qiao.** Meloxicam executes its antitumor effects against hepatocellular carcinoma in COX-2- dependent and -independent pathways. – *PLoS One,* **9**(3), 2014, e92864.
6. **Dyakova, L., D. C. Culita, T. Zhivkova, M. Georgieva, R. Kalfin, G. Miloshev, M. Alexandrov, G. Marinescu, L. Patron, R. Alexandrova.** 3d Metal complexes with meloxicam as terapeutic agents in fight against human glioblastoma multiforme and cervical carcinoma. – *Biotechnology & Biotechnological Equipment*, **29** (6), 2015, 1190-1200.
7. **Half, E., X. M. Tang, K. Gwyn, A. Sahin, K. Wathen, F. A. Sinicrope.** Cyclooxygenase-2 expression in human breast cancers and adjacent ductal carcinoma in situ. – Cancer Res., **62**(6), 2002, 1676-1681.
8. **Hashemi Goradel, N., M. Najafi, E. Salehi, B. Farhood, K. Mortezaee**. Cyclooxygenase-2 in cancer: A review. – *J. Cell Physiol*., **234**(5), 2019, 5683-5699.
9. **Hassan, M. H., H. A. El-Beshbishy, H. Aly, S. M. Attia, S. A. Bahashwan, M. M. Ghobara.** Modulatory effects of meloxicam on cardiotoxicity and antitumor activity of doxorubicin in mice. – *Cancer Chemother. Pharmacol.,* **74**(3), 2014, 559-569.
10. **Li, X., H. L. Xu, Y. X. Liu, N. An, S. Zhao, J. K. Bao.** Autophagy modulation as a target for anticancer drug discovery. – *Acta Pharmacol. Sin.,* **34**(5), 2013, 612-624.
11. **Mosalpuria, K., C. Hall, S. Krishnamurthy, A. Lodhi, D. M. Hallman, M. S. Baraniuk, A. Bhattacharyya, A. Lucci.** Cyclooxygenase-2 expression in non-metastatic triple-negative breast cancer patients. – *Mol. Clin. Oncol.,* **2**(5), 2014, 845-850.
12. **Naruse, T., Y. Nishida, K. Hosono, N. Ishiguro.** Meloxicam inhibits osteosarcoma growth, invasiveness and metastasis by COX-2-dependent and independent routes. – *Carcinogenesis,* **27**(3), 2006, 584-592.
13. **Ozturk, M., O. D. Ozsoylemez, F. K. Dagistanli.** The Detection Techniques for Autophagy-Associated Cell Death-Related Genes and Proteins: Gene Expression Assay and Immunohistochemistry. – *Methods Mol. Biol*., **1854,** 2019, 119-130.
14. **Xin, B., Y. Yokoyama, T. Shigeto, M. Futagami, H. Mizunuma.** Inhibitory effect of meloxicam, a selective cyclooxygenase-2 inhibitor, and ciglitazone, a peroxisome proliferator-activated receptor gamma ligand, on the growth of human ovarian cancers. – *Cancer,* **110**(4), 2007, 791-800.
15. **Yu, C., W. B. Li, J. B. Liu, J. W. Lu, J. F. Feng**. Autophagy: novel applications of nonsteroidal anti-inflammatory drugs for primary cancer. – *Cancer Med*., **7**(2), 2018, 471-484.
16. **Zappavigna, S., A. M. Cossu, A. Grimaldi, M. Bocchetti, G. A. Ferraro, G. F. Nicoletti, R. Filosa, M. Caraglia**. Anti-Inflammatory Drugs as Anticancer Agents. – *Int. J. Mol. Sci*., **21**(7), 2020. pii: E2605. doi: 10.3390/ijms21072605.
17. **Zecchini, S., F. Proietti Serafini, E. Catalani, M. Giovarelli, M. Coazzoli, I. Di Renzo, C. De Palma, C. Perrotta, E. Clementi, F. Buonanno, C. Ortenzi, E. Marcantoni, A. R. Taddei, S. Picchietti, A. M. Fausto, D. Cervia.** Dysfunctional autophagy induced by the pro-apoptotic natural compound climacostol in tumour cells. – *Cell Death Dis.,* **10**, 2019, 10.
18. **Zhong, J., P. Xiu, X. Dong, F. Wang, H. Wei, X. Wang, Z. Xu, F. Liu, T. Li, Y. Wang, J. Li.** Meloxicam combined with sorafenib synergistically inhibits tumor growth of human hepatocellular carcinoma cells via ER stress-related apoptosis. – *Oncol. Rep.,* **34**(4), 2015, 2142-2150.

Institute of Experimental Morphology, Pathology and Anthropology with Museum
Bulgarian Anatomical Society

Acta morphologica et anthropologica, 27 (1-2)
Sofia ● 2020

Gastrointestinal and Pancreatic Involvement in Mediterranean Spotted Fever Fatal Cases

Ivan Baltadzhiev[1], Zaprian Zaprianov[2], Atanas Baltadjiev[3]*

[1] Department of Infectious Diseases, Parasitology and Tropical Medicine, Faculty of Medicine, Medical University and Clinic of Infectious Disease, University hospital St.George, Plovdiv, Bulgaria;
[2] Department of General and Clinical Pathology, Faculty of Medicine, Medical University and Clinic of General and Clinical Pathology, University hospital St. George, Plovdiv, Bulgaria;
[3] Department of Anatomy, Histology and Embryology, Faculty of Medicine, Medical University, Plovdiv, Bulgaria

* Corresponding author e-mail: dr_atanas@abv.bg

Mediterranean spotted fever (MSF) is a rickettsial disease, caused by *Ricketsia conorii*. It is a tick-borne infection endemic for several regions in Bulgaria along the Maritza River and the Black Sea coast. The characteristic features of MSF include a skin eschar (tache noite) at the site of tick bite, fever, flu-like symptoms and maculopapular rash spread on the body and extremities, not sparing the palms and feet. MSF has usually mild or moderate course, however severe, so-called "malignant" forms have been observed with involvement of vital organ systems and lethal outcome. We present two rare and fatal complications of MSF – gastrointestinal bleeding and pancreatic steatonecrosis. In both cases the organ involvement had histomorphological confirmation at autopsy. MSF diagnosis was confirmed serologically by an indirect immunofluorescent assay. Awareness of the possibility of gastrointestinal bleeding and necrotizing pancreatitis in MSF patients is essential to professionals for conducting a convenient behaviour and help.

Key words: Mediterranean spotted fever, fatal complications, gastrointestinal bleeding, necrotizing pancreatitis, histomorphology

Introduction

Mediterranean spotted fever (MSF) is caused by *Ricketsia conorii*. It is a tick-borne rickettsial infection endemic for several regions in Bulgaria along the Maritza River and the Black Sea coast. The life cycle of rickettsiae involves insect vector – *Ripicephalus sanguineus*, and mammal reservoirs – mainly domestic and stray dogs. Humans are accidental hosts. The main clinical signs and symptoms of MSF include a skin eschar (tache noite) at the site of tick bite, fever, flu-like symptoms and maculopapular rash spread on the body and extremities, not sparing the palms and feet. MSF has usually mild or moderate course and had long been considered a benign disease, however the so-called "malignant" forms have been observed with involvement of vital organ systems and lethal outcome [1, 8]. A hallmark of MSF pathology is the rickettsial vasculitis.

Gastrointestinal system is involved in the disseminated rickettsiosis with perivascular lymphohistiocytic infiltrates in tela submucosa and tunica muscularis of the organs' wall. Submucosal vasculitis can lead to mucosal erosions, ulcers, petechiae or hemorrhage. The pancreatic gland involvement in rickettsial vasculitis ranges from catarrhal to hemorrhagic-necrotizing pancreatitis [2, 4]. The mentioned MSF complications are almost unknown among patients and health professionals especially in non-endemic regions of Bulgaria similarly the imported rickettsioses in non-endemic countries. The purpose of this communication is to make the medical community aware of the possibility of gastrointestinal hemorrhage and concomitant necrotizing pancreatitis in the most severe, often fatal forms of MSF.

Patients and Methods

We present two rare and fatal complications of Mediterranean spotted fever – gastrointestinal bleeding and acute necrotizing pancreatitis. The organ involvement had histomorphological confirmation at autopsy. We conducted a histopathological study including complete post-mortem examinations of the specimens of liver, lung, kidneys, stomach, pancreas and brain. The samples were fixed in 4% neutral buffered solution of formaldehyde, embedded in paraffin, sectioned at 5 μm thicknesses, and processed by staining with hematoxylin/eosin for evaluation of histopathology. The MSF diagnosis was confirmed by an indirect fluorescent antibody assay, with IgG ≥128 and/or IgM ≥64 being considered indicative of acute infection.

Ethical consideration: Informed autopsy consent was signed by the relatives of the deceased patient. The case we described is completely anonymous and the histological examination of autopsy samples did not reveal its identity.

Results

In our previous research we investigated 55 patients with a very severe, so called "malignant" form of MSF named "MSF form with multiple organ involvement". Gastrointestinal system was involved in 8 of these patients and 6 of them were lethal [1]. Here we present the clinical characteristic and histomorphological data of one of the deceased patients with involvement of the digestive tract (gastrointestinal system and pancreatic gland) in the rickettsial infection.

Case description: A 61-year-old woman, with a previous history of long-standing diabetes mellitus type 2, had a seven-day history of fever (39.5˚C), chills, headache, vomiting and myalgia. She had contacts with her pet dog. On day 4 after the onset of symptoms, a rash appeared on her body and limbs. Within two days, her condition deteriorated severely. She was admitted to the hospital intensive care facility in the state of shock – in circulatory collapse, sweating, with thready rapid pulse, pale skin and mucous membranes. She was confused and hypoactive. There was an abundant maculopapular and hemorrhagic rash on the body and limbs, hands and feet, and an eschar (tache noire) under the left scapula. Melena and hematemesis appeared on the second day of admission. Erosive gastritis was diagnosed on upper endoscopy. Ulcers were not detected. Despite the complex resuscitation efforts exitus letalis occurred 34 h after admission. The serology was positive for *Rickettsia conorii*.

Autopsy protocol: Generalized thrombo-vasculitis with perivascular lympho-histiocytic infiltration; multiple petechial hemorrhages on all mucous and serous

membranes; three acute ulcers in the stomach fundus with massive bleeding in the digestive tract; acute post-hemorrhage anemia; acute pancreatic steatonecrosis; focal interstitial nephritis with thrombotic vasculitis of the renal microcirculation; brain edema and pulmonary edema.

Microphotographs of histopathological changes in the gastric mucosa serve as illustrations of the presented case (**Fig. 1; Fig. 2**). At the same time, we present microphotographs of catarrhal gastritis with inflammatory perivascular infiltrates in a patient who died from other MSF complications, thus highlighting the different extent of the gastric mucosa involvement in the rickettsial vasculitis. (**Fig. 3; Fig. 4**).

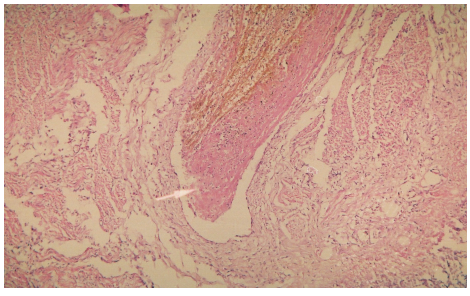

Fig. 1. Bottom of an acute ulcer. Gastric wall mixed thrombus in an arteriole (arrow). (Hematoxylin-Eosin, ×200)

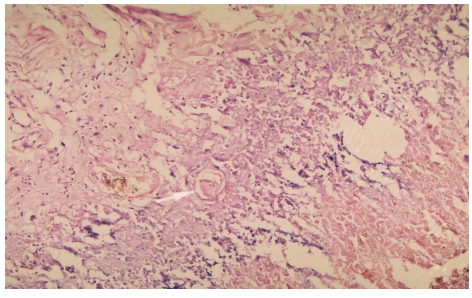

Fig. 2. Gastric mucosa with hemorrhage and necrosis; hyaline thrombus at the base (arrow). (Hematoxylin-Eosin, ×200)

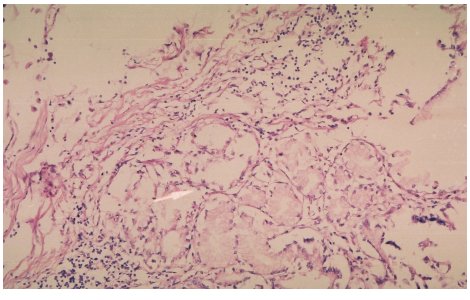

Fig. 3. Gastric wall. Relatively preserved gastric mucosa. Catarrhal gastritis with perivascular round cell infiltrates (arrow)
(Hematoxylin-Eosin, ×200)

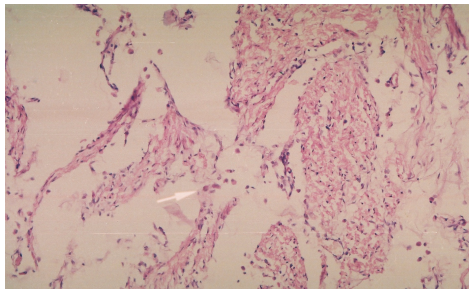

Fig. 4. Gastric wall with edema and inflammatory infiltrate of lymphocytes and plasma cells (arrow)
(Hematoxylin-Eosin, ×200)

Pancreatic involvement in the MSF rickettsial vasculitis is not a common event. Our previous investigation showed that among 55 patients with malignant MSF cases the pancreatic gland was involved in 5 patients and 4 of them died [1]. In an attempt to demonstrate the different amplitude of pancreatic involvement in the rickettsial microvascular injury we present a microphotograph of the pancreatic gland preserved structure in a patient who died from other MSF complications (**Fig. 5**) and a microphotograph of pancreas lytic steatonecrosis in the patient we described above (**Fig. 6**).

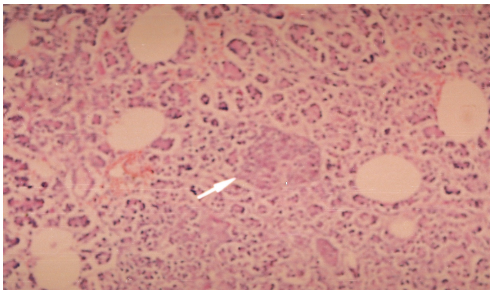

Fig. 5. Pancreas. Centrally located Langerhans island (arrow); around – exocrine part of the gland. (Hematoxylin-Eosin, ×200)

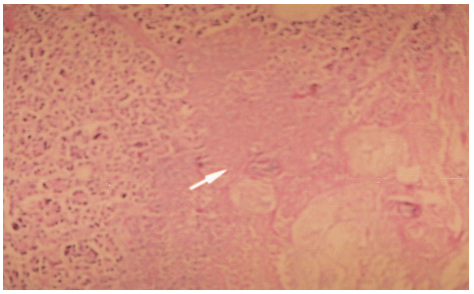

Fig 6. Pancreas Lytic necrosis (steatonecrosis) (arrow)
(Hematoxylin-Eosin, ×200)

Discussion

The most likely pathophysiological mechanisms of the organ involvement in rickettsioses seem to be the increased vascular permeability, caused by numerous closely spaced foci of endothelial cell damages in the microcirculatory system [12]. The major observed pathological lesions in rickettsial diseases consist in vascular and perivascular mononuclear cell-rich inflammatory foci with or without thrombosis and necrotic hemorrhages [4].

Mediterranean spotted fever is a rickettsial disease that affects multiple organs due to the widespread microvascular damage. Submucosal and muscularis perivascular lymphohistiocytic infiltrates and vasculitis are the most frequent findings in the stomach. Mucosa is involved only secondary in the underlying vascular lesions resulting in mucosal petechiae, erosions, ulcers and hemorrhage. Hemorrhages in the gastrointestinal tract are severe, although uncommon complication of vasculitic changes in malignant forms of MSF. In a study by Ruiz-Beltrán et al. bleeding appeared as a consequence of multiple acute superficial erosions of the gastric mucosa. The histological substrate for these lesions was identified as a lymphohistiocytic vasculitic process affecting the small vessels of the gastric wall [10]. Erosions and several ulcers in the gastric wall of MSF patients have been reported by other authors as well [6]. Vascular inflammation, capillaritis, or lymphohistiocytic vasculitis like those in a whole gastrointestinal tract with or without vascular dilation and endothelial cell swelling was identified in esophageal and intestinal lesions, though infrequent and vascular injuries were moderate only [4]. Similarly, in some MSF fatal cases because of crucial organ involvement, we found moderately expressed scattered lymphohistiocytic perivascular infiltrates in the gastric mucosa referred as a catarrhal gastritis thus highlighting the different range of gastric mucosa involvement in the rickettsial vasculitis.

Acute necrotizing pancreatitis is characterized by necrosis in and around the pancreas. It is subdivided anatomically into parenchymal, peripancreatic, and combined subtypes, depending on whether it involves pancreatic parenchyma only, or peripancreatic tissues with the peripancreatic fat, or both [3, 11]. Pancreatic involvement in MSF appears to be less frequent than gastrointestinal involvement and has been rarely reported in literature [5, 9, 12]. In this report we present a case of gastrointestinal bleeding with concomitant pancreatic steatonecrosis considering both lesions related to a common cause – rickettsial microvascular damage. However, we have also described hemorrhagic-necrotizing pancreatitis and pancreatic fat necrosis in MSF patients

without gastrointestinal hemorrhage [2], suggesting that the observed phenomena are not necessarily related and interdependent.

Existing opinions suggest that although the pancreatic interlobular vasculature is a frequent site of perivascular lymphohistiocytic infiltrates, the lesions in MSF are small and scattered; vasculitis with endothelial cell damage is much less frequent and its contribution to the clinical picture is uncertain [4]. According to some reports, however, rickettsial vascular injury of the pancreas occurred frequently, although the parenchymal lesions might not be severe enough to qualify as pancreatitis [7]. In one of the cases reported in the literature, the pancreatic involvement was mild, with a prompt response to antibiotic therapy [5]. Other report, however, announced a serious multiorgan involvement, including the pancreas in South African tick bite fever (*R.conorii)* patients with 2 fatal cases. Immunofluorescent organisms of *R.conorii* were demonstrated in vascular endothelium of pancreatic septa [12].

Conclusion

Awareness of the possibility of gastrointestinal bleeding and necrotizing pancreatitis in MSF patients is essential to the critical care of professionals for conducting prompt practical management and providing an appropriate treatment.

Acknowledgements: The authors thank Prof. N. Popivanova for the valuable advice on the overall presentation of the disease and its complications.

References

1. **Baltadzhiev, I., N. Popivanova, Z. Zaprianov**. Malignant forms of Mediterranean spotted fever: risk factors for fatal outcomes. – *Braz. J. Infect Dis*., **20**(5), 2016, 511-512.
2. **Baltadzhiev, I., N. Popivanova, Y. Stoilova, A. Kevorkian**. Mediterranean spotted fever – classification by disease course and criteria for determining the disease severity. – *Folia Med.*, **54**(4), 2012, 53-61.
3. **Banks, P., T. Bollen, C. Dervenis**. Classification of acute pancreatitis 2012: revision of the Atlanta classification and definitions by international consensus. – *Gut,* **62**(1), 2013, 102-111.
4. **Procop, G., P. Bobbi**. Rickettsia, Esherichia and Anaplasma infections. In: *Pathology of infectious diseases a volume in the series: foundations in diagnostic pathology.* Elsevier, 1st Edition, Chapter 19, 2014, 393.
5. **Mansueto, S., R. Di Leo, G. Tringali**. Unusual abdominal involvement in rickettsial diseases. – *JAMA*, **249**, 1983, 1709-1710.
6. **Pereira, M. J., J. M. Romãozinho, C. Sofia.** Mediterranean spotted fever with involvement of the gastrointestinal tract. – *BMJ Case Rep.,* 2013, doi: 10.1136/bcr-2013-200186
7. **Randall, M. B., D. H. Walker.** Rocky Mountain spotted fever: gastrointestinal and pancreatic lesions and rickettsial infection. – *Arch. Pathol. Lab. Med.*, **108**, 1984, 963–967.
8. **Raoult, D., H. Gallais, A. Ottomani, J. P. Resch, D. Tichadou, P. De Micco, P. Casanova.** Malignant form of Mediterranean boutonneuse fever. 6 cases. – *Presse Med.,* **12**, 1983, 2375-2378.
9. **Rombola, F.** Mediterranean spotted fever presenting as an acute pancreatitis. – *Acta Gastroenterol. Belg.*, **74**(1), 2011, 91-92.
10. **Ruiz-Beltrán, R., J. L. Herrero-Herrero, D. H. Walker.** Mechanisms of upper gastrointestinal hemorrhage in Mediterranean spotted fever. – *Trop. Geogr. Med.,* **42***,* 1990, 78–82.
11. **Shyu, J. Y., N. I. Sainani, V. A. Sahni, J. F. Chick, N. R. Chauhan, D. L. Conwell, T.E. Clancy, P.A. Banks, S.G. Silverman.** Necrotizing pancreatitis: diagnosis, imaging, and intervention. – *Radiographics,* **34**(5), 2014, 1218-1239.
12. **Walker, D. H., J. H. Gear.** Correlation of the distribution of Rickettsia conorii, microscopic lesions, and clinical features in South African tick bite fever. – *Am. J. Trop. Med. Hyg.*, **34,** 1985, 361-371.

Institute of Experimental Morphology, Pathology and Anthropology with Museum
Bulgarian Anatomical Society

Acta morphologica et anthropologica, 27 (1-2)
Sofia ● 2020

Review Articles

Effects of Gut Microbiome on the Nervous and Immune Systems – a Novel Concept of Gut-Brain Axis in Multiple Sclerosis

Stephan Engibarov[1], Rumyana Eneva[1], Iskra Sainova[2], Desislava Drenska[3], Vera Kolyovska[2], Dimitar Maslarov[4]*

[1] The "Stephan Angeloff" Institute of Microbiology, Bulgarian Academy of Sciences, Sofia, Bulgaria
[2] Institute of Experimental Morphology, Pathology and Anthropology with Museum, Bulgarian Academy of Sciences, Sofia, Bulgaria
[3] Neurology Clinic, University First MHAT-Sofia, "St. John Krastitel", Sofia, Bulgaria
[4] Neurology Clinic University First MHAT-Sofia, "St. John Krastitel", Medical University of Sofia, Medical College "Y. Filaretova", Sofia, Bulgaria

* Corresponding author e-mail: verakol@abv.bg

The gut and brain form the gut-brain axis through bidirectional nervous, endocrine, and immune communications. Disorders in the composition and quantity of gut microorganisms can eventually affect both enteric nervous system and central nervous system (CNS), thereby confirming the possible existence of a microbiota-gut-brain axis. Due to the intricate interactions between the gut and the brain, gut symbiotic microorganisms are closely associated with various CNS diseases, such as Parkinson's disease, Alzheimer's disease, chronic fatigue syndrome and irritable bowel syndrome, schizophrenia, autism and multiple sclerosis (MS). Alterations in gut microbiota composition in MS patients under long-term drug treatment have been established. Increased levels of *Bacteroidaceae*, *Faecalibacterium*, *Ruminococcus*, *Lactobacillaceae*, *Clostridium*, and other members of the class *Clostridiales* have been assessed compared to untreated MS individuals. Our understanding is that neuroinflammation might be initiated by gastrointestinal tract (GIT) infections in which the GIT immune system is implicated.

Key words: microbiome-gut-brain axis, neuroinflammation, nervous system diseases, multiple sclerosis

Introduction

The importance of the gut microbiome for the pathogenesis of multiple sclerosis (MS) has been established, although the underlying signaling mechanisms of this relationship have not been studied yet. Many authors suggest that serotonin, a microbial modulated

neurotransmitter (NT) could be a potent candidate for mediator of the bowel and brain in demyelinating disorders [29]. It has been proved that serotonin levels in the gut are controlled by the microbiome, by both secretion and regulation of metabolites. In addition, gut microbiome is supposed to influence the formation of the serotonergic system in the brain. More frequent spread of depression and euphoria is observed in patients with MS. Changes in the serotonergic system have been suggested to be related with the directly altered MS expression of serotonin carriers in the central nervous system (CNS). Serotonin modulating drugs exert indirect beneficial effects in the course of the disease. The role of other microbiome-modulated NTs as γ-aminobutyric acid (GABA) and dopamine in MS has also been discussed. New direction for future research aimed at linking microbiome-regulated NTs to demyelinating disorders is needed [29].

Multiple sclerosis. First described by the French Professor Jean-Martin Charcot in 1868, MS has recently been determined as the primary demyelinating disease with significant loss of myelin and relatively preserved neurons and axons. MS is the most common autoimmune inflammatory neurodegenerative disease of the CNS, characterized by demyelination, neuroaxonal loss and a heterogeneous clinical course [10]. Neuronal and axonal damages have been shown to go along with the demyelination. A person with MS can have almost any neurological symptom, with autonomic, visual, motor, and sensory problems being the most common [8]. In 85% of the patients the disorder is in relapsing-remitting (RRMS) form [15].

There are various methods of treating MS by administering drugs depending on the form and phase of the disease. If the diagnosis and initiation of neuroprotective therapy are timely, the effectiveness of the treatment is more successful. RRMS treatment is expensive and long-lasting, but it is effective in large number of young patients [40]. According to recent studies over 60% of MS patients use complementary and alternative medicine (diet, gymnastics, bee sting in acupuncture points) as helping methods to the conventional treatments. The future of MS treatment should be aimed at combining anti-inflammatory agent and such with a neuroprotective effects. The goal is to prevent demyelination and to reduce axonal loss [25]. It is especially important for young MS patients to lead a normal lifestyle, to work, to have families and children. Any supportive therapy that improves quality of life is of great importance.

In recent years understanding of treatment goals has been changed. The concept of "no evidence of disease activity" (NEDA) has become attractive, not only in the assessment of clinical trial data, but also as a treatment target in clinical practice. This concept focuses on clinical and Magnetic Resonance Imaging (MRI) measures of disease activity. It also reflects patient-reported outcomes - progression of symptoms, adverse effects of treatment, and inability to tolerate injections, which may lead to a switch in treatments. The increasing number of highly active treatments becoming available raises the possibility of treatment election when necessary. That is why truly achieving NEDA will require the development of agents that directly target mechanisms of disease progression. Furthermore, the next revolution in MS therapeutics is remyelination. Such strategies will likely warrant rationally designed combination therapy approaches to both prevent further disease activity and push central nervous system repair [15].

Multiple human epidemiological studies have revealed the effects of environmental factors on the prevalence of MS and demonstrated that viral infections, lack of sun exposure, vitamin D and vitamin A deficiency, active or passive smoking, season of birth, obesity, dietary habits (especially high levels of salt and fat), stress and the intestinal microflora play a significant role in the initiation of the disease. Epstein–Barr virus (EBV) is a widely recognized risk factor. A seroepidemiological study of MS found that nearly 100% of the patients were infected with EBV. If EBV infection occurs in late childhood, it is considered the largest risk factor for the development of MS.

There is a strong EBV-specific CD8+ response in the blood during the onset of MS; the intensity of the response decreases during the course of the illness [1].

Nowdays, it is accepted that MS is a CD4+ T helper (Th) 1-mediated autoimmune disease; however, CD8+ T cells may be involved in the pathogenesis as they are the predominant lymphocyte found in MS lesions. The cells that form myelin in the CNS (oligodendrocytes) are thought to be the main target for attack in MS, and the inflammatory demyelinating lesions characteristic of MS can occur in the optic nerve, brainstem, spinal cord and periventricular white matter [12, 15]. MS has also been suggested to arise from a negative interaction between genetic and environmental factors. A large number of genes promote autoimmune response against brain cells [8, 40]. New experimental and clinical studies indicate that autoimmune attacks are triggered by interaction between brain immune cells and gut microbiota. The pathophysiology of MS involves several aspects of abnormalities: redox, inflammatory/autoimmune, vascular, neuroendocrine and neurodegenerative [15].

Life with MS. Patients with MS are often best cared for in multidisciplinary approach [23, 24]. The diet has been associated with improvements in the majority of the population in terms of mood, fatigue and cognitive impairment - all issues that factor significantly in MS. Such results, particularly concerning mood modification, are reported in a study on a Mediterranean-style diet [12].

Microbiome. Commensal and symbiotic microbes densely populate the human body, the majority of which being bacteria. These microbes occupy different habitats such as gut, skin, vagina and oral cavity. The types and abundance of microbes differ not only in various organs, but also in the different individuals. The genome of these microorganisms and their ecosystems constitute the microbiome. Factors such as diet, environment, host genetics and way of birth may be factors influencing the wide microbial diversity [11]. Diet and gut microbiota composition are probably related to the leaky gut phenomenon [1, 20].

Probiotics and Prebiotics. About 100 000 billion bacteria are present in the human intestines [21, 32]. The beneficial and harmful bacteria in the gut are in balance.

Probiotics are living bacteria in the group of good ones – they maintain the electrolyte balance in the body and the good microflora in the gut [21, 32, 33].

Prebiotics are indigestible dietary fibers that stimulate the growth of good bacteria inhabiting the colon. They pass through the gastrointestinal tract unchanged and stimulate the growth and development of beneficial bacteria in the gut. Prebiotics are resistant to heat amplitudes and the increased stomach acidity, i.e. they are the perfect food for the existence and growth of beneficial gut microorganisms [32]. Probiotics and prebiotics play key role in prevention and neutralization of the harmfull effects of many pathogenic bacteria as *Helicobacter pylory* and *Escherichia coli*.

Gut-brain axis. Hippocrates has wisely remarked: “all diseases begin in the gut” and “death sits in the bowel”, thereby creating the hypothesis that gut is responsible for many disorders including neurodegenerative diseases [27]. Nowadays, the main concept of the gut-brain axis represents a major shift of our understanding about the brain health [30]. Gastrointestinal tract (GIT) infections could be initiated by neuroinflammation in which the GIT immune system is implicated.

Microbiome is shaped by host factors such as genetics and nutrients but in turn is able to influence host biology in health and disease. Gut microbiome is probably plaing a crucial role in the bidirectional gut-brain axis that integrates both gut and CNS activities, and thus the concept of microbiome-gut-brain axis has emerged. Many studies reveal how diverse forms of neuro-immune and neuro-psychiatric disorders are correlated with or modulated by variations of microbiome, microbiota-derived products

as well as antibiotics and probiotics. The microbiome probably poises the peripheral immune homeostasis and predisposes the host susceptibility to CNS autoimmune diseases such as MS [39].

Larger studies are necessary to investigate the changes within the gut microbiome and MS, in order to find potential disease biomarkers and therapies. These findings might contribute to development of new therapeutic strategies that modulate gut microbiota.

Therefore, the aim of the current review article is to summarize the available literature data about the impact of microbiome on MS development.

How does the microbiome influence the MS? GIT is a point of combined influence of the body's largest concentration of immune cells, a vast network of 500 million neurons and the gut microbiota. It also serves as a primary barrier between the outside world of potential pathogens and the internal environment of the body [19]. This interaction is constituted as early as the postnatal period of life. The postnatal period is a critical developmental phase of the GIT. Various GI functions, such as intestinal epithelial barrier (IEB) role and motility undergo profound changes during this period.

The human gut microbiome may influence human brain health by several different mechanisms. Structural components of bacterial cell wall such as lipopolysaccharides provide low-grade tonic stimulation of the innate immune system. Excessive stimulation due to bacterial dysbiosis, small intestinal bacterial overgrowth, or increased intestinal permeability may lead to inflammation in the CNS. Dysfunctional responses of the adaptive immunity by cross-reaction with human antigens could be caused by bacterial proteins. The functions of different bacterial enzymes may produce neurotoxic metabolites as D-lactic acid and ammonia. [14]. Some beneficial metabolites as short-chain fatty acids may also cause neurotoxic effects. Production of neurotransmitters and other hormones from some gut microbes are identical or similar to the produced by humans. In this way bacterial receptors for these substances may influence microbial growth and virulence. Direct stimulation of afferent neurons in the enteric nervous system by gut bacteria makes them able to send signals to the brain via the *vagus nerve.* Through these different pathways gut microbes shape the architecture of sleep and stress reactivity of the hypothalamic-pituitary-adrenal axis. In such a way these microorganisms influence the memory, mood and cognition. Thus, they are clinically and therapeutically relevant to a variety of disorders, including alcoholism, chronic fatigue syndrome, fibromyalgia and restless legs syndrome [14].

The bidirectional communication via the gut-brain axis is suggested to play a substantial role in neurologic diseases, including anxiety, depression, autism, MS, Parkinson's disease (PD), Alzheimer's disease (AD), etc. [9]. Although subtle differences in the exact composition of gut microflora have been found within the patient versus control populations (as would be expected considering the differences in geographical location), the overwhelming conclusion is that, indeed, microbial dysbiosis is present in the intestine of MS patients [7]. The intestinal microflora in MS patients has greater inter-individual variability than that of healthy controls. A decrease in the percentage of several *Bacteroides* species, including *B. stercoris*, *B. coprocola,* and *B. coprophilus* in the intestinal microflora in patients with MS has been shown [1]. Significant differences in microbiota structure between patients with MS and healthy controls have been found in a cohort of 31 patients with RRMS compared with 36 healthy controls. According to several studies, MS patients have distinct microbial profile compared to healthy controls. Increased abundance of *Pseudomonas*, *Mycoplana*, *Haemophilus*, *Blautia*, and *Dorea* genera in MS patients have been established, whereas control group has shown increased abundance of *Parabacteroides*, *Adlercreutzia* and *Prevotella* genera [6, 19, 30].

This is consistent with the hypothesis that MS patients have gut microbial dysbiosis and further study is needed to better understand their role in the etiopathogenesis of

MS [6]. However, there was no difference in overall species richness (α-diversity) between healthy controls and MS patients but within the MS patient cohort there was a trend toward reduced species richness in individuals with active disease whereas those in remission were similar to the healthy controls. Such changes in α-diversity could suggest a role of the gut microbiome in disease exacerbation but future longitudinal studies are necessary to establish correlation [7].

Besides the microorganisms, other environmental factors as toxins might start a pathological process within enteric nerve cell plexus, causing mucosal inflammation and oxidative stress. In this way gut leakiness could be initiated which could disrupt the integrity of the blood brain barrier (BBB) and thus increase its permeability [1]. Numerous data are emerging on the effect of gut microflora on the immune system in human and mouse models of MS. According to recent studies there are data of probiotic influence on stress markers and immunoregulatory responses on healthy volunteers both *in vivo* and *in vitro*. In many animal models and in human studies the probiotics have been found to influence the intestinal microbiota and immunity, and in this way to stabilize the mucosal barrier. It has recently been shown that probiotics influence the 'gut-brain' axis modeling the behavior in the way that significantly reduces anxiety, depression, and stress [35]. There is evidence that epsilon toxin causes BBB permeability and in this way kills the brain myelin producing cells oligodendrocytes - the same cells that die in MS lesions [28, 38]. Epsilon toxin may be responsible for triggering MS. It is produced by certain strains of *Clostridium perfringens*, a spore-forming bacterium that is one of the most common causes of foodborne illness in the United States [1]. *C. perfringens* is a spore-forming gram-positive bacterium found in many environmental sources as well as in the intestines of humans and animals. It prefers to grow in conditions with very little or no oxygen, and under ideal conditions can multiply very rapidly. There is a relation between the GIT and physiological stress expressed by the levels of cortisol and immunoglobulin A (IgA) in the saliva in patients with MS [1, 38].

Typical microbial agents associated with some neurodegenerative autoimmune disorders in humans. Prevalence of Haptoglobin I (88%) in patients with Alzheimer Disease and 46.7% in controls both infected with *H. pylori* have been established [27]. Probably this is the main reason for the assessed iron deficiency in patients with autism. Very strong correlation of *Desulfovibrio* with the severity of autism manifestations has been noted, represented by the Autism Spectrum Disorders restricted/repetitive behavior subscale score [35]. Toxins B and D from *C. perfringens* have also been suggested to influence the neurological symptoms in MS patients [1]. A lot of alterations in gut microflora composition have been observed in patients with MS. Increased levels of *Methanobrevibacter* and *Akkermansia* have been assessed but decreased amounts of *Butyricimonas* and *Lachnospiraceae* have been found [17, 18]. Alterations in gut microflora composition in MS patients under treatment with glatiramer acetate (long-term drug) have been noted. There are increased levels of *Bacteroidaceae*, *Faecalibacterium*, *Ruminococcus*, *Lactobacillaceae*, *Clostridium*, and other members of the class *Clostridiales* compared to untreated MS patients [1]. Epsilon Toxin from *C. perfringens* has been determined as a candidate-trigger for new lesion formation in MS [38]. *Campylobacter jejuni* has been found in 154 patients with Guillain-Barre Syndrome (GBS), 63 patients with other neurological diseases, and 50 normal controls [16]. Using quantitative PCR, alterations in gut microflora composition have been found in patients with PD compared to normal controls. Decreased levels of *Bacteroidetes* and *Prevotella* and increased amounts of *Enterobacteriaceae* in PD have been assessed [36]. Additionally, fecal short chain fatty acids concentrations were significantly reduced in PD patients compared to controls.

Effects of probiotics/prebiotics on the nervous and immune systems in healthy volunteers. Significantly decreased levels of cortisol in saliva in administration of *Lactobacillus plantarum* 299v [4] and in urine – in administration of strains *Lactobacillus helveticus* R0052 and *Bifidobacterium longum* R0175 [31] have been observed, compared to placebo treated individuals. According to other studies, attenuated increases in cortisol levels and subjective anxiety in response to acute stressor have been observed in application of *B. longum* 1714 [3]. No overall effect has been noted in treatment with *Lactobacillus rhamnosus* (JB-1) [22]. In another group of healthy controls in administration of *Bifidobacterium infantis* increased secretion of IL-10 and enhanced *Foxp3* expression in peripheral blood has been assessed [26]. This gene codes protein FOXP3 (forkhead box P3) also known as scurfin, which is involved in immune system responses. It appears to function as a master regulator of the regulatory pathway in the development and function of regulatory T cells (T_{regs}), which generally turn the immune response down [26]. The same authors have established activated immunoregulatory responses on dendritic cells from healthy donors in *in vitro* studies. Decreased serum concentrations of the inflammatory markers CRP, IL- 1β, and TNF-α have been noted in application of *Lactobacillus salivarius* UBL S22 fructooligosaccharides (FOS). In *in vitro* study of whole blood from healthy human individuals appearance of Zwitterionic polysaccharides, up-regulated immunologic synapse components, as well as, activated induction on $CD39^{+}Foxp3^{+}$, IL-10, IFNγ and increased frequency of CD39-expressing T_{regs} have been observed compared to patients with gastro-intestinal problems [34]. One of two prebiotics (FOS or Bimuno®-galactooligosaccharides – B-GOS) has led to decreased salivary cortisol awakening response after B-GOS intake. However, no effects after administration of FOS have been shown [32]. According to many authors in treatment of children with autism by *Lactobacillus acidophilus*, *L. rhamnosus* and *L. acidophilus* strain *Rosell*-11 have been noted decreased body weight and BMI as well as decreased severity in administration together with *B. longum* [33, 35]. Probiotic capsule significantly improves ability of concentration and carrying out orders in autistic children [21].

Probiotics/prebiotics therapeutic strategies in MS. Treatment paradigms based on the hygiene hypothesis include probiotic strategies, that is directed to administration of non-pathogenic live microorganisms which, when given in adequate amounts, confer a health benefit on the host. There are statistically significant differences in the microbiome composition of MS patients versus healthy volunteers. Many experiments of probiotic/prebiotic treatment were carried out on animal models and the reported effects are:

– Increased effectiveness in combined treated stress-induced visceral pain than with single probiotic;
– Less stress-induced anxiety-like behaviour and prevented deficits in social interaction with conspecifics are available;
– Low intestinal permeability *in vivo* under basal conditions and in response to MS or WAS (water avoidance stress);
– Attenuated rise of corticosterone levels in response to MS or WAS by the probiotic;
– Increased IFN-γ levels;
– Higher locomotion and exploratory behavior;
– No alterations in the development of aggressor avoidance following social defeat [2, 5, 37].

The role of microbe-based interventions in stress-related disorders has been shown in mouse model [5]. Usability of *Lactobacillus fermentum* as a novel tool for the prevention

and/or treatment of gastrointestinal disorders associated with altered intestinal epithelial barrier (IEB) functions in the newborn rats has been suggested [37]. In patients with MS the combination of *L. helveticus* and *B. longum* has been more effective in regulating glucocorticoid negative feedback on the HPA axis than probiotic alone [2].

Fecal microbiota transplantation has a 1700-year history [13]. This forgotten treatment method has been put into use again during the last 50 years. There are case reports that it is effective in the treatment of MS, and also of autism, PD, chronic fatigue syndrome and irritable bowel syndrome [13].

As the etiology and pathogenesis of MS are not fully understood, an individual approach is needed. Since it is an autoimmune disease, it is of great importance to reduce the immune system stimuli. For all patients, an appropriate diet, clean water consumption, rest and a longer stay in clean air, providing a suitable lifestyle, is important [23, 24, 25].

Conclusions

The type of diet has been characterized as critically important for patients with MS. From this point of view, the microbial-related therapies can be suggested as supportive treatment in parallel with the accepted medical protocol. As far as the etiology and the pathogenesis of MS are still unknown, it would be reasonable to forward the research in the direction of the gut-brain axis. If such clue is proved, a new, probiotic approach could be developed in addition to the unified MS protocol. Having in mind the positive influence of probiotics on MS aspects of human health, such approach might improve the quality of life of patients with this disorder.

References

1. **Adamczyk-Sowa, M., A. Medrek, P. Madej, W. Michlicka, P. Dobrakowski.** Does the gut microbiota influence immunity and inflammation in multiple sclerosis pathophysiology? – *J. Immunol. Res*., **2017**, 2017, 7904821.
2. **Ait-Belgnaoui, A., I. Payard, C. Rolland, C. Harkat, V. Braniste, V. Théodorou, T. A. Tompkins.** *Bifidobacterium longum* and *Lactobacillus helveticus* synergistically suppress stress-related visceral hypersensitivity through hypothalamic-pituitary-adrenal axis modulation. – *J. Neurogastroenterol. Motil*., **24**(1), 2018, 138-146.
3. **Allen, A. P., W. Hutch, Y. E. Borre, P. J. Kennedy, A. Temko, G. Boylan, E. Murphy, G. F. Cryan, T. J. Dinan, G. Clarke.** *Bifidobacterium longum* 1714 as a translational psychobiotic: modulation of stress, electrophysiology and neurocognition in healthy volunteers. – *Transl. Psychiatry*, **6**(11), 2016, e939.
4. **Andersson, H., C. Tullberg, S. Ahrne, K. Hamberg, I. L. Ahren, G. Molin, M. Sonesson, A. Håkansson.** Oral administration of *Lactobacillus plantarum* 299v reduces cortisol levels in human saliva during examination induced stress: a randomized, double-blind controlled trial. – *Int. J. Microbiol*., **2016**, 2016, 8469018.
5. **Bharwani, A., M. F. Mian, M. G. Surette, J. Bienenstock, P. Forsythe.** Oral treatment with *Lactobacillus rhamnosus* attenuates behavioural deficits and immune changes in chronic social stress. – *BMC Med*., **15**, 2017, 7.
6. **Chen, J., N. Chia, K. R. Kalari, J. Z. Yao, M. Novotna, M. M. P. Soldan, D. H. Luckey, E. V. Marietta, P. R. Jeraldo, X. Chen, B. G. Weinshenker, M. Rodriguez, O. H. Kantarci, H. Nelson, J. A. Murray, A. K. Mangalam.** Multiple sclerosis patients have a distinct gut microbiota compared to healthy controls. – *Sci. Rep*., **6**, 2016, 28484.
7. **Colpitts, S. L., L. H. Kasper.** Influence of the gut microbiome on autoimmunity in the central nervous system. – *J. Immunol*., **198**(2), 2017, 596-604.

8. **Compston, A., A. Coles.** Multiple sclerosis. – *Lancet*, **372**(9648), 2008, 1502-1517.
9. **Cox, L. M., H. L. Weiner.** Microbiota signaling pathways that influence neurologic disease. – *Neurotherapeutics*, **15**(1), 2018, 135-145.
10. **De Angelis, F., D. Plantone, J. Chataway.** Pharmacotherapy in secondary progressive multiple sclerosis: an overview. - *CNS Drugs*, **32**(6), 2018, 499-526.
11. **De Luca, F., Y. Shoenfeld.** The microbiome in autoimmune diseases. – *Clin. Exp. Immunol*., **195**(1), 2019, 74-85.
12. **Eskandarieh, S., P. Heydarpour, A. Minagar, S. Pourmand, M. A. Sahraian.** Multiple sclerosis epidemiology in East Asia, South East Asia and South Asia: a systematic review. – *Neuroepidemiology*, **46**, 2016, 209-221.
13. **Evrensel, A., M. E. Ceylan.** Fecal microbiota transplantation and its usage in neuropsychiatric disorders. – *Clin. Psychopharmacol. Neurosci*., **14**(3), 2016, 231-237.
14. **Galland, L.** The gut microbiome and the brain. - *J. Med. Food*, **17**(12), 2014, 1261-1272.
15. **Ivanova, S., V. Kolyovska.** Complecated face of multiple sclerosis. – *Proceedings of the eleventh workshop "Biological activity of metals, synthetic compounds and natural products" (Sofia), 14-16 December*, 2016, 111-117.
16. **Jacobs, B. C., P. A. van Doorn, P. I. Schmitz, A. P. Tio-Gillen, P. Herbrink, L. H. Visser, H. Hooijkass, F. G. van der Meché.** Campylobacter jejuni infections and anti-GM1 antibodies in *Guillain-Barré* syndrome. – Ann. Neurol., **40**(2), 1996, 181-187.
17. **Jangi, S., R. Gandhi, L. M. Cox, N. Li, F. von Glehn, R. Yan, B. Patel, M. A. Mazzola, S. Liu, B. L. Glanz, S. Cook, S. Tankou, F. Stuart, K. Melo, P. Nejad, K. Smith, B. D. Topçuolu, J. Holden, P. Kivisäkk, T. Chitnis, P. L. De Jager, F. J. Quintana, G. K. Gerber, L. Bry, H. L. Weiner.** Alterations of the human gut microbiome in multiple sclerosis. – *Nat. Commun*., **7**, 2016, 12015.
18. **Jhangi, S., R. Gandhi, B. Glanz, S. Cook, P. Nejad, D. Ward, N. Li, G. Gerber, L. Bry, H. Weiner.** Increased *Archaea* species and changes with therapy in gut microbiome of multiple sclerosis subjects (S24.001). – *Neurology*, **82**(10 Suppl.), 2014.
19. **Joscelyn, J., L. H. Kasper.** Digesting the emerging role for the gut microbiome in central nervous system demyelination. – *Mult. Scler*., **20**(12), 2014, 1553-1559.
20. **Julio-Pieper, M., J. A. Bravo.** Intestinal barrier and behavior. – *Int. Rev. Neurobiol*., **131**, 2016, 127-141.
21. **Ka1uzna-Czaplinska, J., S. Blaszczyk.** The level of arabinitol in autistic children after probiotic therapy. – *Nutrition*, **28**, 2012, 124-126.
22. **Kelly, J. R., A. P. Allen, A. Temko, W. Hutch, P. J. Kennedy, N. Farid, E. Murphy, G. Boylan, J. Bienestock, J. F. Cryan, G. Clarke, T. G. Dinan.** Lost in translation? The potential psychobiotic *Lactobacillus rhamnosus* (JB-1) fails to modulate stress or cognitive performance in healthy male subjects. – *Brain Behav. Immun*., **61**, 2017, 50-59.
23. **Kolyovska, V., S. Todorov, D. Kadiysky, D. Maslarov.** Modeling of nutrition in patient with relapsing remitting multiple sclerosis whit aim to reduce exacerbation. – *Proceedings of the Sixth workshop "Experimental models and methods in biomedical research"*, 2015, 147-151.
24. **Kolyovska, V., S. Todorov, D. Maslarov.** New perspectives in multiple sclerosis treatment. – *Medical Data*, **5**(3), 2013, 241-244.
25. **Kolyovska, V., V. Pavlova, I. Iliev, D. Kadiysky, D. Maslarov.** Complementary and alternative medicine for multiple sclerosis treatment. Yes or no? – *Medical Data*, **7**(3), 2015, 207-209.
26. **Konieczna, P., D. Groeger, M. Ziegler, R. Frei, R. Ferstl, F. Shanahan, E. M. Quigley, B. Kiely, C. A. Akdis, L. O'Mahony.** *Bifidobacterium infantis* 35624 administration induces Foxp3 T regulatory cells in human peripheral blood: potential role for myeloid and plasmacytoid dendritic cells. – *Gut*, **61**, 2012, 354-366.
27. **Kountouras, J, Tsolaki M, Gavalas E, M. Boziki, C. Zavos, P. Karatzoglou, D. Chatzopoulos, I. Venizelos.** Relationship between *Helicobacter pylori* infection and *Alzheimer* disease. – Neurology, **66**, 2006, 938-940.
28. **Linden, J. R., Y. Ma, B. Zhao, J. M. Harris, K. R. Rumah, N. Schaeren-Wiemers, T. Vartanian.** *Clostridium perfringens* epsilon toxin causes selective death of mature oligodendrocytes and central nervous system demyelination. – *mBio*, **6**(3), 2015, e02513-14.
29. **Malinova, T. S., C. D. Dijkstra, H. E. de Vries.** Serotonin: a mediator of the gut-brain axis in multiple sclerosis. – *Mult. Scler*., 2018, **24**(9), 1144-1150.

30. **McKay, K. A., K. Kowalec, F. Brinkman, B. B. Finlay, M. Horwitz, A. R. Manges, L. Osborne, H. Tremlett.** From bugs to brains: The microbiome in neurological health. – *Mult. Scler. Relat. Disord*., **12**, 2017, 1-3.
31. **Messaoudi, M., R. Lalonde, N. Violle, H. Javelot, D. Desor, A. Najdi, J. Basson, C. Rougeot, M. Pichelin, M. Cazalbiel, J. Cazalbiel.** Assessment of psychotropic-like properties of a probiotic formulation (*Lactobacillus helveticus* R0052 and *Bifidobacterium longum* R0175) in rats and human subjects. – *Br. J. Nutr*., **105**(5), 2011, 755-764.
32. **Schmidt, K., P. J. Cowen, C. J. Harmer, G. Tzortzis, S. Errington, P. W. J. Burnet.** Prebiotic intake reduces the waking cortisol response and alters emotional bias in healthy volunteers. – *Psychopharmacology (Berl.)*, **232**(10), 2015, 1793-1801.
33. **Shaaban, S. Y., Y. G. Gendy, N. S. Mehanna, W. M. El-Senousy, H. S. A. El-Feki, K. Saad, O. M. El-Asheer.** The role of probiotics in children with autism spectrum disorder: a prospective, open-label study. – *Nutr. Neurosci*., **7**, 2017, 1-6.
34. **Telesford, K. M., W. Yan, J. Ochoa-Reparaz, A. Pant, C. Kircher, M. A. Christy, S. Begum-Haque, D. L. Kasper, L. H. Kasper.** A commensal symbiotic factor derived from Bacteroides fragilispromotes human CD39+Foxp3+T cells and Treg function. – *Gut Microbes*, **6**(4), 2015, 234-242.
35. **Tomova, A., V. Husarova, S. Lakatosova, J. Bakos, B. Vlkova, K. Babinska, D. Ostatnikova.** Gastrointestinal microbiota in children with autism in Slovakia. – *Physiology & Behavior*, **138**, 2015, 179-187.
36. **Unger, M. M., J. Spiegel, K. U. Dillmann, D. Grundmann, H. Philippeit, J. Burmann, K. Faßbender, A. Schwiertz, K. H. Schäfer.** Short chain fatty acids and gut microbiota differ between patients with *Parkinson's* disease and age-matched controls. – *Parkinsonism Relat. Disord*., **32**, 2016, 66-72.
37. **Vanhaecke, T., P. Aubert, P. A. Grohard, T. Durand, P. Hulin, P. Paul-Gilloteaux, A. Fournier, F. Docagne, A. Ligneul, C. Fressenge-Mazda, P. Naveilhan, H. Boudin, P. Le Ruyet, M. Neunlist.** *L. fermentum* CECT 5716 prevents stress-induced intestinal barrier dysfunction in newborn rats. – *Neurogastroenterol. Motil*., **29**(8), 2017. Epub 2017 Mar 31. doi: 10.1111/nmo.13069.
38. **Vartanian, T., K. Rumah, J. Linden.** Identification of *Clostridium perfringens* epsilon toxin as a candidate trigger for new lesion formation in multiple sclerosis (P6.151). – *Neurology*, **82**(**10** Suppl.), 2014.
39. **Wang, Y., S. Begum-Haque, K. M. Telesford, J. Ochoa-Repáraz, M. Christy, E. J. Kasper.** A commensal bacterial product elicits and modulates migratory capacity of $CD39^+$ CD4 T regulatory subsets in the suppression of neuroinflammation. – *Gut Microbes*, **5**(4), 2014, 552-561.
40. **Zaprianova, E., D. Deleva, B. Sultanov, V. Kolyovska.** Current knowledge of multiple sclerosis pathogenesis. – *Acta morphol. anthropol.*, **14**, 2009, 136-140.

Institute of Experimental Morphology, Pathology and Anthropology with Museum
Bulgarian Anatomical Society

Acta morphologica et anthropologica, 27 (1-2)
Sofia ● 2020

ANTHROPOLOGY AND ANATOMY 27 (2)

Original Articles

Digital Morphometric Analysis and Comparison of Orbital Region in Metopic and Non-metopic Cranial Series

Silviya Nikolova[1], Diana Toneva[1], Angel Dandov[2]*

[1]Department of Anthropology and Anatomy, Institute of Experimental Morphology, Pathology and Anthropology with Museum, Bulgarian Academy of Sciences, Sofia, Bulgaria
[2]Department of Anatomy and Histology, Medical University, Sofia, Bulgaria

* Corresponding author e-mail: sil_nikolova@abv.bg

The study aimed to compare the orbital region in metopic and non-metopic series and to ascertain if its morphology differs considerably in both of them. A total of 278 (control, n = 207; metopic series, n = 71) dry skulls of contemporary adult males were scanned with a hand-held laser scanner. Digital morphometry was performed by recording the 3D coordinates of five bilateral landmarks. The linear measurements were calculated as Euclidian distances between the landmarks. Orbital index and orbital aperture area were also computed. The results showed that the metopic skulls had significantly larger upper biorbital (fmo-fmo), biorbital (ek-ek) and maxillofrontal (mf-mf) breadths. The orbital aperture area, orbital index and its distribution by categories did not differ considerably between the series. Generally, the metopic suture persistence was related to aspecific orbital region morphology. The established greater biorbital breadths in the metopic series were due to the enlarged intraorbital distance.

Key words: metopic suture, metopism, orbital region, polygonal 3D models, digital morphometry

Introduction

The frontal bone undergoes intramembranous ossification during embryogenesis and develops from two ossification centres. The metopic suture forms at the borderline between both halves of the growing frontal bone and runs from the *nasion* to the anterior fontanelle. The metopic suture allows enlargement of the frontal part of neurocranoium

perpendicular to it. This suture is the first one which physiologically obliterates, usually by the end of the second postnatal year. The fusion is initiated at the *nasion* and progresses towards the anterior fontanelle [3]. Sometimes, however, the closure is delayed and the metopic suture persists during the adulthood. In such cases, the frontal bone remains bipartite and this condition is known as *metopism*. The hypothetical factors causing *metopism* are with heterogeneous etiology and are still unclear. The reported frequency varies in wide ranges among the different groups [1, 8, 12, 15, 16].

It is known that the cranial sutures allow growth of the adjacent bone plates in direction perpendicular to the suture line. In accordance to this regularity, the metopic skulls have been observed to possess a considerably wider frontal bone [15, 16, 19]. The orbital region of the skull includes the two orbits, which are symmetrical bony cavities. Each orbit is shaped like a four-sided pyramid, with its apex situated posteriorly and its base anteriorly. The orbital aperture is enclosed by the frontal bone superiorly, the zygomatic bone laterally and the maxilla inferiorly. Since the frontal bone partakes in the orbit formation, it is reasonable to suppose that the orbital region in metopic skulls differs as well. Therefore, the aim of this study was to compare the orbital region in metopic and non-metopic cranial series using digital morphometric analysis. This way we intended to assess the relation of the metopic suture persistence to the orbital region morphology.

Materials and Methods

A total of 278 dry adult male skulls without mandibles were investigated. The skulls were distributed into two groups: a metopic series (n = 71) with a patent metopic suture extending from *nasion* to *bregma* and a control series (n = 207) without any traces of metopic suture. The skulls belonged to soldiers who died in the wars at the beginning of the 20th century. The bone remains were preserved at the Military Mausoleum with Ossuary and were kindly provided for investigation by the Bulgarian National Museum of Military History.

Generation of 3D polygonal models

The skulls were scanned with a hand-held laser scanner CreaformVIUscan. The scanning was performed at a resolution of 0.40 mm and a texture resolution of 150 DPI. The accuracy of the laser scanner was up to 0.05 mm. The collected surface data were post-processed in the scanner software platform VXelements™.

Digital morphometry

Digital morphometry was performed on the polygonal models (**Fig. 1**) by recording the 3D coordinates of five bilateral landmarks (**Table 1**) using the "Pick Points" tool in the free software MeshLab version2016.12 [2] (**Fig. 2**). The linear distances were calculated as Euclidian distances using the software PAST version 2.17c. [4]. The measurements obtained from 3D models generated by laser scanning have been proved to be accurate and reliable [20-22].

The orbital index was calculated and distributed by categories according to the following borderline values [5]:

Chamaeconch × – 75.9
Mesoconch 76.0 – 84.9
Hypsiconch 85.0 – ×

The orbital aperture area was also computed using the formula for rectangle area calculation as was suggested by Kadanoff and Mutafov [5]. Accordingly, the orbital area was calculated as follows:

Orbital aperture area = Orbital breadth × Orbital height

Statistics

Basic descriptive statistics, including the mean, standard deviation (SD), minimum and maximum values, were calculated for both metopic and control series. The significance of the differences between groups was assessed by the independent samples t-test. The Mann-Whitney U-test was used in cases when the normality test or the equal variance test failed. Chi-square test was used to assess the intergroup differences in the distribution of the orbital index categories. The significance level for all tests was set at $p \leq 0.05$.

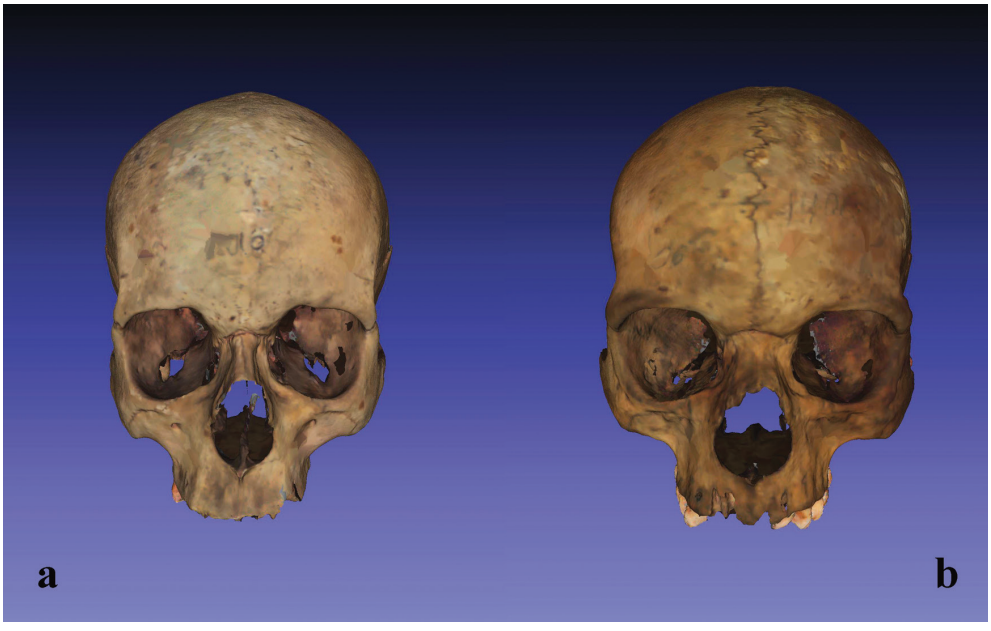

Fig. 1. Polygonal 3D models of skulls generated by laser scanning: a) a skull from the control series; b) a skull from the metopic series.

Table 1. Description of the landmarks and measurements

Landmarks	**Description**
Frontomalareorbitale (fmo)	The point of intersection of the zygomaticofrontal suture with the lateral orbital rim;
Ektoconchion (ek)	The point where the outer orbital rim length line, parallel to the upper border, meets the outer rim;
Maxillofrontale (mf)	The point of intersection of the anterior lacrimal crest with the frontomaxillary suture;
Supraorbitale (so)	The most superior point at the upper orbital rim;
Zygoorbitale (zo)	The point of intersection of the zygomaticomaxillary suture with the lower orbital rim;

Measurements	Description
Upper biorbital breadth (fmo-fmo)	The linear distance between both landmarks frontomalareorbitale;
Biorbital breadth (ek-ek)	The linear distance between both landmarks ektoconchion;
Orbital breadth R/L (mf-ek)	The linear distance between the landmarks maxillofrontale and ektoconchion;
Orbital height R/L (so-zo)	The linear distance between the landmarks supraorbitale andzygoorbitale;
Maxillofrontal breadth (mf-mf)	The linear distance between both landmarks maxillofrontale;
Indices	**Description**
Orbital index R/L (so-zo/mf-ek)	The ratio between the orbital height and the orbital length;
Area	**Description**
Orbital aperture area R/L	The multiplication of orbital width with orbital height.

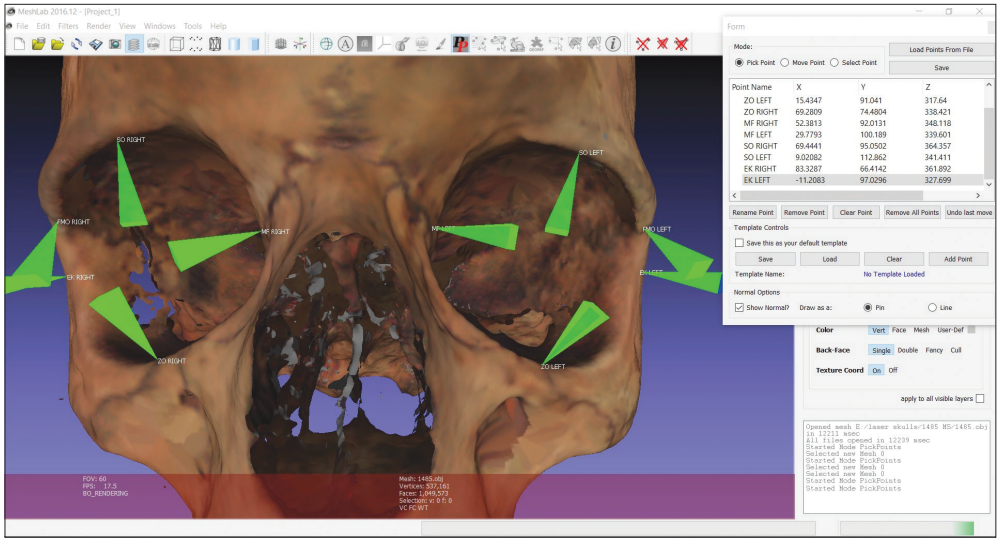

Fig. 2. Designation of the landmarks picked on a 3D model in MeshLab. Abbreviations: FMO – frontomalareorbitale; EK – ektoconchion; MF – maxillofrontale; SO – supraorbitale; ZO – zygoorbitale.

Results

Statistically significant differences between both series were observed in the upper biorbital breadth (fmo-fmo), biorbital breadth (ek-ek) and maxillofrontal breadth (mf-mf), which were larger in the metopic series. Besides, the orbital breadth (mf-ek) on the right side was significantly larger in the control series (**Table 2**). The orbital aperture area along with the orbital index and its distribution by categories did not differ significantly between the series (**Table 2, Table 3; Table 4**).

Table 2. Descriptive and test statistics of the measurements. The linear measurements are in mm and the area is in mm^2

Measurements	Metopic series					Control series					t-test/U-test (p-value)
	n	mean	SD	min	max	n	mean	SD	min	max	
Upper biorbital breadth (fmo-fmo)	70	98.97	3.03	93.02	106.66	207	97.35	3.64	88.12	109.04	t = 3.344 (P = <0.001)
Biorbital breadth (ek-ek)	70	97.86	2.64	91.83	104.06	206	96.69	3.52	88.90	108.21	U = 5670.50 (P = 0.008)
Orbital breadth R (mf-ek)	70	41.09	1.84	37.43	45.29	206	41.67	1.92	37.02	46.48	t = -2.192 (P = 0.029)
Orbital breadth L (mf-ek)	72	41.17	1.64	37.37	44.68	206	41.33	1.87	36.56	46.52	t = -0.649 (P = 0.517)
Orbital height R (so-zo)	70	33.48	2.33	27.13	38.90	207	33.56	2.10	27.49	39.52	t = -0.247 (P = 0.805)
Orbital height L (so-zo)	71	33.51	2.28	26.32	38.27	207	33.66	2.02	27.74	39.71	t = -0.547 (P = 0.585)
Maxillofrontal breadth (mf-mf)	71	22.57	2.12	18.13	28.78	206	19.95	2.06	15.04	26.63	t = 9.190 (P = <0.001)
Orbital index R (so-zo R/mf-ek R)	70	81.55	5.61	68.80	94.58	206	80.70	5.21	65.29	97.41	t = 1.157 (P = 0.248)
Orbital index L (so-zo L/mf-ek L)	71	81.45	5.72	63.71	93.02	207	81.54	4.98	64.94	95.32	t = -0.124 (P = 0.902)
Orbital area R (so-zo R*mf-ek R)	70	1377.33	130.39	1084.33	1641.17	207	1400.65	122.83	1088.22	1747.11	t = -1.351 (P = 0.178)
Orbital area L (so-zoL*mf-ekL)	71	1380.63	119.17	1087.56	1620.46	206	1392.87	122.37	1075.26	1847.24	t = -0.731 (P = 0.465)

Table 3. Distribution by orbital index categories

Orbital index categories	Metopic series R		Metopic series L		Control R		Control L	
	n	%	n	%	n	%	n	%
Chamaeconch	14	20.00	12	16.90	37	17.96	26	12.62
Mesoconch	37	52.86	41	57.75	125	60.68	124	60.19
Hypsiconch	19	27.14	18	25.35	44	21.36	56	27.18
Total	**70**	**100**	**71**	**100**	**206**	**100**	**206**	**100**

Table 4. Comparison between the distributions of orbital index categories in metopic and control series

Comparisons	χ^2(k = 2)	***p* value**
MS (R) : Control (R)	1.4279	0.489718
MS (L) : Control (L)	0.8246	0.662142

Discussion

The persistence of the metopic suture in adults has not been reported to cause any abnormalities by itself, though it has been found as a concomitant finding in some disorders [9, 11]. Furthermore, the metopic skulls often manifest additional bones, arising from non-fusion of normal ossification centres or from additional ones [9, 10, 13, 19]. It has also been observed that the metopic skulls possess a specific distinctive configuration of the neurocranium [15, 16, 19]. However, despite the close developmental interrelation between the neuro- and basicranium, the persisting metopic suture has not been associated with an alteration in the cranial base assessed by the cranial base angle constructed between the landmarks *nasion*, *sella* and *basion* [14]. The main differences concern the frontal bone, which is considerably shorter, wider and more convex in the metopic skulls [15, 19]. The significantly broad and high forehead in the metopic series, however, is not related to a greater frontal sinus pneumatization. On the contrary, recent morphometric investigations have revealed a tendency for metopic suture persistence to be frequently related to frontal sinus underdevelopment. Furthermore, the frontal sinus pneumatization seems to be a spatially-coordinated process progressing proportionately in the vertical and horizontal plates of the frontal bone [12, 15-18].

According to the functional matrix concept of Moss [6, 7] the adult human frontal bone is a single morphological structure, but not a single functional unit. The shape of the frontal bone accurately reflects the functional demands to protect and support the soft tissues and cavities. Thus, the metopic suture persistence could be considered not as a causative for the distinctive skull configuration, but rather as an expression of the underlying neural mass specific demands. The results obtained in this study show that besides the specific configuration on the frontal bone, the orbital region morphology in metopic skulls differs as well. As it could be seen, the orbital

aperture area and measurements do not differ considerably between the series, and the greater biorbital breadths in the metopic series are due to the significantly enlarged intraorbital distance, which in turn is a precondition for a broad nasal bridge. The tendency for a wider frontal bone and orbital region in metopic skulls is apparent, but the issue if the metopic suture retention causes this specific appearance, or all these features are the expression of underlying neural mass demands is still unclear and an object of further investigations.

Conclusion

It could be concluded that the persistence of a metopic suture is related to a distinct morphology of the orbital region, which is significantly wider in the metopic skulls. The greater biorbital breadths are not at the expense of enlarged orbital apertures, but are due to a greater interorbital distance.

Acknowledgements: The study was supported by the Bulgarian National Science Fund, Grants No DN01/15-20.12.2016 and DN11/9-15.12.2017. The authors thank Dr. Ivan Georgiev for the image generation.

References

1. **Berry, A. C.** Factors affecting the incidence of non-metrical skeletal variants. – *J. Anat.*, **120**, 1975, 519-535.
2. **Cignoni, P., M. Callieri, M. Corsini, M. Dellepiane, F. Ganovelli, G. Ranzuglia.** MeshLab: an open-source mesh processing tool. – *In: Eurographics*, *Italian Chapter Conference* (Eds. V. Scarano, R. De Chiara, U. Erra). Eurographics Association, 2008, 1-8.
3. **Faro, C., B. Benoit, P. Wegrzyn, R. Chaoui, K. Nicolaides.** Three-dimensional sonographic description of the fetal frontal bones and metopic suture. – *Ultrasound in Obstetrics & Gynecology*, **26**, 2005, 618-621.
4. **Hammer, Ø., D. Harper, P. Ryan.** PAST: paleontological statistics software package for education and data analysis. – *Palaeontologia Electronica*, **4**, 2001, 9-18.
5. **Kadanoff, D., S. Mutafov.** *The human skull in a medico-anthropological aspect: form, dimensions and variability*. Sofia, Prof. Marin Drinov Academic Publishing House. 1984, 236 pp
6. **Moss, M. L.** Functional anatomy of cranial synostosis. – *Childs Brain*., **1**, 1975, 22-33.
7. **Moss, M. L., R. W. Young.**A functional approach to craniology. – *Am. J. Phys. Anthropol.,* **18**, 1960, 281-292.
8. **Nikolova, S., D. Toneva.** Frequency of metopic suture in male and female medieval cranial series. – *Acta Morphol. Anthropol*., **19**, 2012, 250–252.
9. **Nikolova, S., D.Toneva, Y. Yordanov, N. Lazarov**. Multiple Wormian bones and their relation with definite pathological conditions in a case of an adult cranium. – *Anthropol. Anz.*, **71**, 2014, 169-190.
10. **Nikolova, S., D. Toneva, Y. Yordanov, N. Lazarov**. Variations in the squamous part of the occipital bone in medieval and contemporary cranial series from Bulgaria. – *Folia Morphol*., **73**, 2014, 429-438.
11. **Nikolova, S., D. Toneva, I. Georgiev.** A case of skeletal dysplasia in bone remains from a contemporary male individual. – *Acta Morphol. Anthropol*., **22**, 2015, 97-107.
12. **Nikolova, S., D. Toneva, I. Georgiev**. A persistent metopic suture – incidence and influence on the frontal sinus development (preliminary data). – *Acta Morphol. Anthropol*., **23**, 2016, 83-90.
13. **Nikolova, S., D. Toneva, I. Georgiev, Y. Yordanov, N. Lazarov**. Two cases of large bregmatic bone along with a persistent metopic suture from necropoles on the northern Black Sea coast of Bulgaria. – *Anthropological Science*, **124**, 2016, 145-153.
14. **Nikolova, S., D. Toneva, I. Georgiev**. Cranial base angulation in metopic and non-metopic cranial series. – *Acta Morphol. Anthropol.,* **24**, 2017, 45-49.

15. **Nikolova, S., D. Toneva, I. Georgiev, N. Lazarov**. Digital radiomorphometric analysis of the frontal sinus and assessment of the relation between persistent metopic suture and frontal sinus development. – *Am. J. Phys. Anthropol*., **165**, 2018, 492-506.
16. **Nikolova, S., D. Toneva, I. Georgiev,N. Lazarov**. Relation between metopic suture persistence and frontal sinus development. – In: *Challenging issues on paranasal sinuses* (Ed. Tang-Chuan Wang), IntechOpen, 2018, 3-23.
17. **Nikolova, S., D. Toneva, I. Georgiev, A. Dandov, N. Lazarov**. Morphometric analysis of the frontal sinus: application of industrial digital radiography and virtual endocast. – *JOFRI*, **12**, 2018, 31-39.
18. **Nikolova, S., D. Toneva.** Frontal sinus dimensions in the presence of persistent metopic suture**.** – *Acta Morphol. Anthropol*., **26**, 2019, 92-98.
19. **Nikolova, S., D. Toneva, G. Agre, N. Lazarov**. Data mining for peculiarities in the configuration of neurocranium when the metopic suture persists. – *Anthropol. Anz.,* 2019 (*in press*) DOI: 10.1127/anthranz/2019/1051
20. **Toneva, D., S. Nikolova, I. Georgiev.** Reliability and accuracy of angular measurements on laser scanning created 3D models of dry skulls. **–** *J. Anthropol.*, **2016**, 2016, 1-6.
21. **Toneva, D., S. Nikolova, I. Georgiev, A. Tchorbadjieff.** Accuracy of linear craniometric measurements obtained from laser scanning created 3D models of dry skulls. – In: *Advanced computing in industrial mathematics. Studies in computational intelligence* (Eds. Georgiev, K., M. Todorov, I. Georgiev), **681**, Springer, 2017, 215-229.
22. **Toneva, D., S. Nikolova, I. Georgiev, N. Lazarov**. Impact of resolution and texture of laser scanning generated 3D models on landmark identification. – *Anat. Rec.* (Hoboken), 2019 (*in press)* DOI: 10.1002/ar.24272

Institute of Experimental Morphology, Pathology and Anthropology with Museum
Bulgarian Anatomical Society

Acta morphologica et anthropologica, 27 (1-2)
Sofia ● 2020

Segmental Body Composition and its Association with Age and Menopausal Status

Priyanka Das[1], Arup Ratan Bandyopadhyay[2], Jyoti Ratan Ghosh[3]*

[1] *Department of Anthropology, UCSTA, University of Calcutta, Calcutta, India*
[2] *Department of Anthropology, UCSTA, University of Calcutta, Calcutta, India*
[3] *Department of Anthropology, Visva-Bharati University, Santiniketan, India*

***** Corresponding author e-mail: jrghosh@rediffmail.com; jrghosh@visva-bharati.ac.in

The aim of the present study was to evaluate age and menopausal status related changes in body composition among adult Bengali women of West Bengal, India. A total of 750 adult women were measured. The results revealed significant age group wise variations in PBF, subcutaneous fat and skeletal muscles. Correlation analysis revealed that PBF and subcutaneous fat at SFWB, SFT, SFA and SFL was increased with increasing age. However, skeletal muscles at SMWB, SMT, SMA and SML demonstrated inverse correlation with age. The results also revealed that PBF, SFWB, SFT and SFA were higher among post-menopausal women compared to pre-menopausal women. On the other hand, skeletal muscles were higher among pre-menopausal women compared to post-menopausal women. In conclusion, body composition in terms of PBF, subcutaneous fat and skeletal muscle changes with age and menopausal status in women. However, the patterns of changes were different for fat mass and skeletal muscle.

*Key words***:** aging, menopause, segmental body composition, skeletal muscle, subcutaneous fat

Introduction

Body composition refers to the different components that make up a person's body weight [1] and includes both fat and fat-free mass. Body composition changes throughout the human life span by genetically determined aging processes [2, 3, 4]. Age related changes in body composition are characterized by a decrease in fat-free mass (FFM) and an increase in fat mass (FM) [5, 6, 7]. Many women also experience weight gain, increases in central adiposity and other changes in body composition around menopause [8, 9, 10]. Menopause is a condition of female hypogonadism that is characterized by ovarian failure and a rapid and dramatic decrease in female sex hormone production [11]. Epidemiological studies suggested that weight gain during the menopausal transition is associated with aging, physical inactivity and hormonal changes [12]. Studies also demonstrated that age induced changes in body composition have widespread consequences on women's health and functional capacity [11, 13, 14]. Body fat especially that located on the trunk is associated with an increased risk of cardiovascular diseases, type 2 diabetes, hypertension and breast cancer [15, 16].

It is recognized that studies on segmental body composition changes with advancement of age and menopausal status are important for better understanding of adiposity and related mortality and morbidity [4]. Precise techniques used to measure total body fat {under water weighing, dual-energy X-ray absorptiometry (DXA)} and its distribution {computed tomography (CT) scan and magnetic resonance imaging (MRI)} in humans are not appropriate for use in field-based studies because of its cost, radiation exposure, limited availability outside the research setting and also time consuming [17]. However, to obtain a reasonable estimation of body composition bioelectrical impedance analysis (BIA) method is widely used [2, 17]. The BIA is also considered a valid method of total and regional body composition analysis and also less time consuming, non-invasive and inexpensive [18].

There are few data on age and menopausal status related changes in segmental body composition, especially in Indian women. Therefore, the present study was undertaken to evaluate age and menopausal status related changes in body composition among adult Bengali women of West Bengal, India.

Materials and Methods

The present cross-sectional study was conducted on 750 apparently healthy Bengali speaking Hindu adult women from in and around Kolkata, West Bengal, India. Age range of the participants were between 18 to 73 years. The period of data collection was from March, 2015 to April, 2017**.** All participants were asked to complete a questionnaire that included specific information on bio-social information including ethnicity and age. Information about menopausal status was obtained through interviews. Anthropometric measurements namely height and weight were measured using standard procedure [19]. Height was measured using anthropometer to the nearest 0.1 cm. Weight was measured using a weighing machine to the nearest 0.1 kg. Body compositions were measured using Omron body composition monitor (Karada Scan, HBF-375). Body composition variables include percent body fat (PBF), subcutaneous fat at whole body (SFWB), trunk (SFT), arm (SFA) and leg (SFL) as well as skeletal muscle at regions like whole body (SMWB), trunk (SMT), arm (SMA) and leg (SML). Prior to the study informed consent was obtained from each participant. Pregnant, lactating women and individuals with low bone density were excluded from the study. Ethical clearance was taken from institutional ethical clearance board. Descriptive statistics includes mean and standard deviation (SD). Inferential statistics including t-test, one-way ANOVA and Pearson correlation have been applied. A p-value of 0.05 was considered as significant. All analyses were performed using the statistical program SPSS, Inc., Chicago, IL; version, 16.

Results

Characteristics of the studied participants were presented in **Table 1.** Mean age of the studied population was 41.19 ± 13.89 years. **Table 2** shows age specific changes in body composition. The participants were categorized in five age (≤30, 31-40, 41-50, 51-60, >61) groups. The results revealed significant ($p<0.05$) age group wise variations in PBF as well as in subcutaneous fat and skeletal muscle. The results of the Pearson correlation analysis revealed that body fat in terms of PBF and subcutaneous fat at whole body, trunk, arm and leg was increasing with increasing age significantly ($p<0.05$; **Table 3**).

Table 1. Characteristics of the studied participants

Variables	Mean	SD
Age (year)	41.19	13.89
Height (cm)	150.53	5.69
Weight (kg)	59.82	12.00
PBF (%)	35.19	6.27
SFWB (%)	31.93	5.10
SFT (%)	28.61	5.12
SFA (%)	49.77	5.52
SFL (%)	44.77	6.62
SMWB (%)	22.10	2.38
SMT (%)	16.69	2.58
SMA (%)	23.16	4.16
SML (%)	34.35	2.66

PBF= percent body fat, SFWB= subcutaneous fat at whole body, SFT= subcutaneous fat at trunk, SFA = subcutaneous fat at arm, SFL = subcutaneous fat at leg, SMWB = skeletal muscle at whole body, SMT = skeletal muscle at trunk, SMA = skeletal muscle at arm, SML = skeletal muscle at leg

Table 2. Age specific changes in body composition

Variables	≤ 30years		31-40years		41-50years		51-60years		> 61years		
	n = 198		n= 191		n=163		n=127		n=71		
	Mean	SD	Mean	SD	Mean	SD	Mean	SD	Mean	SD	*P*
PBF (%)	33.31	6.62	34.99	5.61	35.82	6.32	36.57	6.03	37.12	6.03	<0.05
SFWB (%)	30.06	5.55	31.91	4.67	32.73	4.81	33.08	4.90	33.34	4.59	<0.05
SFT (%)	26.41	5.65	28.31	4.45	29.36	4.59	30.38	4.98	30.73	4.33	<0.05
SFA (%)	47.51	6.01	49.59	5.03	50.68	5.31	51.54	4.94	51.65	4.60	<0.05
SFL (%)	43.56	7.21	45.43	6.28	45.58	6.61	44.91	6.17	44.35	6.31	<0.05
SMWB (%)	23.78	2.22	22.70	2.15	21.61	1.69	20.60	1.65	19.62	1.71	<0.05
SMT (%)	18.78	2.48	17.28	2.01	16.01	1.86	14.95	1.69	13.96	1.64	<0.05
SMA (%)	25.26	4.56	23.42	3.71	22.40	3.91	21.70	3.49	20.98	3.02	<0.05
SML (%)	35.87	2.28	34.89	2.44	34.07	2.27	32.92	2.41	31.87	2.29	<0.05

Table 3. Correlation of age with body composition measures

Variables	r	*p*
PBF (%)	0.208	<0.05
SFWB (%)	0.232	<0.05
SFT (%)	0.309	<0.05
SFA (%)	0.279	<0.05
SFL (%)	0.050	<0.05
SMWB (%)	-0.592	<0.05
SMT (%)	-0.637	<0.05
SMA (%)	-0.355	<0.05
SML (%)	-0.504	<0.05

However, skeletal muscles at whole body, trunk, arm and leg demonstrated significant ($p<0.05$) negative correlation with age. Menopausal status wise comparison in body compositions were presented in **Table 4**. Result revealed significant ($p<0.05$) differences in all body composition variables except SFL ($p>0.05$) between pre-menopausal and post-menopausal women. The results also revealed that PBF, SFWB, SFT and SFA were significantly higher among post-menopausal women compared to pre-menopausal women. However, SFL was also comparatively higher among post-menopausal women as compared to pre-menopausal women. On the other hand, skeletal muscles (SMWB, SMT, SMA and SML) were significantly ($p<0.05$) higher among pre-menopausal women compared to post-menopausal women.

Table 4. Menopausal status wise comparison in body composition

Variables	Pre-menopause		Post-menopause		*p*
	n = 456		n = 294		
	Mean	SD	Mean	SD	
PBF (%)	34.43	6.17	36.38	6.27	<0.05
SFWB (%)	31.21	5.26	33.06	4.65	<0.05
SFT (%)	27.59	5.21	30.20	4.57	<0.05
SFA (%)	48.75	5.69	51.44	4.82	<0.05
SFL (%)	44.60	6.90	45.11	6.24	>0.05
SMWB (%)	23.06	2.25	20.62	1.73	<0.05
SMT (%)	17.77	2.46	15.03	1.78	<0.05
SMA (%)	24.10	4.33	21.71	3.42	<0.05
SML (%)	35.26	2.42	32.95	2.40	<0.05

Discussion

The loss of FFM and increased FM with age has been acknowledged in a number of previous studies [14, 20, 21, 22]. The present study is the first attempt among adult Bengali women to evaluate age and menopausal status related changes in segmental body composition. We found that body composition in terms of PBF as well as subcutaneous fat and skeletal muscle changes with age. However, the pattern of changes was different for fat mass and skeletal muscle. It was observed that fat mass measures like PBF and subcutaneous fat at whole body, trunk, arms and legs were increased with age. Contrary to that, fat free mass like skeletal muscles at whole body, trunk, arms and legs were decreased with the advancement of age.

The results of the present study corroborate with both cross sectional [3] and longitudinal [23] studies that demonstrated the amount of FM increases with age. In accordance with the present study, previous study by Cohn et al. [24] also observed that increasing age was associated with a greater decrease in muscle than non-muscle mass. In a recent study among Han, He et al. [7] also demonstrated a decrease in FFM and increase in PBF with age. Similar findings of greater loss in skeletal muscle mass than non-skeletal muscle mass with age were also observed by Kyle et al. [20].

The loss of FFM is interrelated with a number of factors in the elderly like decline resting metabolic rate [25], sarcopenia and related impaired mobility, increased morbidity and mortality as well as lower quality of life [20, 21] and increased risk for cardiovascular diseases [26].

Study demonstrated that these changes in body composition with aging may be due to an imbalance between energy intake and energy needs associated with increasing sedentary lifestyle [20]. Other mechanisms associated with these age-related changes include neuronal and hormonal changes as well as inflammation [27]. Moreover, among women, notable age-related changes in body composition were also observed particularly after menopause [3]. In the present study we also found a comparatively higher fat mass in terms of PBF, SFWB, SFT, SFA and SFL among post-menopausal women than pre-menopausal women. However, different patterns were observed for skeletal muscles (SMWB, SMT, SMA and SML), which were higher among pre-menopausal women as compared to post-menopausal women. In a study Gambacciani et al. [28] also demonstrated significantly higher mean PBF and regional fat percentage at trunk and arm in post-menopausal women than in the pre-menopausal women. In that study total lean tissue was also significantly less in post-menopausal women than in pre-menopausal women. Svendsen et al. [29] demonstrated that total body fat and abdominal fat increases and lean tissue mass decreases after menopause. Study also demonstrated that the decrease in FFM is more menopause related, whereas the shift toward upper body fat distribution and overall adiposity are more age related [30]. However, in contrary to the results of the present study a previous study by Toth et al. [31] demonstrated no differences in FFM or appendicular skeletal muscle mass between pre-menopausal and post-menopausal women, though PBF was higher in post-menopausal women as compared with pre-menopausal women. The relationship between menopausal status and changes in body composition may be associated with the hormonal changes in terms of decreased estrogen and progesterone concentrations and increase gonadotrophins, follicle-stimulating and luteinizing hormones [11].

Conclusion

In conclusion, body composition in terms of PBF as well as subcutaneous fat and skeletal muscle changes with age and menopausal status in women. However, the patterns of changes were different for fat mass and skeletal muscle.

Acknowledgements: The authors are grateful to all the participants of the study. Authors are also grateful to Swami Vivekananda Single Girl Child Scholarship for Research in Social Sciences (SVSGC-UGC), Government of India for providing financial support.

References

1. **Shah, A. H., R. Bilai.** Body composition, its significance and model for assessment. – *Pak. J. Nutr.,* **8**, 2009, 198-202.
2. **Sillanpaa, E., S. Cheng, K. Hakkinen, T. Finni, S. Walker, A. Pesola, J. Ahtiainen, L. Stenroth, H. Selanne, S. Sipil.** Body composition in 18 to 88-year old adults: comparison of multifrequencybioimpedance and dual energy X-ray absorptiometry. – *Obesity,* **22,** 2014, 101-109.
3. **Gaba, A., M. Pridalova.** Age-related changes in body composition in a sample of Czech women aged 18-89 years: a cross-sectional study. – *Eur. J. Nutr.,* **53**, 2014, 167-176.
4. **Tian, S, B. Morio, J. B. Denis, L. Mioche.** Age related changes in segmental body composition by ethnicity and history of weight change across the adult lifespan. – *Int. J. Environ. Res. Public Health,* **13,** 2016, 821-838.
5. **Hughes, V., W. Frontera, R. Roubenoff, W. Evans, M. Singh.** Longitudinal changes in body composition in older men and women: role of body weight change and physical activity. – *Am. J. Clin. Nutr.*, **76**, 2002, 473-481.
6. **Stenholm, S., T. B. Harris, T. Rantanen, M. Visser, S. B. Kritchevsky, L. Ferrucci.** Sarcopenic obesity – definition, etiology and consequences. – *Curr. Opin. Clin. Nutr. Metab. Care*, **11**, 2008, 693-700.
7. **He, X., Z. Li, X. Tang, L. Zhang, L. Wang, Y. He, T. Jin, D. Yuan.** Age- and sex-related differences in body composition in healthy subjects aged 18 to 82 years. – *Medicine*, **97**, 2018, 25- 30.
8. **Weiner, J. S., J. A. Lourie.** *Human biology: a guide to field methods*. Academic Press Inc, London. 1981.
9. **Simkin-Silverman, L. R., R. R. Wing, M. A. Boraz, L. H. Kuller.** Lifestyle intervention can prevent weight gain during menopause: results from a 5-year randomized clinical trial. – *Ann. Behav. Med.,* **26**, 2003, 212-220.
10. **Freeman, E.W., M. D. Sammel, H. Lin, C. R. Gracia.** Obesity and reproductive hormone levels in the transition to menopause. – *Menopause*, ***17***, 2010, 718-726.
11. **Sipila, S**. Body composition and muscle performance during menopause and hormone replacement therapy. – *J. Endocrinol. Invest.,* **26**, 2003, 893-901.
12. **Spadafranca, A., L. Vignati, A. Battezzati, S. Bertoli.** Body composition and metabolic risk factors in postmenopausal women: effects of a dietary weight loss program. – *F. N. S.*, **4**, 2013, 420-429.
13. **Lahmann, P. H., L. Lissner, B. Gullberg, G. Berglund.** A prospective study of adiposity and all-cause mortality: the Malmö diet and cancer study. – *Obes. Res.*, **10**, 2002, 361-369.
14. **Makizako, H., H. Shimada, T. Doi, K. Tsutsumimoto, S. Lee, S. C. Lee, K. Harada, R. Hotta, S. Nakakubo, S. Bae, K. Harada, D. Yoshida, K. Uemura, Y. Anan, H. Park, T. Suzuki.** Age-dependent changes in physical performance and body composition in community-dwelling Japanese older adults. – *J. Cachexia Sarcopenia Muscle,* **8**, 2017, 607-614.
15. **Ulijaszek, S. J., S. S. Strickland.** 1996. Body mass index and fat patterning of adults in rural Sarawak. – *Malays. J. Nutr.,* **2**, 1996, 128-136.
16. **Brown, D. E., P. T. Katzmarzyk, L. A. Gotshalkb.** Physical activity level and body composition in a multiethnic sample of school children in Hawaii. – *Ann. Hum. Biol.,* **45**, 2018, 244-248.
17. **Taing, K. Y., M. E. Farkouh, R. Moineddin, J. V. Tu, P. Jha.** Comparative associations between anthropometric and bioelectric impedance analysis derived adiposity measures with blood pressure and hypertension in India: a cross-sectional analysis. – *B.M.C. Obesity*, **4**, 2017, 37-47.

18. **Malavolti, M., C. Mussi, M. Poli, A. L. Fantuzzi, G. Salvioli, N. Battistini, G. Bedogni.** Cross-calibration of eight-polar bioelectrical impedance analysis versus dual-energy X-ray absorptiometry for the assessment of total and appendicular body composition in healthy subjects aged 21-82 years. – *Ann. Hum. Biol.*, **30**, 2003, 380-391.
19. **Wannamethee, S. G., J. L. Atkins.** Muscle loss and obesity: the health implications of sarcopenia and sarcopenic obesity. – *Proc. Nutr. Soc.,* **74**, 2015, 405-412.
20. **Kyle, U. G., L. Genton,** D**. Hans, L. Karsegard, D. O. Slosman, C. Pichard.** Age-related differences in fat-free mass, skeletal muscle, body cell mass and fat mass between 18 and 94 years. – *Eur. J. Clin. Nutr.,* **55,** 2001, 663-672.
21. **Campbell, T. M,. L. A. Vallis.** Predicting fat-freemass index and sarcopenia in assisted-living older adults. – *Age*, **36**, 2014, 9674-9687.
22. **Pedrera-Zamorano, J. D., R. Roncero-Martin, J. M. Lavado-Garcia, J. F. Calderon-Garcia, P. Rey-Sanchez, V. Vera, M. Martinez, J. M. Moran.** Segmental fat free and fat mass measurements by bioelectrical impedance analysis in 2,224 healthy Spanish women aged 18-85 years. – *Am. J. Hum. Biol.,* **27**, 2015, 468-474.
23. **Kyle, U. G., K. Melzer, B. Kayser, M. Picard-Kossovsky, G. Gremion, C. Pichard.** Eight-year longitudinal changes in body composition in healthy Swiss adults. – *J. Am. Coll. Nutr.,* **25**, 2006, 493-501.
24. **Cohn, S. H., A. N. Vaswani, S. Yasumura, K. Yuen, K. J. Ellis.** Assessment of cellular mass and lean body mass by noninvasive nuclear techniques. – *J. Lab. Clin. Med.*, **105**, 1985, 305 -311.
25. **Tzankoff, S. P., A. H. Norris.** Effect of muscle mass decrease on age related BMR changes. – *J. Appl. Physiol.*, **43**, 1977, 1001-1006.
26. **Heitmann, B. L., H. Erikson, B. M. Ellsinger, K. L. Mikkelsen, B. Larsson.** Mortality associated with body fat, fat-free mass and body mass index among 60-year-old Swedish men-a 22-year follow-up: the study of men born in 1913. – *Int. J. Obes. Relat. Metab. Disord.*, **24**, 2000, 33- 37.
27. **Wing, R.R., K. A. Matthews, L. H. Kuller, E. N. Meilahn, P. L. Plantinga.** Weight gain at the time of menopause. – *Arch. Intern. Med.,* 151, 1991, 97-102.
28. **Gambacciani, M., M. Ciaponi, B. Cappagli, C. Benussi, L. De Simone, A. R. Genazzani.** Climacteric modifications in body weight and fat tissue distribution. – *Climacteric,* **2**, 1999, 37-44.
29. **Svendsen, O. L., C. Hassager, C. Christiansen.** Age and menopause-associated variations in body composition and fat distribution in healthy women as measured by dual-energy x-ray absorptiometry. – *Metabolism,* **44**, 1995, 369-373.
30. **Douchi, T., S. Yamamoto, N. Yoshimitsu, T. Andoh, T. Matsuo, Y Nagata.** Relative contribution of aging and menopause to changes in lean and fat mass in segmental regions. – *Maturitas*, **42**, 2002, 301-306.
31. **Toth, M. J., A. Tchernof, C. K. Sites, E. T. Poehlman.** Effects of menopausal status on body composition and abdominal fat distribution. – *Int. J. Obes.,* **24**, 2000, 226-231.

Institute of Experimental Morphology, Pathology and Anthropology with Museum
Bulgarian Anatomical Society

Acta morphologica et anthropologica, 27 (1-2)
Sofia ● 2020

High Origin of the Superficial Palmar Branch of the Radial Artery Extending into the Princeps pollicis Artery

*Nikoleta Vulova, Todor Kirov, Lina Malinova, Lazar Jelev**

Department of Anatomy, Histology and Embryology, Medical University, Sofia, Bulgaria

* Corresponding author e-mail:ljelev@abv.bg

The clinical applications of the radial artery depend on its "standard" anatomy. In the literature, however, there are many variations of the radial artery described, that may hamper clinical procedures. In this case report, we present some variations in the branching pattern of radial artery, foundin the right upper limb of an embalmed male cadaver. The superficial palmar branch of the radial artery started from the radial artery at unusually high level - nearly 10 cm proximal to the wrist. The aberrant vessel passed just under the thenar muscle fascia and underneath the palmar aponeurosis it bifurcated into the princeps pollicis and radialis indicis arteries. Based on the presence of a small sized anastomosis at the level of the superficial palmar arch, it seemed that the main thumb arterial supply in this case depends on the variant superficial palmar branch of the radial arteryof high origin.

Key words: radial artery, superficial palmar branch of the radial artery, princeps pollicis artery, arterial variations, upper limb

Introduction

The radial artery is a mid-sized vessel (external diameter about 3mm) [16] that follows the radial side of the anterior forearm, covered by the brachioradialis muscle [4, 7]. At the wrist, the radial artery sends a superficial branch to the superficial palmar arch from the ulnar artery and turning dorsally around the scaphoid and trapezium it passes through the muscles of the first interosseus (web) space. Here, the artery sends several branches to the palmar and dorsal sides of the thumb [4, 7]. The wrist portion of the radial artery is superficially located and with a proper diameter to provide a good vascular access site for interventional procedures [6, 21, 2]. The wide clinical application of the radial artery, either harvested as an arterial conduit for surgery or temporarily occluded for catheterization procedures, is based on the presumption that its anatomy is nearly corresponding to the classical textbook descriptions [4, 7] and most importantly – a good collateral system exists between the superficial and deep palmar arches [18, 22]. As a matter of fact, however, the radial artery system is variable in its antebrachial [10, 12, 22] and especially its distal parts [11, 16, 17], thus presenting a real danger of radial catheterization failure [24] or post-procedure thumb ischemia [13, 18, 23, 25].

Materials and Methods

The variations reported were observed during routine student dissections of the right upper limb of an adult formalin-fixed male cadaver of Caucasian descent. All dissections took place at the Department of Anatomy, Histology and Embryology, Medical University of Sofia.

Case report

The present case report describes variations in the branching pattern of radial artery in the distal third of the forearm, wrist and hand. The most noticeable finding was a large sized superficial palmar branch of the radial artery supplying the thumb. Upon dissecting the forearm vessels we noticed that the radial artery bifurcated nearly 10 cm above the distal wrist crease into two equal in size branches (**Fig. 1a; Fig. 2b**).

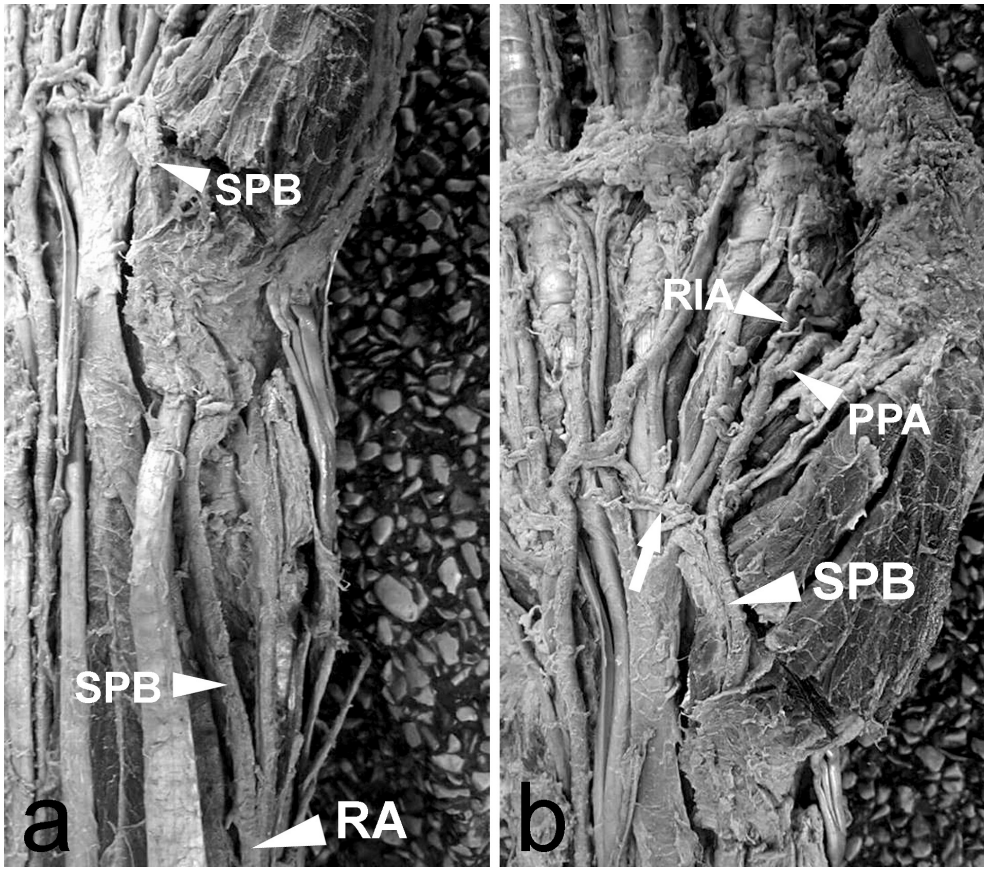

Fig. 1a, b. Anterior view of the forearm and wrist (**a**) and hand (**b**) demonstrating the variant branching pattern of the radial artery. Arteries: RA – radial artery; SPB – superficial palmar branch; PPA – princeps pollicis artery; RIA – radialisindicis artery. The white arrow indicates the small anastomosis between the superficial palmar branch of the radial artery and the distal ulnar artery within the superficial palmar arch.

The following dissection revealed that the medial one continued into the superficial palmar branch of the radial artery, while the lateral one extended into the distal part of the radial artery. The superficial palmar branch of the radial artery measured about 2.5 mm of external diameter and initially coursed parallel to the main radial artery, on its medial site, and lateral to the median nerve and flexor carpi radialis muscle. The superficial palmar branch crossed the thenar muscle tendons superficially and continued underneath the palmar aponeurosis. A dissection of this vessel showed that it bifurcated further into the princeps pollicis artery, providing radial and ulnar palmar arteries to the thumb and the radialisindicis artery (**Fig. 1b; Fig. 2b**). At the level of the origin of the flexor pollicis brevis muscle, the superficial palmar branch of the radial artery sent a small anastomosing branch (less than 1 mm in diameter) to the superficial palmar arch. The distal part of the usual radial artery had a normal course through the anatomical snuff box and first interosseous space without giving significant side branches. Entering the deep palmar region of the hand, the radial artery extended into the deep palmar arch that anastomosed at the end with a small deep palmar branch of the ulnar artery.

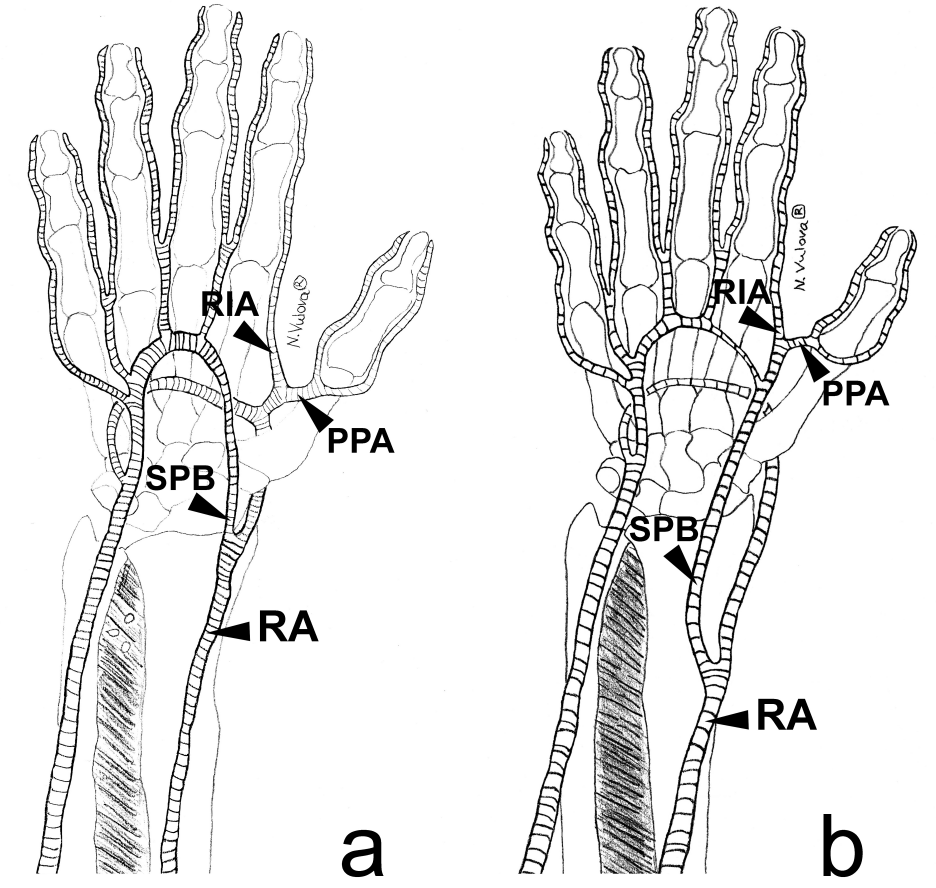

Fig. 2a, b. Schemes of the normal (**a**) and variant (**b**) branching pattern of the distal radial artery as described in our case. Arteries: RA – radial artery; SPB – superficial palmar branch; PPA – princeps pollicis artery; RIA – radialis indicis artery.

Discussion

In the case reported, there are variations of both antebrachial and distal parts of the radial artery, each one presenting distinctive clinical problems. Radial artery at the distal forearm and wrist is safe and effective vascular access site for the coronary and cerebrovascular interventional procedures [21]. This artery is preferred over brachial, axillary and femoral arteries for smaller size catheters based on its anatomical features [5, 8]. Moreover, the anterbrachial portion of the radial artery is about 20 cm long and is considered an adequate auto-conduit for coronary system routinely harvested for coronary artery bypass graft surgery [1, 3]. Because of the high division of the radial artery, as reported here, at the typical wrist site instead of one large, two parallel smaller arteries were identified. Such a variant pattern has already been recognized as a potential problem for radial artery catheterization [12]. Moreover harvesting of such a bifurcated radial artery will not be desired for surgery.

Regarding the distal part of radial artery, the presence of a large sized superficial palmar branch providing mainly the blood supply of the thumb might be important in plastic and reconstructive surgery of the hand [20]. The presence of only small sized anastomosing branches between the distal parts of the radial and ulnar arteries, as reported in our case, might create a higher risk of thumb ischemia if radial artery is harvested for surgery or occluded by catheter. The higher origin of the superficial palmar branch of the radial artery has been reported previously [9], so is its branching into princeps pollicis and radialis indicis arteries [2, 14, 15, 19]. However, such a high origin of the superficial palmar branch of the radial artery providing mainly the thumb blood supply has not been described previously. In our dissection series, it was the only case in over 50 upper limbs dissected.

References

1. **Alameddine, A. K., V. K. Alimov, R. M. Engelman, J. A. Rousou, J. E. Flack, D. W. Deaton, D. T. Engelman**. Anatomic variations of the radial artery: significance when harvesting for coronary artery bypass grafting. – *J. Thorac. Cardiovasc. Surg.*, **127**, 2004, 1825-1827.
2. **Ames, E. L., M. Bissonnette, R. Acland, G. Lister, J. Firrell**. Arterial anatomy of the thumb. – *J. Hand Surg. Br.*, **18**, 1993, 427-436.
3. **Baikoussis, N. G., N. A. Papakonstantinou, E. Apostolakis**. Radial artery as graft for coronary artery bypass surgery: Advantages and disadvantages for its usage focused on structural and biological characteristics. – *J. Cardiol*., **63**, 2014, 321-328.
4. **Bannister, L. H., M. Berry, P. Collins, M. Dyson, M. W. J. Ferguson** (Eds.). *Gray's Anatomy*, 38th Ed, Edinburgh, Churchill Livingstone, 1995, 1540-1544.
5. **Bianchi, R., L. D'Acierno, M. Crisci, D. Tartaglione, M. Cappelli Bigazzi, M. Canonico, M. Albanese, F. Gragnano, F. Fimiani, M. Russo, P. Cirillo, P. Calabrò**. From femoral to radial approach in coronary intervention angiology. – *Angiology*, **68**, 2017, 281-287.
6. **Chugh, S. K., Y. Chugh, S. Chugh**. How to tackle complications in radial procedures: Tip and tricks. – *Indian Heart J*., **67**, 2015, 275–281.
7. **Clemente, C. D.** (Ed.). *Anatomy of the Human Body,* 30th Ed, Philadelphia, Lea and Febiger, 1985, 715-728.
8. **Franchi, E., P. Marino, G. G. Biondi-Zoccai, G. De Luca, C. Vassanelli, P. Agostoni**. Transradial versus transfemoral approach for percutaneous coronary procedures. – *Curr. Cardiol. Rep*., **11**, 2009, 391-397.
9. **Gupta, C., B. Ray, A. S. Dsouza, N. Nair, S. R. Pai, M. Manju**. A morphological study of variations in the branching pattern and termination of the radial artery. – *Singapore Med. J*., **53**, 2012, 208-211.
10. **Icten, N., Y. Sullu, I. Tuncer**. Variant high-origin radial artery: a bilateral case. – *Surg. Radiol. Anat.*, **18**, 1996, 63-66.

11. **Ilić, M., M. Milisavljević, A. Maliković, D. Laketić, D. Erić, J. Boljanović, A. Dožić, B. V. Štimec**, **R. Manojlovic**. The superficial palmar branch of the radial artery: a corrosion cast study. – *Folia Morphol. (Warsz),* **77**, 2018, 649-655.
12. **Jelev, L, L.Surchev.** Radial artery coursing behind the biceps brachii tendon: Significance for the transradial catheterization and a clinically oriented classification of the radial artery variations. – *CardioVasc. And Intervent. Radiol.*, **31**, 2008, 1008-1012.
13**. Kleinert, J. M., S. G.Fleming, C. S. Abel, J. Firrell.** Radial and ulnar artery dominance in normal digits. – *J. Hand Surg. Am.*, **14**, 1989, 504-508.
14. **Loukas, M., S. Tubbs, R. G. Jr Louis, N. Apaydin.** Princeps pollicis artery arising from the superficial palmar arch. – *Singapore Med. J.*, **50**, 2009, 391-392.
15. **Madhyastha, S., B. V. Murlimanju, P. J. Jiji, V. V. Saralaya, A. Rai, R. Vadgaonkar.** Morphological variants of the human superficial palmar arch and their clinical implications. – *J. Morphol. Sci.*, **28**, 2011, 261-264.
16. **Nasr, A**. The radial artery and its variations: Anatomical study and clinical implications. – *Folia Morphol.*, **71**, 2012, 252-262.
17. **Ottone, N., N. Prum, M. Dominguez, E. Blasi, C. Medan, S. Shinzato, D. Finkelstein, V. Bertone.** Analysis and clinical importance of superficial arterial palmar irrigation and its variants over 86 cases. – *Int. J. Morphol.*, **28**, 2010, 157-164.
18. **Parks, B. J., J. Arbelaez, R. L. Horner.** Medical and surgical importance of the arterial blood supply of the thumb. – *J. Hand Surg. Am.*, **3**, 1978, 383-385.
19. **Ramirez, A. R., S. M. Gonzalez.** Arteries of the thumb: Description of anatomical variations and review of the literature. – *PlasticReconstr. Surg.*, **29**, 2012, 468-476.
20. **Rinker, B.** Fingertip reconstruction with the laterally based thenar flap: Indications and long-term functional results. - *Hand (NY),* **1**, 2006, 2-8.
21. **Satti, S. R., A. Z. Vance, T. Sivapatham.** Radial access for cerebrovascular procedures: Case report and technical note. – *Interv. Neuroradiol*., **22**, 2016, 227-235.
22. **Schussler, J. M.** Effectiveness and safety of transradial artery access for cardiac catheterization. – *Proc.(Bayl. Univ. Med. Cent.)*, **24**, 2011, 205–209.
23. **Türker, T., N. Capdarest-Arest.** Acute hand ischemia after radial artery cannulation resulting in amputation. – *Chir. Main*., **33**, 2014, 299-302.
24. **Valsecchi, O., A. Vassileva, G. Musumeci, R. Rossini, M. Tespili, G. Guagliumi, L. Mihalcsik, A. Gavazzi, P. Ferrazzi.** Failure of transradial approach during coronary interventions: anatomic considerations. – *Catheter Cardiovasc. Interv.*, **67**, 2006, 870-878.
25. **Wilkins, R.G.** Radial artery cannulation and ischaemic damage: A review. – *Anaesthesia*, **40**, 1985, 896-899.

Institute of Experimental Morphology, Pathology and Anthropology with Museum
Bulgarian Anatomical Society

Acta morphologica et anthropologica, 27 (1-2)
Sofia ● 2020

Absence of Palmaris Longus Muscle and Flexor Digitorum Superficialis Muscle Tendon to the Little Finger – Incidence in the Bulgarian Population

Matei Popnikolov[1], Mustafa Barzev[1], Alexandar Iliev[1], Boycho Landzhov[1], Georgi P. Georgiev[2]*

[1] *Department of Anatomy, Histology and Embryology, Medical University, Sofia, Bulgaria*
[2] *Department of Orthopaedics and Traumatology, University Hospital Queen Giovanna – ISUL, Medical University, Sofia, Bulgaria*

* Corresponding author e-mail: dralexiliev@abv.bg

Palmaris longus (PL) and flexor digitorum superficialis muscles (FDS) are some of the variable muscles in the human body. The absence of PL and FDS tendon of the little finger are the two most frequently reported variations. The aim of the study was to analyse the absence of PL and absence of FDS tendon of the little finger with clinical tests. We examined 100 cases using three tests to visualize the tendons of PL and FDS. We found bilateral absence of PL in 29% of the cases and bilateral absence of FDS tendon of the little finger in 15% of cases. In conclusion, absence of PL in the Bulgarian population is higher than this in other Caucasian populations (5.5% - 24%). Conversely, our results for absence of tendon of the little finger FDS showed that it is approximately the same as in other Caucasians (15% - 22%).

Key words: upper limb, palmaris longus muscle, flexor digitorum superficialis muscle, variations, clinical significance

Introduction

The palmaris longus muscle (PL) has a thin, elongated muscle body which is located medially to the flexor carpi radialis muscle. It arises from the medial epicondyle of the humerus via the common flexor tendon and is attached to the distal portion of the flexor retinaculum and the palmar aponeurosis [4]. This muscle body prolongs into a short tendon between the flexor carpi radialis and the flexor carpi ulnaris. PL is described as an additional weak flexor of the wrist which cramps the palmar aponeurosis [4]. In the human body, PL is one of the most variable muscles and the main reported variation is its absence [4]. Earlier reports have pointed out that absence of PL is found in 5.5% to 24% of Caucasian populations (European and North American) and 4.6% to 26.6% of Asian populations (Chinese, Japanese, Indian, Turkish and Malaysian) [4, 14, 15].

The flexor digitorum superficialis muscle (FDS) of the forearm has a flat muscle body, which arises from the medial epicondyle of the humerus and passes through the

carpal tunnel. FDS is one of the largest superficial flexor muscles of the forearm and is situated medially and deep to the PL and flexor carpi ulnaris muscle [8]. The terminal tendons of FDS split into smaller ones that insert at the bases of the intermediate phalanges of the second to fifth fingers. The function of FDS is to flex the proximal interphalangeal joints and the metacarpophalangeal joints of the hand [8]. Similar to PL, FDS is also a very variable muscle. The most frequently observed variation is the absence of its tendon to the little finger [8, 9]. According to one study in the Indian population, FDS tendon to the little finger was bilaterally absent in 42% of subjects [1, 13]. Unilateral absence was reported in 6.1% of cases on the right side and 8.6% of cases on the left. The prevalence of the absence of FDS tendon to the little finger has also been studied in other studied populations – for instance, in the Caucasian population (15–21%) and in the Chinese population (6.4%) [14, 15].

Considering the fact that both muscles share the same innervation, have similar functions, belong to the same muscle lodge and are highly variable in existence and function, it has been hypothesised that their absence may be related [17]. Embryologically, the flexor muscles of the forearm expand from the flexor mass following its division into two layers – superficial and deep. FDS, the flexor digitorum profundus (FDP) and the flexor pollicis longus arise from the deep layer, while the pronator teres, PL, flexor carpi radialis and flexor carpi ulnaris muscle arise from the superficial one [8, 9]. Failure of cleavage of the superficial layer of the forearm flexor mass during the embryological development could be a possible reason for the absence of PL. Failure of cleavage of the deep layer of the forearm flexor mass could, respectively, lead to anatomical variations of FDS [10].

The tendon of PL can be observed through several clinical tests. One of the methods is by touching the pads of the little finger and thumb and flexing the wrist. The presence of the tendon can be seen in the middle of the anterior wrist. This examination is known as Schaeffer's standard test [14]. Thompson's test is another test, where a person clenches his/her fist, followed by flexing the wrist against resistance with the thumb flexed over the fingers [11, 12]. The presence of FDS's tendon for the little finger is usually examined by asking the patient to flex the little finger with the rest positioned in extension at the interphalangeal joints to neutralize the action of FDP. FDS tendon of the little finger is reported absent when there is no ability to flex the little finger within 20° of the passive range of motion of the finger [11, 12].

The aim of the current study was to analyse the absence of PL and FDS tendon of the little finger and functional deficiency of FDS through different clinical tests and to establish a possible correlation in the Bulgarian population.

Materials and Methods

In the present study, we examined 100 students from both sexes at the Department of Anatomy, Histology and Embryology of the Medical University of Sofia. All participants provided their informed consent. The examinations were performed through Schaeffer's standard test and Thompson's test for visualisation of the tendon of PL and the test for visualization of FDS tendon of the little finger as described above. Photos were taken and the obtained data were summarised and analysed through Microsoft Excel 2010. The obtained quantitative data were demonstrated with diagrams.

Results

In the present study, we reported absence of PL in 29 cases (29%). Absence of FDS tendon of the little finger was noted in 15 cases (15%). In 2 cases (2%), we noted bilateral absence of PL and absence of FDS tendon of the little finger. Only 2 cases (2%) had unilateral absence of PL and FDS on the left or right hand. Bilateral presence of these muscles was documented in 38 cases (38%). Furthermore, 12 (12%) of the examined cases had bilateral absence of PL and bilateral presence of FDS. On the other hand, there were 10 cases (10%) that had bilateral presence of PL and bilateral absence of FDS (**Fig. 1; Fig. 2; Fig. 3**).

In line with the above findings, we divided the cases into six different groups. The groups were distinguished according to the absence or presence of each of the examined muscles. Thus, we established the following groups:

Group 1: Bilateral presence of PL and bilateral presence of FDS – 21 males and 17 females (38%);
Group 2: Bilateral absence of PL and bilateral presence of FDS – 7 males and 5 females (12%);
Group 3: Right presence of PL (left absence) and bilateral presence of FDS – 8 males and 4 females (12%);
Group 4: Bilateral presence of PL and right presence of FDS (left absence) – 4 males and 6 females (10%);
Group 5: Bilateral presence of PL and bilateral absence of FDS – 1 male and 9 females (10%);
Group 6: Bilateral presence of PL and left presence of FDS (right absence) – 2 males and 4 females (6%).

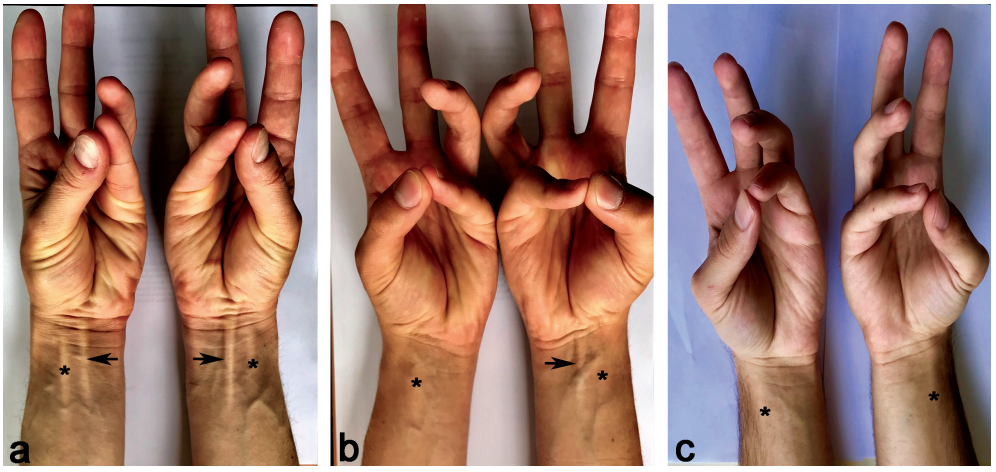

Fig. 1. Schaeffer's standard test for visualization of the tendon of the palmaris longus muscle (PL): bilateral presence of PL (a); right presence of PL (b); bilateral absence of PL (c); arrows - tendons of the tested muscles; asterisks – flexor carpi radialis muscle

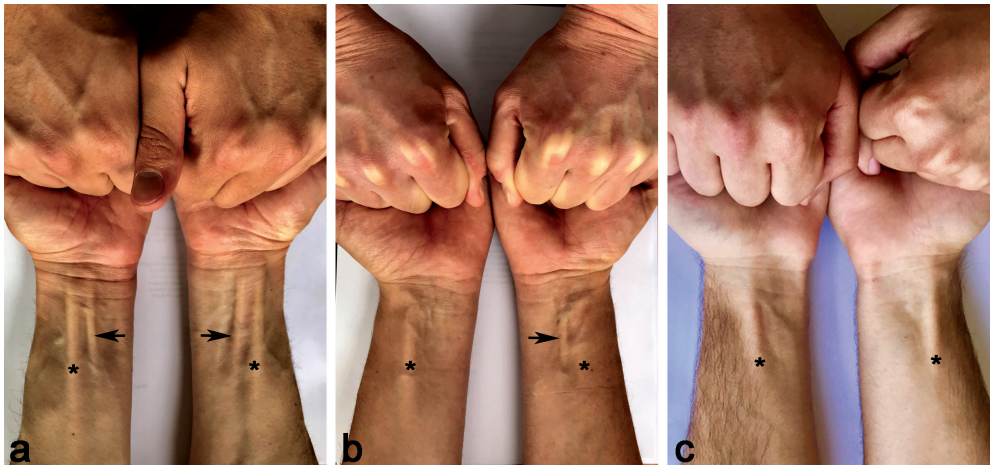

Fig. 2. Thompson's test for visualization of the tendon of the palmaris longus muscle (PL): bilateral presence of PL (a); right presence of PL (b); bilateral absence of PL (c) arrows - tendons of the tested muscles; asterisks – flexor carpi radialis muscle

Fig. 3. Test for visualization of the tendon of flexor digitorum superficialis muscle (FDS) for the little finger: bilateral presence of FDS tendon (a); right presence of FDS tendon (b); bilateral absence of FDS tendon (c)

The distribution of the cases in the groups after cluster analysis is summarized in the following tables (**Table 1; Table 2**) and figures (**Fig. 4; Fig. 5**):

Table 1. Data on the examination of palmaris longus muscle in males and females.

Palmaris longus muscle	Schaeffer's standard test		Thompson's test	
	Males (%)	Females (%)	Males (%)	Females (%)
Bilateral presence	42	64	52	66
Right absence	2	8	6	8
Left absence	18	8	16	8
Bilateral absence	38	20	26	18

Table 2. Data on the examination of flexor digitorum superficialis muscle in males and females.

Flexor digitorum superficialis muscle	Males (%)	Females (%)
Bilateral presence	74	56
Right absence	6	10
Left absence	12	12
Bilateral absence	8	22

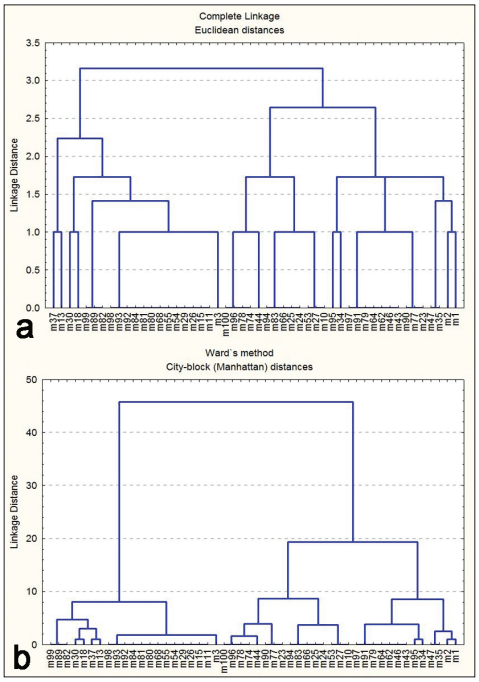

Fig. 4. Cluster analysis of male cases: Complete-linkage clustering (a); Ward's method (b); m-male

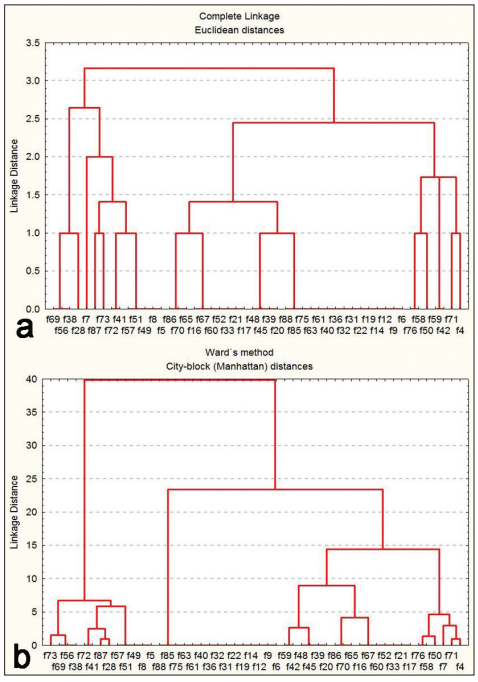

Fig. 5. Cluster analysis of female cases: Complete-linkage clustering (a); Ward's method (b); f-female

Discussion

Muscular variations of the flexor compartment of the forearm are often encountered and could result in multiple clinical conditions limiting the functions of the forearm and hand. In cases in which the median nerve represents the most superficial structure in this compartment, an injury to it is often possible which may compromise the innervation of the respective region [1].

The PL is the most variable muscle in the human upper limb and in the human body. In the literature, there are examples of an aberrant PL occurring together with other anatomical variations, such as persistent median artery and flexor carpi

ulnaris muscle [5]. PL is a retrogressive muscle, the presence of which is restricted to mammals and especially to those that use load to walk [2]. A number of species (such as orangutan) still use the muscle to snatch different items while climbing. Other primate relatives (such as the chimpanzee and gorilla), like humans, do not actively use the muscle which provides the basis for the multitude of observed variations [16]. One really important advantage of the PL tendon is the protection of the median nerve which passes deep to it. In case of an absence of the PL tendon, the median nerve, which would be the most superficial structure in the wrist, could be injured during trauma and surgical incisions [1]. PL plays an important role in orthopaedic and plastic surgeries. Its presence in most of the population and its superficial location makes it the most common donor material for tendon and joint reconstructive surgeries [1].

According to our results, 29% of all subjects (male and female) tested with Schaeffer's standard test had bilateral absence of PL. Only 5% had right absence and 13% had left absence of the muscle. The majority of the examined subjects (53%) had bilateral presence of PL. While there was a slight difference in the results as measured by the two tests (as evident by **Table 1**), PL was present in both upper limbs of the predominant number of subjects. These results also demonstrate that minimal differences exist between the different tests used for visualization of the tendon of PL.

The FDS is also a variable muscle [8, 9]. Our findings of concomitant variations of PL and FDS lead to the conclusion that there could be a connection between the absence of one muscle or the other. The absence of FDS tendon to the little finger may compromise hand function in case of an injury to the tendon of FDP, which would lead to an impaired flexion of the little finger, thus causing difficulties in grip function. This injury may necessitate the use of a tendon graft that would usually be easily mobilised from the PL of the same hand. Therefore, hand surgeons should be aware if any link exists between the absences of the two muscles [8, 9]. During physiotherapy, therapists should take into account the lower results achieved when examining grip strength of FDS-absent or FDS-common individuals [3].

Independent FDS function, as some studies suggest, is important for professional musicians [6]. Also, in patients with absolute little finger FDS functional deficit, special attention should be paid when the little finger is injured. As a result, it is of utmost importance that FDP tendon be properly treated in order to avoid any permanent functional deficit [7].

According to our study, 65% of cases had bilateral presence of FDS. Bilateral absence of FDS tendon to the little finger was observed in 15% of cases, 8% of cases had right absence of the muscle and 12% had left absence. Bilateral absence of both muscles was only observed in 2% of the examined cases. In addition, our observations revealed that PL is more variable in males than females, while FDS is more variable in females than males. The dominance of hands was not related to the tested variables.

Conclusion

In conclusion, the majority of the examined subjects (62%) had either bilateral absence or absence of either PL or FDS tendon of the little finger in one of their upper limbs. The remaining cases had bilateral presence of both muscles.

PL muscle absence was an independent entity for FDS muscle absence. Bilateral absence of PL and FDS was observed in 29% and 15% of cases, respectively. For PL, these results are higher than those previously observed in Caucasian populations (European and North American), which range between 5.5% and 24%. For FDS, our results are similar to those reported for other Caucasian populations (15% – 22%).

Acknowledgement: The authors of the present manuscript are deeply indebted to Associate Professor Jordanka A. Angelova, PhD, the University of Chemical Technology and Metallurgy, Sofia, Bulgaria, for her kind assistance in the preparation of the statistical analysis the obtained results. We would also like to thank Dr. Georgi Kotov of the Medical University of Sofia for his help in the preparation of the manuscript and the proofreading of the English text.

References

1. **Agarwal, P.** Absence of the palmaris longus tendon in Indian population. – *Indian J. Orthop.,* **44**, 2010, 212-215.
2. **Angelini Júnior, L. C., F. B. Angelini, B. C. de Oliveira, S. A. Soares, L. C. Angelini, R. H. Cabral.** Use of the tendon of the palmaris longus muscle in surgical procedures: study on cadavers. – *Acta Ortop. Bras.,* **20**, 2012, 226-229.
3. **Bowman, P., L. Johnson, A. Chiapetta, A. Mitchell, E. Belusko.** The clinical impact of the presence or absence of the fifth finger flexor digitorum superficialis on grip strength. – *J. Hand Ther.,* **16**, 2003, 245-248.
4. **Georgiev, G. P., A. Iliev, I. N. Dimitrova, G. Kotov, L. Malinova, B. Landzhov.** Palmaris longus muscle variations: significance for hand surgery and proposal of new classifications. – *Fol. Med. (Plovdiv),* **59**, 2017, 289-297.
5. **Georgiev, G. P., L. Jelev, W. A. Ovtscharoff.** Unusual combination of muscular and arterial variations in the upper extremity: a case report of a variant palmaris longus and an additional tendinous portion of the flexor carpi ulnaris together with a persistent median artery. – *Anatomy,* **3**, 2009, 58-61.
6. **Godwin, Y., G. A. Wheble, C. Feig.** Assessment of the presence of independent flexor digitorum superficialis function in the small fingers of professional string players: is this an example of natural selection? – *J. Hand Surg. Eur. Vol.,* **39**, 2014, 93-100.
7. **Gupta, A., V. Kumar.** Bilateral absence of flexor digitorum superficialis (FDS) tendon of the little finger: clinical significance. – *J. Clin. Diagn. Res.,* **8**, 2014, 135-136.
8. **Kigera, J. W. M., A. Katusiime.** Prevalence of agenesis of flexor digitorum superficialis of the fifth digit in East Africa through clinical examination. – *SA Orthop. J.,* **10**, 2011, 75-77.
9. **Kigera, J. W. M., S. Mukwaya, A. Katusiime.** The relationship between functional absence of the flexor digitorum superficialis to the fifth digit and absence of the palmaris longus. – *E. A. O. J.,* **7**, 2013, 11-13.
10. **Kumar, V., N. S. Naveen, B. V. Murlimanju, P. S. DaSouza.** A rare muscular variation in the flexor compartment of the forearm. – *Int. J. Anat. Var.,* **4**, 2011, 115– 116.
11. **Mishra, S.** A new test for demonstrating the action of flexor digitorum superficialis (FDS) tendon. – *J. Plast. Reconstr. Aesthet. Surg.*. **59**, 2006, 1342-1344.
12. **Mishra, S.** Alternative tests in demonstrating the presence of palmaris longus. – *Indian J. Plast. Surg*., **34**, 2001, 12.
13. **Mugalur, A, S. M. Shahane, A. Samant, A. C. Pathak, A. Patil, R. Reddy.** Anatomic variation of palmaris longus and flexor digitorum superficialis of little finger in Indian population. – *SICOT J.,* **1**, 2015, 5.
14. **Sandeep, J. S., Y. T. L. Aymeric, W. Hwee-Bee.** Clinical assessment of absence of the palmaris longus and its association with other anatomical anomalies-a Chinese population study. – *Ann. Acad. Med. Singap*., 35, 2006, 249-253.
15. **Sebastin, S. J., A. Y. Lim.** Clinical assessment of absence of the palmaris longus and its association with other anatomical anomalies - a Chinese population study. – *Ann. Acad. Med. Singapore,* **35**, 2006, 249-253.
16. **Thejodhar, P., B. K. Potu, R. G. Vasavi.** Unusual palmaris longus muscle. – *Indian J. Plast. Surg.,* **41**, 2008, 95-96.
17. **Vučinić, N., M. Erić, M. Savić.** How often absence of palmaris longus and functional deficiencyof flexor digitorum superficialis occurs? – *Acta Orthop. Belg.,* **82**, 2016, 405-411.

Institute of Experimental Morphology, Pathology and Anthropology with Museum
Bulgarian Anatomical Society

Acta morphologica et anthropologica, 27 (1-2)
Sofia ● 2020

A Case of Well Developed Median Superficial Sural Artery (Small Saphenous Artery) Piercing Through the Medial Sural Cutaneous Nerve

Lazar Jelev, Nikolai Krastev, Lina Malinova,*

Department of Anatomy, Histology and Embryology, Medical University, Sofia, Bulgaria

* Corresponding author e-mail: ljelev@abv.bg

A case of well-developed median superficial sural artery (small saphenous artery) is reported here, found during routine student dissections of the left lower limb of an adult formalin-fixed male cadaver. This small sized artery was starting from the posterior surface of the popliteal artery and passed between the main tibial nerve and its muscular branch to the gastrocnemius medial head. Further distally, the artery pierced through the initial part of the medial sural cutaneous nerve. Along the upper calf region, the small arterial vessel was located on the lateral side of the small saphenous vein and cutaneous nerves and terminated in the lower part of the leg. The literature descriptions concerning the cutaneous popliteal artery branches are reviewed, including their application in the field of plastic and reconstructive surgery.

Key words: popliteal artery; cutaneous branches; median superficial sural artery, sural nerve, human

Introduction

In the detailed anatomy textbooks [5, 13, 16, 19], the branches of the popliteal artery are divided into muscular, genicular (articular) and superficial. The superficial branches are described as occasionally present arteries of small size, starting directly from the popliteal artery or some of its branches and piercing through the crural fascia they supply the skin over the calf. Despite not included in Terminologia Anatomica [6], these superficial branches have clinical importance as vascular pedicles of fasciocutaneous flaps [2, 8, 12, 15, 18, 20, 21] or vascularized nerve grafts [7, 14] for plastic and reconstructive surgery and microsurgery.

In this report, we present a demonstrative case of such a well-developed superficial artery branching from the popliteal artery.

Materials and Methods

The reported findings were observed during routine student dissections of the left lower limb of an adult formalin-fixed male cadaver of a Caucasian descent. All dissections took place at the Department of Anatomy, Histology and Embryology, Medical University of Sofia.

Case report

After removal of the skin of posterior crural region, a dissection was started in the subcutaneous fat tissue in order to demonstrate the superficial veins and cutaneous nerves branches. A common way of formation of the sural nerve was observed by fusion of the medial sural cutaneous nerve, piercing through the crural fascia, and sural communicating branch from the lateral sural cutaneous nerve, which fusion happened in the middle of the leg. The sural nerve and medial sural cutaneous nerve were accompanied by the small (lesser) saphenous vein, as usual. A small-sized artery (external diameter 1.8 mm) was also observed in companion to the cutaneous nerves and vein (**Fig. 1a**). Dissecting completely the crural fascia and popliteal fossa revealed the origin of this arterial vessel (**Fig. 1b**). It was starting from the posterior surface of the lower part of the popliteal artery. Then, the small artery passed between the main tibial nerve and its muscular branch to the gastrocnemius medial head. Further distally, the artery pierced through the initial part of the medial sural cutaneous nerve and continued downwards on the lateral side of the small saphenous vein and the cutaneous nerves. By fine dissection, this artery was traced to the lower third of the posterior leg and did not reach the ankle. Because of its midline position and superficial location, the small artery can be identified as "median superficial sural artery" [11] or according to its close relation to the small saphenous vein as "small saphenous artery" [1].

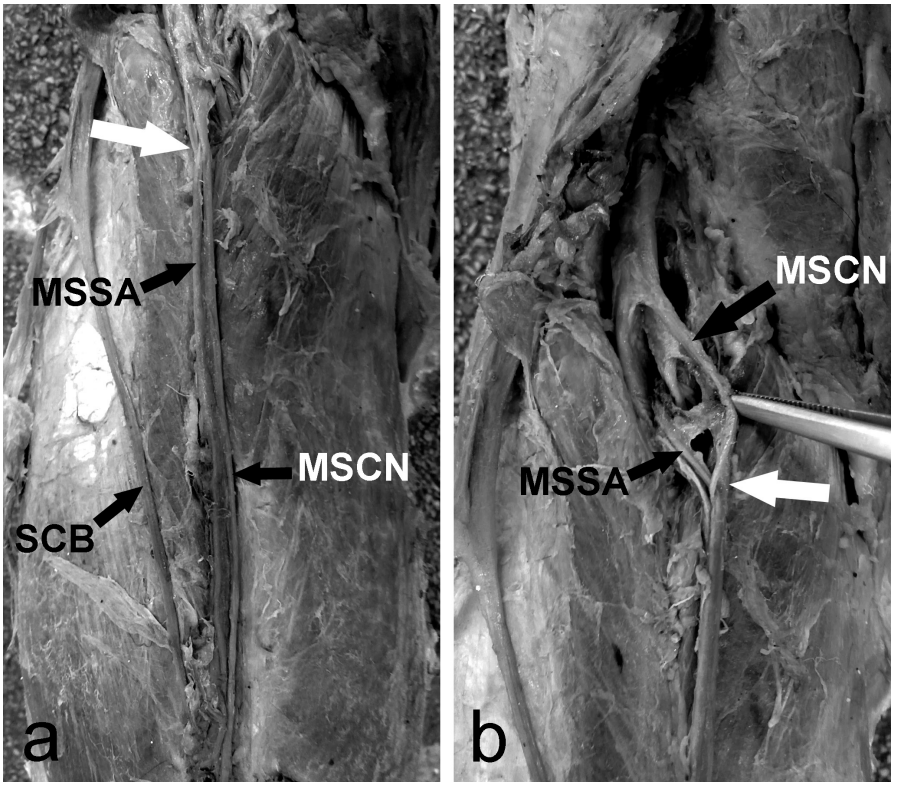

Fig. 1. Photographs of the reported case, presenting dissection of the upper calf region (a) and popliteal fossa (b). The nerve piercing point is indicated with white arrow. Artery: MSSA - median superficial sural artery. Nerves: MSCN – medial sural cutaneous nerve; SCB - sural communicating branch from the lateral sural cutaneous nerve.

Discussion

In the classical textbooks of anatomy, the superficial branches of the popliteal artery usually do not have their proper names [5, 13, 19]. According to these sources, the largest and most constant of all is the small artery passing between the gastrocnemius heads, which accompanies the small saphenous vein and medial sural cutaneous and sural nerves.

In the texts of anatomical variations, the small superficial artery between the heads of gastrocnemius is either not mentioned [9, 17] or described as the occasionally present "small saphenous artery" [3] or "arteria saphena parva" ("a. suralis superficialis media") [1]. Such an artery was described in 2 out of 180 lower limbs dissected but only when of larger size and anastomosing with the tarsal arteries [1]. Obviously, the superficial sural arteries did not attract much attention of variational anatomists.

The most detailed descriptions of the superficial sural arteries can be found in the clinically oriented texts such as the profound book on the cutaneous arteries in the human body by Manchot [11], and in a number of papers [7, 10, 15, 18]. Three cutaneous arteries are identified in these texts - the median (central), medial and lateral superficial sural arteries [7, 10, 15, 18]. It was reported that the median superficial sural artery is usually the largest one (0.9-2.6 mm) [10] and is present in more than 90% of the lower limbs. This artery may start from the popliteal artery (most commonly), from the other superficial sural arteries or from the genicular arteries [7, 10, 15, 18]. In plastic and reconstructive surgery a number of fasciocutaneous flaps have been described, which are based on the vascular pedicles of superficial sural arteries [2, 8, 12, 15, 18, 20, 21]. The median superficial sural artery is also providing extensive blood supply to the sural nerve, which make possible a useful vascularized nerve graft to be developed [7, 14].

In summary, the median superficial sural artery, a small-sized cutaneous vessel, is scarcely described in the classical anatomical texts, despite well-known in the area of plastic and reconstructive surgery. The reported here course of the median superficial sural artery through the fibers of the medial sural cutaneous nerve might be a reason for sural nerve entrapment [4], as well as its passage together with the small saphenous vein and medial sural cutaneous (or sural) nerve through the unyielding fibrous arcade of the crural fascia.

References

1. **Adachi, B**. *Anatomy of Japanese I. The arterial system of Japanese*, Vol. II: Aorta thoracalis – Arcus plantaris profundus. Kyoto, Verlag der Keiserlich-Japanischen Universitat zu Kioto, 1928, 213. [in German]
2. **Al-Qattan, M. M**. A modified technique for harvesting the reverse sural artery flap from the upper part of the leg: inclusion of a gastrocnemius muscle "cuff" around the sural pedicle. – *Ann. Plast. Surg*., **47**, 2001, 269-278.
3. **Bergman, R. A., A. K. Afifi, R. Miyauchi**. *Illustrated encyclopaedia of human anatomic variation*. Opus II: Cardiovascular system, 2020. Available at: https://www.anatomyatlases.org/AnatomicVariants/Cardiovascular/Text/Arteries/Popliteal.shtml.
4. **Brown, M. N., B. S. Pearce, T. K. Vanetti**. Sural nerve entrapment. – In: *Peripheral nerve entrapments* (Ed. M. Trescot), Switzerland, Spinger, 2016, 795-810.
5. **Clemente, C.D.** (Ed.). *Anatomy of the human body*, 30th Ed, Philadelphia, Lea and Febiger, 1985, 770.
6. **Federative Committee of Anatomical Terminology (FCAT)**. *Terminologia anatomica: International anatomical terminology*, Stuttgart, Georg ThiemeVerlag, 1998, 1-292.
7. **Frachinelli, A., A. Masquelet, J. Restrepo**. The vascularized sural nerve. – *Int. J. Microsurg*., **3**, 1984, 57.

8. **Karacalar, A**. Axial bilobed flap based on the median and medial superficial sural arteries: a case report. – *Scand. J. Plast. Reconstr. Surg. Hand. Surg*., **35**, 2001, 207-210.
9. **Lippert, H., R. Pabst**. *Arterial variations in man*, München, J.F. Bergmann Verlag, 1985, 1-121.
10. **Magden, A. O., A. Menderes, M. Yilmaz, A. Barutcu**. Anatomical study of the origin and course of the median superficial sural artery. – *Eur. J. Plast. Surg*., **19**, 1996, 29–32.
11. **Manchot, C**. *The cutaneous arteries of the human body*, New York, Springer, 1983, 105-131. English translation of: Manchot C. Die Hautarterien des menschlichen Körpers, 1889.
12. **Mazur, N., R. Osinga, S. Lo**. Split median superficial sural artery perforator (MSSAP) flap and medial sural artery perforator (MSAP) flap for posterior thigh sarcoma reconstruction. – BMJ Case Rep., **13**, 2020, 1-2.
13. **Moore, K. L**. *Clinically oriented anatomy*, 3rd Ed., Baltimore, Williams & Wilkins, 1992, 423-426.
14. **Riordan, C. L., L. B. Nanney, J. Upton, III3, S. F. Wolfort**. Vascularized medial sural cutaneous nerve based on the superficial sural artery: A reliable nerve graft. – *J. Reconstr. Microsurg*., **18**, 2002, 147-152
15. **Satoh, K., F. Fukuya, A. Matsui, T. Onizuka**. Lower leg reconstruction using a sural fasciocutaneous flap. – *Ann. Plast. Surg*., **23,** 1989, 97-103.
16. **Standring, S.** (Ed.). *Gray's Anatomy - The Anatomical Basis of Clinical Practice*, 41th Ed, London, Elsevier, 2016, 983-986.
17. **Tubbs, R. S., M. M. Shoja, M. Loukas.** (Eds.). *Bergman's comprehensive encyclopedia of human anatomic variation*, Hoboken, New Jersey, John Wiley & Sons, Inc., 2016, 741-751.
18. **Walton, R. L., J. Bunkis**. The posterior calf fasciocutaneous free flap. – *Plast. Reconstr. Surg*., **74**, 1984, 76-85.
19. **Williams, P. L., L. H. Bannister, M. M. Berry, P. Collins, M. Dyson, J. E. Dussek, M. W. J. Ferguson** (Eds.). *Gray's anatomy*, 38th Ed, Edinburgh, Churchill Livingstone, 1995, 1568-1570.
20. **Wolff, K.-D., F. Hölzle**. *Rising of microvascular flaps*, Berlin, Springer, 2018, 273-291.
21. **Xie, X. T., Y. M. Chai**. Medial sural artery perforator flap. – *Ann. Plast. Surg.,* **68**, 2012, 105-110.

Institute of Experimental Morphology, Pathology and Anthropology with Museum
Bulgarian Anatomical Society

Acta morphologica et anthropologica, 27 (1-2)
Sofia ● 2020

Morphometric Studies on Skulls of Male Mole Rats [Nannospalax nehringi (2n = 50)] (Satunin 1898) (Rodentia: Spalacidae) Collected from Kars Province

Semine Dalga[1], Kadir Aslan[1], Barış Yıldız[2]*

[1] *Kafkas University, Faculty of Veterinary Medicine, Department of Anatomy, Kars, Turkey*
[2] *Kafkas University, Faculty of Veterinary Medicine, Department of Physiology, Kars Turkey*

* Corresponding author e-mail: sdalga91@gmail.com

Thirteen adult male *Nannospalax nehringi* skulls were collected from Kars province. Lengths of 19 different points on skulls were measured with the aid of an electronic caliper (0.00, BTS, UK). Macroanatomic examination of male *Nannospalax nehringi* mole rat skulls revealed that, there were no clear external occipital crest formations, nuchael crest was quite long and sharp, external saggital crest was in a wavy form, tympanic bulla was large and long, and foramen magnum was pretty large and high. Also there was a bilateral protrusion on the midline of molar teeth on the os palatinum and holes on the premaxillo-nasal sutures and nasal bone were seen. The average lengths of the skulls were calculated 49.02 ± 4.62 mm. As a result of the correlation of the distances between measured points, strong positive correlations were determined between lengths of L2/L3, L2/L4 and L3/L4 and no insignificant or negative result was obtained.

Key words: Macroanatomy, Cephalometry, *Nannospalax nehringi*

Introduction

The Spalacidae family members adapted to underground life. It is thought to be they emerged in Anatolia during the Upper Oligocene and extensively subsided into Balkans, Russian steppes, Central Asia and extended to North Africa [22]. Members of the Spalacidae family can be found in Southeast Europe, Anatolia, the Caucasus, Trans-Caucasus, Ukraine, Armenia, Syria, Palestine, Israel, Iraq, Jordan and North Africa [1, 10, 22]. This family is a monophilic group at the family level, characterized by having semi-hypsodont, rooted and strong teeth [17]. Mehely [15] described *Spalax* genus under four sub-genus *(Nannospalax, Mesospalax, Macrospalax and Microspalax)* but Gromov and Baranova [8] gathered them under two genera as *Nannospalax* and *Spalax*. Topachevskii [24], Savic [21], Wilson and Reeder [26], Yigit et al. [27] and Sözen et al. [23], reported that *Nannospalax nehringi* is widely distributed across the Anatolia, Southeastern Anatolia but *Nannospalax ehrenbergi*

and *Nannospalax leucodon* spread on the European side of Turkey especially. They are also known as blind mole rats (BMR).

Morphometric analsis methods are frequently used in the identification of fossil model formations, determination of intrinsic phenotypic variations and evaluationof many internal and external osteological forms [5, 12]. The regional anatomy of skull is important because it contains some important organs such as brain, tongue, eye, lips, teeth, nose andeyelid. The well-known anatomical anatomy allows us to know the details of the structure related to the region in any case, and to practice in terms of clinical and surgical intervention.

There are many published research about the morphological and anatomical characteristics of *Nannospalax nehringi* [3, 4, 14, 15, 16, 24]. In this study, we aimed to determine the morphometric and macroanatomical features, and also craniofacial characteristics of *Nannospalax nehringi* (2n=50) in Kars province.

Material and Methods

Skulls of 13 adult male *Nannospalax nehringi* (2n=50) collected from Kars province for a thesis study in the Faculty of Veterinary Medicine, Department of Physiology, Kafkas University were used in the present study. This study was approved by the Institutional Animal Care and Use Committee of Kafkas University with permission no 2018-077. The skulls were cleaned from skin and coarse flesh and boiled in controlled manner and, cured with hydrogen peroxide for 25-30 minutes. Distances among 19 different points on skulls were measured with an electronic caliper (0.00, BTS, UK) according to literature. For photograph of the BMR skulls, Canon Digital Camera Zoom 5X was used. Dataset was composed from obtained measurements and, mean, standard deviation and correlation values were determined by SPSS 18.0 software.

Measurement points defined on the skull of Mole rats (*Nannospalax nehringi*) – Fig. 1.

Acrocranion (A). The most aboral point on the vertex of the cranium in the median plane, **Basion (B).** Orobasal border of foremen magnum in median plane, **Bregma (Br).** Median point of parietofrontal suture, **Euryon (Eu).** Most lateral point of braincase, **Lambda (L).** Median point of parietooccipital suture, **Nasion (N).** Median point of nasofrontal suture, **Otion (Ot).** Most lateral point of mastoid region, **Prosthion (P).** Most oral points of premaxillae on the median plane, **Postdentale (Pd).** Median point of the line combining the caudal edges of the last molar teeth alveoli on the median line of the oral cavity, **Rhinion (Rh).** Median point of the line combining the most oral points of nasals.

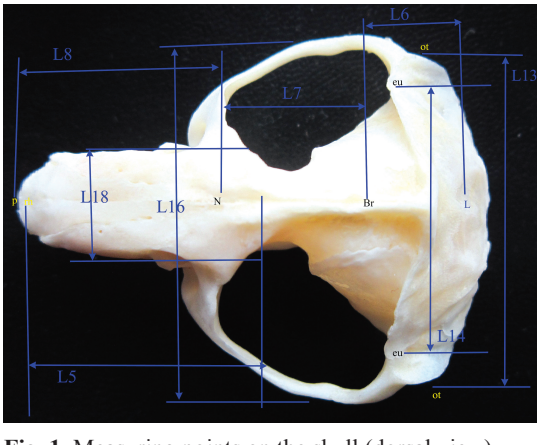

Fig. 1. Measuring points on the skull (dorsal view)

Measurements taken from the skull of Mole rats (*Nannospalax nehringi*) – Fig. 2.

L1. Skull length (acrocranion – prosthion), **L2.**Condylobasal length (aboral borders of occipital condyle - prosthion), **L3.** Basal length, **L4.** Dental length (postdentale – prosthion), **L5.** Largest nasal length, **L6.** Parietal length (lambda – bregma), **L7.** Frontal length (bregma – nasion), **L8.**Viscerocranium length (nasion – prosthion), **L9.** Length of the cheektooth row (measured along the alveoli on the buccal side), **L10.**Diestema length, **L11.** Palatal length, **L12.** Greatest width between the occipital condyles, **L13.** Widest length between the external acoustic meatus (otion – otion), **L14.** Maximum neurocranium width (euryon – euryon), **L15.** Skull width (distance between the temporal fossae), **L16.** Oral zygomatic width (between the oral parts of zygomatic arch), **L17.** Aboral zygomatic width (between the aboral parts of zygomatic arch), **L18.** Largest nasal width, **L19.** Palatal width.

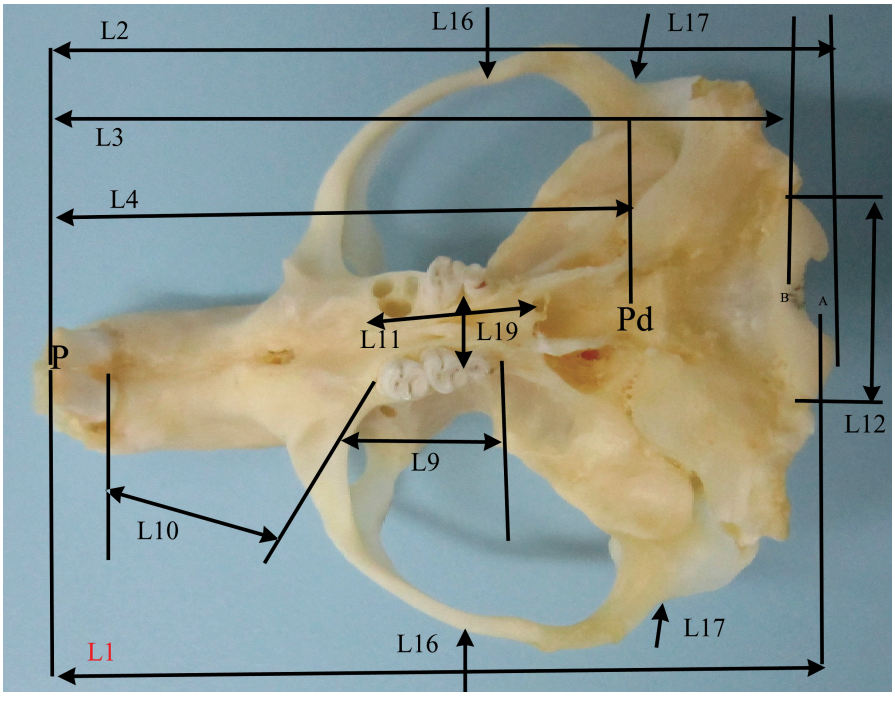

Fig. 2. Measuring points on the skull (ventral view).

Results

According to the macro-anatomic examinations of the *Nannospalax nehringi* skulls, occipital crest formation was not very clear (**Fig. 3**/thin arrow) and crista nuchae was quite long and sharp (**Fig. 3**/thick arrow). It was seen that external sagittal crest continued to descend after the beginning (**Fig. 3**/arrowhead). Tympanic bulla was in a large and long form and foramen magnum was pretty large and high. Also, a clear protrusion was observed bilaterally on the midline of molar teeth on the os palatinum. Additionally, it was seen that there were holes on the premaxillo-nasal sutures and nasal bone, as noted from previously studies (**Fig. 4**).

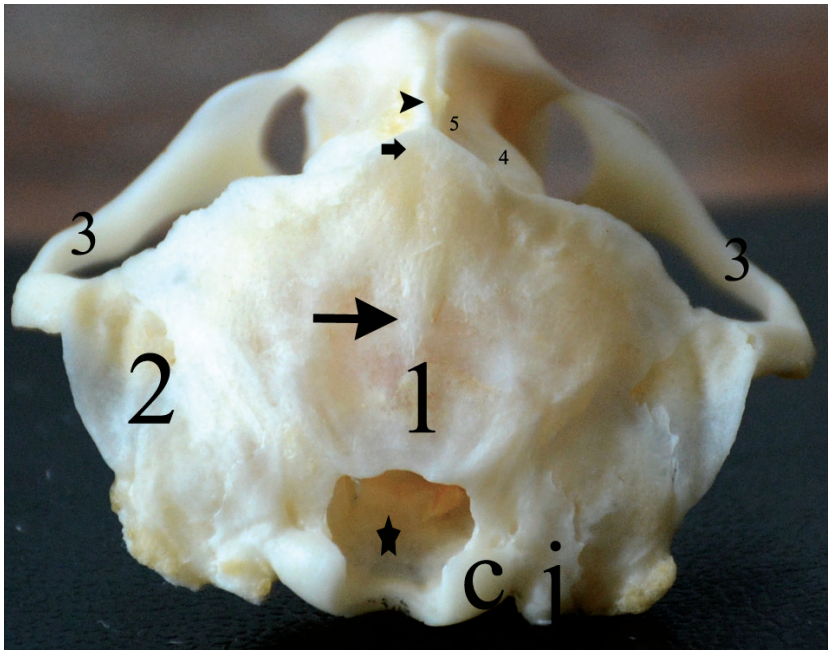

Fig. 3. 1. Occipital bone, 2. Temporal bone, 3. Arcus zygomaticus, 4. Parietal bone, 5. Interparietal bone, c. Condylar process, J. Jugular process

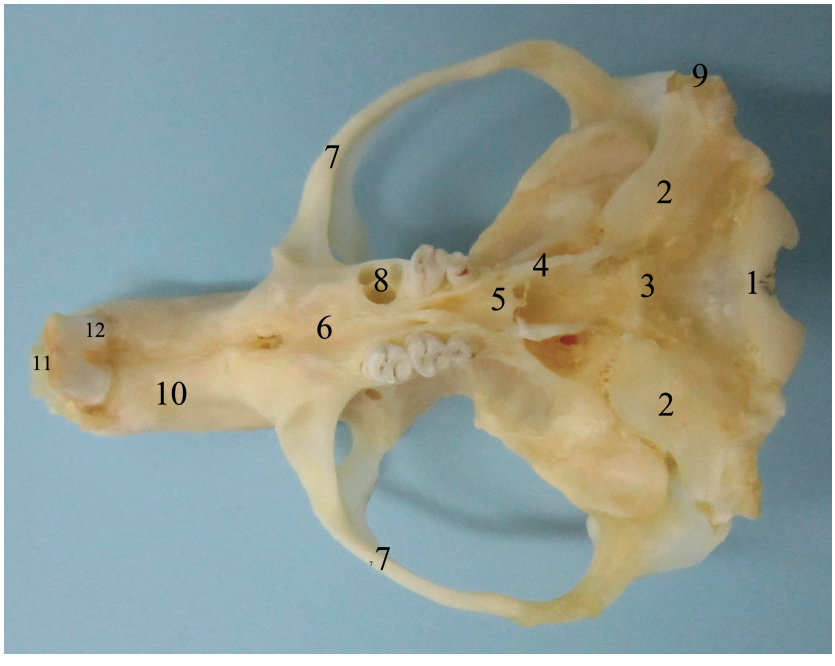

Fig. 4. 1. Occipital bone, 2. Tympanic bulla, 3. Sphenoid bone, 4. Pterygoid bone, 5. Palatin bone, 6.Maxillar bone, 7. Zygomatic arch, 8. Alveoli dentali, 9. Porusacusticus externus, 10. İnciciv bone, 11. Nasal bone, 12. Inciciv tooth.

Mean and standard deviation values of morphometric measurements of the male *Nannospalax nehringi* are shown in **Table 1** and the correlation analysis results of these values are shown in **Table 2**. According to these findings, the skull length was foundas 49.02 ± 4.62 mm on average.

As a result of the correlation analysis of obtained values, we found that there was positive correlation between the lengths of L2 / L3, L2 / L4 and L3 / L4, and no insignificant or negative result was detected.

Table 1. Mean and standard deviation values of morphometric values of skull in blind mole rat

	Mean	**Std. Deviation**
L1	49,0267	4,62838
L2	51,3617	4,15494
L3	49,4242	4,23306
L4	34,7267	3,39918
L5	23,1933	3,25571
L6	16,5675	1,31072
L7	20,2017	2,07067
L8	21,3650	1,83681
L9	7,9800	,69080
L10	18,2467	1,61045
L11	15,5842	1,79532
L12	10,2692	,72231
L13	27,6325	1,96954
L14	13,0767	,99418
L15	25,0375	2,10912
L16	33,8800	3,30935
L17	36,7842	3,52741
L18	8,8250	1,10210
L19	2,9067	,71115

Table 2. Correlation analysis of the morphometric values of the skull in blind mole rat(*P <0.05, **P <0.01).

	L1	L2	L3	L4	L5	L6	L7	L8	L9	L10	L11	L12	L13	L14	L15	L16	L17	L18	L19
L1	1	,931**	,940**	,959**	,902**	,834**	,909**	,901**	,751**	,897**	,881**	,251	,877**	,843**	,844**	,896**	,907**	,856**	,788**
L2		1	,998**	,987**	,919**	,883**	,812**	,909**	,681*	,890**	,921**	,246	,876**	,833**	,848**	,950**	,939**	,922**	,711**
L3			1	,992**	,923**	,882**	,811**	,924**	,681*	,904**	,933**	,246	,880**	,837**	,853**	,957**	,952**	,924**	,731**
L4				1	,942**	,898**	,862**	,910**	,697*	,913**	,937**	,262	,881**	,862**	,864**	,959**	,964**	,913**	,757**
L5					1	,763**	,845**	,882**	,605*	,915**	,871**	,258	,854**	,779**	,894**	,878**	,921**	,823**	,667*
L6						1	,795**	,706*	,545	,680*	,864**	,206	,747**	,774**	,636*	,869**	,878**	,841**	,612*
L7							1	,689*	,676*	,776**	,733**	,200	,781**	,725**	,727**	,775**	,794**	,669*	,691*
L8								1	,635*	,939**	,883**	,270	,812**	,776**	,893**	,893**	,913**	,886**	,791**
L9									1	,716**	,678*	,657*	,607*	,675*	,662*	,595*	,589*	,612*	,816**
L10										1	,880**	,353	,753**	,786**	,948**	,852**	,879**	,792**	,847**
L11											1	,462	,710**	,793**	,860**	,857**	,928**	,831**	,785**
L12												1	,044	,182	,367	,104	,250	,183	,562
L13													1	,724**	,642*	,893**	,856**	,884**	,552
L14														1	,831**	,866**	,799**	,860**	,689*
L15															1	,792**	,817**	,746**	,781**
L16																1	,961**	,945**	,718**
L17																	1	,902**	,761**
L18																		1	,647*
L19																			1

Discussion

Coşkunet Kaya. [2] and Ketani et al. [13] reported that the external saggittal crista was in only one protrusion shape but we observed that external sagittal crista was in a wavy formation in *Nannospalax nehringi* collected in Kars province.

A morphometric study on skulls of New Zealand rabbits reported that average lengths of the skulls are 94.1 mm [9]. In a different study, which was conducted on *Spalax leucodonnordmann,* the average lengths of the skulls were reported as 42.5 mm [19]. Additionally, it is known that, skulls of male rats are significantly longer than female rats have [11]. Olude et al. [18] reported the average skulls lengths of the male and female African giant rats as 63.6 mm and 62.8 mm respectively. In our study, the average length of skulls of the male *Nannospalax nehringi* was measured as 49.02 mm.

In the case of New Zealand rabbits, it was stated that all lengths other than the skull width (L15) and aboral zygomatic width (L17) were higher in the female rabbits than the 19 lengths measured over the skull [9].

Galatius [7] reported that skull measurements of Phocoenaphocoena were higher and significant in females than males.

In addition, Salih [20] reported that the average of 10 values out of a total of 16 lengths measured from rabbit skulls was higher in female rabbits than in male rabbits and that some lengths measured between genders were statistically significant. For example, measurements between 2 arcus zygomaticus and maxillo alveolar distance.

In New Zealand rabbits, all lengths except skull width (L15) and aboral zygomatic width (L17) were reported to be higher in female rabbits [9].

As a result, morphometric analyses are frequently preferred methods in determination of differences between the genders, interspecies modelling and identification of extinct or endangered species.

This study determined the macro-anatomical features, and morphometric characteristics of *Nannospalax nehringi* collected from Kars.

References

1. **Corbet, G. B.** *Mammals of the palearctic region: A Taxonomic review*. British Mus. Nat. History, London, 1978, pp**.** 1-314.
2. **Coşkun, Y., A. Kaya.** Morphological properties of nannospalax *(Rodentia: Spalacidae)* distributed in North-Iraq, Haccettepe. – *J. Biol. And Chem.,* **44**, 2016, 173-179.
3. **Coşkun, Y.** Turkey mole rat's the taxonomic status. XII. National Biology Congress Papers, Zoology Section, Volume VI, Edirne, 1994, pp. 277-283. [In Turkish]
4. **Coşkun, Y.** Morphological properties of Kars, Ağrı and Erzurum Region Spalax. XV. National Biology Congress Papers, Volume I, Ankara, 2000**,** pp. 277-283. [In Turkish]
5. **Çakır, A., İ. G. Yıldırım, O. Ekim.** Craniometric measurements and some anatomical characteristics of the cranium in Mediterranean monk seal (Monachus monachus, Hermann 1779). – *Ankara Üniv. Vet. Fak. Derg.,* **59**, 2012, 155-162.
6. **Dyce, K. M., W. O. Sack, C. J. G. Wensing.** *Textbook of veterinary anatomy*, 2nd edition, Philadelphia, Saunders, 1996
7. **Galatius, A.** Sexually dimorphic proportions of the Harbour Porpoise (Phocoenaphocoena) skeleton. – *J. Anat.,* **206**, 2005, 2, 144-154.
8. **Gromov, I. M., G. I. Baranova.** *Catalogue of mammals in USSR*. Leningrad, Nauka, 1981**.**
9. **Gürbüz, İ, Y. Demiraslan, K. Aslan.** Morphometric analysis of the skull of New Zealand rabbit (Oryctolaguscuniculus L.) According to gender. – *ARC Journal of Animal and Veterinary Sciences (AJAVS),* **1**, 2015, 27-32.

10. **Harrison, D. L., P. J. J. Bates.** *Mammals of Arabia*. Second edition, Harr. Zool. Mus. Pub, 1991 pp. 1-353.
11. **Hughes, P. C. R., J. M. Tanner, J. P. G. Williams.** A longitudinal radyographic study of the growth of the rat skull. – *J. Anat*., **127**, 1978, 83-91.
12. **Ketani, A. M., H. Sağsöz.** Histomorphometric investigation of the effects of gender on the histological structure of the mandibular condyle in rats. – *Atatürk Üniv. Vet. Bil. Derg.*, **4**, 2009, 31-38. [In Turkish].
13. **Ketani, Ş., M. Kilinc, S. Erdogan, A. Kaya, Y. Coskun.** A Macro-anatomical investigation of the some skull bones of Nehring's blind mole rats (Spalacidae: *Nannospalax nehringi*). – *Anat. Histol. Embryol*. **46**, 2017, 232–239.
14. **Kivanc, E.** Turkey mole rat's of geographical variations (Mammalia: Rodentia). *Ph.D. Thesis*, Ank. Univ. Science Fac., Ankara, 1988, 88 pp. [In Turkish]
15. **Mehely, V. L.** A Foldi Kutyak Fajai, Budapest (Mathem. und naturwissenschaftliche Berichteaus Ungarn), **28**, 1909, 4. pp. 1-273. [In German]
16. **Mursaloğlu, B.,** Turkey mole rat's in (Mammalia: Rodentia) Systematic Problems. TÜBİTAK VI. Science Congress, 1979 Communiqués, pp. 83-92. [In Turkish]
17. **Nevo, E., E. Ivanitskaya, M. Filippucci, G. A. Beiles.** Speciation and adaptive radiation of subterranean mole rats, *Spalaxehrenbergi* super species in Jordan. – *Biol. J. Lin. Soc*., **69**, 2001, 263-281.
18. **Olude, M., A. Olopade, J. O. Fatola, S. K. Onwuka.** Some aspects of the neurocraniometry of the African giant rat (Cricetomysgambianus Waterhouse). – *Folia Morphol.,* **68** (4), 2009, 224-227.
19. **Özkan, Z. E.** Macro-anatomical investigations on the skeletons of mole-rat *(Spalax leucodon Nordmann)* III. Skeleton axiale. – *Veterinarski arhiv,* **77** (3), 2007, 281-289.
20. **Salih, K. M.** Gross anatomical and morphometrical studies to the skull bones of the local rabbit (Oryctohgus cuniculus). – *Bas. J. Vet. Res*., **12** (2), 2013, 267-277.
21. **Savic, I.** Familie Spalacidae Gray, 1821 – Blindmouse. *In: Handbuch der saugetiere Europas, band 2/1 Rodentia*. Wiesbaden, Akademishe Verlagsgesellschaft, 1982, pp. 537-584. [in German]
22. **Savic, I., Nevo, E.** The Spalacidae: Evolutionary history, speciation and population biology. *In: Evolution of subterranean mammals at the organismal and molecular levels* (Eds. E. Nevo, A. O. Reig), New York, Alan R. Liss, 1990, pp. 129-153.
23. **Sözen, M., F. Matur, E. Çolak, S. Özkurt, A. Karataş.** Some karyological records and a new chromosomal form for Spalax (Mammalia: Rodenita) in Turkey. – *Folia Zool.*, **55**(3), 2006, 247-251.
24. **Topachevskii, W. A.** *Fauna USSR Spalacidae.* Leningrad, Nauka, 1969 (English translation: US Dept. Commerce. Nat. Info. Serv., Springfield, Virginia).
25. **Von den driesch, A.** A guide to the measurement of animal bones from archaeological sites. In: *Peabody museum bulletin I*, Cambridge MA, Harvard University, 1976, pp. 31-34
26. **Wilson, D. E., D. M. Reeder.** *Mammal species of the world: A taxonomic and geographic reference.* Second Edition, Washington and London, Smithsonian Institution Press, 1993.
27. **Yiğit, N., E. Çolak, M. Sözen, A. Karataş.** Rodents of Turkey. Ankara, Meteksan, 2006, 76-80.

Institute of Experimental Morphology, Pathology and Anthropology with Museum
Bulgarian Anatomical Society

Acta morphologica et anthropologica, 27 (1-2)
Sofia ● 2020

Morphometric Study of the Domestic Swine Auditory Tube

Nikolay Tsandev[1], Angel Vodenicharov[1], Ivaylo Stefanov[2]*

[1] *Department of Veterinary Anatomy, Histology and Embryology, Faculty of Veterinary Medicine, Trakia University, Stara Zagora, Bulgaria*

[2] *Department of Anatomy, Faculty of Medicine, Trakia University, Stara Zagora, Bulgaria*

*Corresponding author e-mail: drcandev@abv.bg

The length and calibre of 60 auditory tubes, collected from 30 longitudinally cut pig heads were measured on Duracryl casts by digital caliper (0.02). It was found that in both sexes, the length was larger at the ventrolateral border compared to the rostrodorsal one. Similar results were obtained for the length of both walls. The small/large diameter ratio of the elliptical *ostium pharyngeum tubae auditivae* showed equal values in male - 0.35 on both sides, whereas in females: 0.28 on the right and 0.27 on the left. The same ratios for *ostium tympanicum tubae auditivae* in males were 0.46 and 0.44 on the right and on the left, and in females: 0.41 and 0.36, respectively. The results allowed assuming the domestic swine's auditory tube was almost identical to that of humans; therefore, this animal species could be successfully used as a model in human medicobiological studies and for transplantology.

Key words: auditory tube, morphometry, domestic swine, corrosion cast

Introduction

The use of mammals as models in research studies on the organ of hearing, whose data with their advantages and disadvantages could be interpreted for men, evidenced a continuously increasing interest over the last three decades [2]. With this regard, the available data in domestic mammalian species are scarce and refer to studies on middle ear diseases in two sheep breeds and one domestic pig breed, having shown that these species were promising for use as human models [6, 8]. Recently, the interest to domestic swine, especially after publication of its genome, was substantially increased as a best-fit model for a number of human biomedical studies, including transplantology [3, 4, 5, 9]. Despite the numerous data proving the anatomical, physiological, biochemical and immunological similarity of men and domestic swine, there are still no detailed data on dimensions of the porcine auditory tube. This was the motivation of the present study, undertaken to elucidate and complete the knowledge on anatomical features of auditory tube of domestic swine.

Materials and Methods

Heads of 20 male and 20 female pigs, six months of age and live weight of 95-110 kg were used in this study. The pigs were slaughtered for meat consumption in a licensed slaughterhouse as per National regulations, and heads were transported in a cooling bag to the Department of Veterinary Anatomy, Histology and Embryology, Faculty of Veterinary Medicine, Trakia University, Stara Zagora, Bulgaria.

Before processing, heads were cut with electric saw into two equal halves along the median line. The surface around *ostium pharyngeum tubae auditivae* was cleaned with a gauze swab. After washing with physiological saline warmed to 37°C, each half was positioned horizontally with the *ostium pharyngeum tubae auditivae* (tube opening) upwards. The tube lumen was filled via opening with the metacrylate polymer Duracryl Plus O (Spofa Dental, Czech Republic). The liquid phase of Duracryl Plus was brought to 20°C. To it, a colorant was added: blue for male pigs and green for female pigs. The coloured liquid was mixed with the powder phase of Duracryl Plus O while stirring slowly and thoroughly at a ratio of 2.5:1 for one minute to prevent the formation of bubbles in the chemopolymerisable resin. Immediately after that, 2 ml of the mixture were manually injected in individual left and right auditory tubes until it flowed freely from the tube (tympanic) opening. Thus prepared models were left for 60 min at room temperature until the final polymerization (curing) of the material. Then, using tweezers, casts were removed from the tube lumen with gentle shaking, cleaned carefully and prepared for measurements.

Morphometry

Length of both medial and lateral wall (PhO-TyOM/PhO-TyOL) of each corrosion cast was defined by measuring the distance from the medial/lateral margin of the cast from pharyngeal orifice to the medial/lateral margin of the cast from tympanic orifice. Morphometric values were defined on corrosion casts of the auditory tube using a digital electronic caliper (accuracy 0.02 mm). (Length of the lateral wall (PhO-TyOL) of corrosion cast from the tube was measured between the lateral margin of the cast from pharyngeal orifice and the lateral margin of the cast from tympanic orifice).

Statistical analysis

Data were processed by GraphPad Prism 6 for Windows (GraphPad Software, Inc., USA) via one-way analysis of variance (one-way ANOVA) followed by Tukey-Kramer's post-hoc test and were presented as mean ± SD. P-values < 0.05 were considered statistically significant.

The terminology was consistent with the Nomina Anatomica Veterinaria [7].

Results

All casts from auditory tube lumens were elliptical, with the shape of flattened truncated cone, with obvious rostrodorsal (cranial) and ventrocaudal borders (walls) (**Fig.1; Fig.2**).

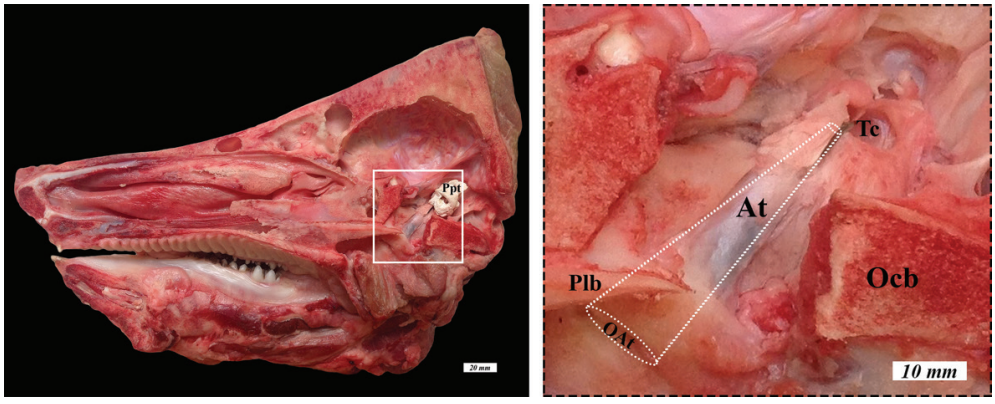

Fig. 1. Native model of porcine right auditory tube. At – auditory tube. Ppt – petrous part of the temporal bone. OAt – opening of the auditory tube. Ocb – occipital bone. Plb – palatine bone. Tc – tympanic cavity. Bar = 20 mm (left); 10 = mm (right).

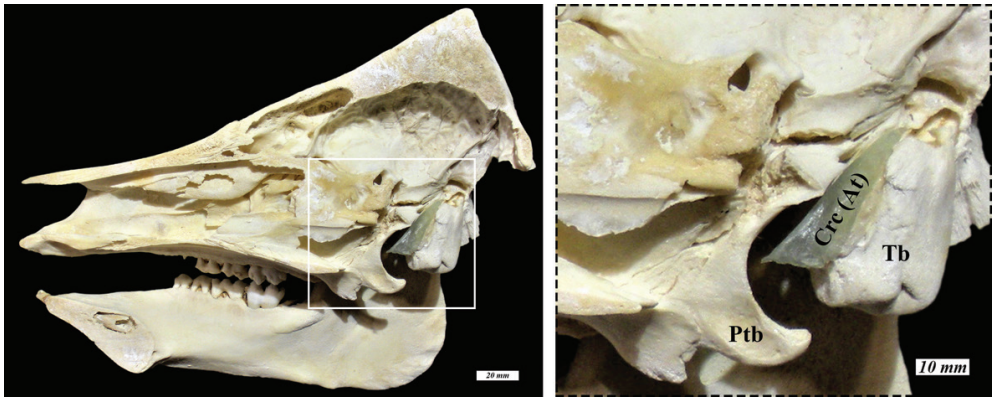

Fig. 2. Macerated acrylate model of porcine right auditory tube. Crc (At) – corrosion cast of the auditory tube (At). Tb – tympanic bulla. Ptb – pterygoid bone Bar = 20 mm (left); 10 = mm (right).

As seen from the data in **Table 1**, tube lengths were higher in female pigs, both from right and left sides.

It should be noted that in male pigs, the difference between the length of the ventrocaudal border was by 2.39 mm higher than the rostrocaudal border in right side casts and by 1.99 mm in left-side casts. The respective values in females were by 0.67 mm (from the right) and by 1.77 mm (from the left). There were also differences in the length of both walls (medial and lateral) measured between two points located in the middle of cast from the respective opening – rostrodorsal and ventrocaudal with higher values for the latter wall. For the right and left tube casts, these differences were 4.34 and 4.59 mm respectively in males and 3.29 and 2.81 mm respectively in females.

The dimensions of the large and small diameters of casts from the right and left ostium pharyngeum tubae auditivae did not show any sex dimorphism (**Table 2**).

The measurements of the calibre of *ostium tympanicum tubae auditivae* of right and left auditory tubes showed equal size of the large diameter in both sexes, while the small diameter of the left tube was larger in male pigs.

The small to large diameter ratio of *ostium pharyngeum tubae auditivae* in males was 0.35 from both sides, and 0.28 (right side) and 0.27 (left side) in females. The same ratios for *ostium tympanicum tubae auditivae* were as followed: in males: right side – 0.46; left side -0.44, and respective values in female pigs were 0.41 and 0.36.

Discussion

This study presents the first detailed morphometric data and statistical analysis of dimensions of auditory tube (caliber) in domestic swine. Our results are a contribution to the body of knowledge on the length of auditory tube in pigs (about 3 cm), similar to that of men [1, 8]. The data from this study were comparable to values reported by [6]

Table 1. Macrometric values regarding the length of the corrosion casts of the lumen of the right and left auditory tubes (PhO-TyOM is the length of the medial wall and PhO-TyOL – the length of the lateral wall of the corrosion casts).

PARAMETERS	Male Pigs	Female Pigs
LENGTH OF THE AUDITORY TUBE		
– Rostrodorsal wall		
Right	26.99 ± 4.71	29.96 ± 2.71
max-min	36.89 – 22.59	34.67 – 26.23
Left	27.44 ± 5.80	29.52 ± 3.72
max-min	36.72 – 19.20	36.75 – 23.92
– Medial length of the tube (PhO-TyOM)		
Right	26.98 ± 4.03	29.43 ± 2.49
max-min	34.30 – 23.09	34.19 – 26.29
Left	27.75 ± 5.54	29.28 ± 3.13
max-min	36.33 – 18.66	33.76 – 24.43
– Lateral lenght of the tube (PhO-TyOL)		
Right	31.32 ±4.26	32.72 ±2.674
max-min	40.31 – 26.90	38.28 – 28.73
Left	32.34 ± 6.74	32.09 ±3.26
max-min	44.83 – 22.99	36.93 – 25.32
– Ventrocaudal wall		
Right	29.38 ± 4.05	30.63 ± 3.83
max-min	38.47 – 25.09	35.87 – 22.25
Left	29.43 ± 5.04	31.29 ± 2.85
max-min	37.62 – 19.93	35.47 – 24.94

Table 2. Macrometric values regarding the large and small diameter of the corrosion casts of the two openings of the right and left auditory tubes

PARAMETERS	Male Pigs	Female Pigs
DIAMETERS OF THE PHARINGEAL OPENING OF THE AUDITORY TUBE		
– Large diameter	13.25 ± 1.84	13.12 ± 0.92
Right	16.09 – 10.08	14.97 – 11.91
max-min	12.02 ± 1.27	12.45 ± 1.71
Left	14.59–10.37	14.48–8.82
max-min		
– Small diameter		
Right	4.65 ± 1.56	3.48 ± 0.80
max-min	7.66 – 2.95	5.06 – 2.47
Left	4.26 ± 0.72	3.36 ± 1.28
max-min	5.17 – 2.98	5.57 – 1.04
DIAMETERS OF THE TYMPANIC OPENING OF THE AUDITORY TUBE		
– Large diameter		
Right	1.53±0.23	1.52± 0.24
max-min	1.23 – 1.93	1.14 – 1.93
Left	1.81± 0.38	1.48± 0.16*
max-min	1.24 – 2.68	1.28 – 1.85
Small diameter	0.70± 0.27	0.63± 0.17
Right	0.32 – 1.17	0.32 – 0.95
max-min	0.80± 0.21	0.53± 0.16*
Left	0.47 – 1.23	0.31 – 0.80
max-min		

*P< 0.05 Significant difference in measurements of left tympanic opening between males and females.

in silicone casts from two sheep breeds - Heathland sheep (30.4 mm ± 2) and Blackface sheep (31.1 mm ± 1.4 mm). This allowed confirming the statements of researchers that both animal species were appropriate models for investigations of disorders in auditory tube and middle ear functions. All data accumulated during the recent year about the similarity between men and domestic swine demonstrated categorically that swine were more relevant in such studies, including middle ear infections [8].

Data about ratios between the small and large diameters of both auditory tube openings were also interesting. It should be noted that there was no statistically significant differences between sexes with regard to lengths of tube casts. Furthermore, small/large diameter ratios were equal for ostium pharyngeum tubae auditivae in male pigs and insignificantly different between right and lift tube in females. The differences were more obvious for ostium tympanicum tubae auditivae only for the left tube opening ($p< 0.05$). The results allowed affirming that the macrometric parameters of the auditory tube have relatively equal proportions in domestic swine from both sexes.

Conclusion

In conclusion, the original data from this study are a contribution to the commonly agreed opinion that the domestic swine is the most appropriate animal mammalian species to serve as model in human medicobiological and transplantation (xenotransplantation) research studies.

References

1. **Bluestone, Ch. D., W. J. Doyle**. Anatomy and physiology of eustachian tube and middle ear related to otitis media. – *J. Allergy Clin Immunol*., **81**, 1988, 997-1003.
2. **dos Reis, A., S. P. Dalmolin, E. Dallegrave**. Animal models for hearing evaluations: a literature review. – *Revista CEFAC*, **19**, 2017, 417-427.
3. **Eberlova, L. V. Liska, H. Mirka, T. Gregor, Z. Tonar, R. Palek, M. Skala J. Bruha, O. Vycita, K. Kalusova, S. Haviar, M. Kralickova, A. Lametschwandtner**. Porcine liver vascular bed in Biodur E20 corrosion casts. – *Folia Morphol*., **75**, 2015, 154-161.
4. **Eberlova, L., V. Liska, H. Mirka, Z. Tonar, S. Haviar, M. Svoboda, J. Benes, R. Palek, M. Emingr, J. Rosendorf, P. Mik, S. Leupen, A. Lametschwandtner**. The use of porcine corrosion casts for teaching human anatomy. – *Annals of Anatomy*, **213**, 2017, 69–77.
5. **Kuzmuk, K. N., L. B. Schook**. Pigs as model in Biomedical Science. In: *The Genetic of the Pig*. (Eds. M. F. Rothschild, A. Ruvinsky) CAB International, 2011, 426-444.
6. **Miller, F., A. Burghard, R. Salcher, V. Scheper, W. Leibold, Th. Lenarz, G. Paasche**. Treatment of middle ear ventilation disorders: Sheep as animal model for stenting the human Eustachian tube – a cadaves. – *PLOS ONE*, **24**, 2014, 1-13.DOI:10.1371/journal.pone.0113906
7. Nomina Anatomica Veterinaria. International Committee on Veterinary Gross Anatomical Nomenclature (I.C.V.G.A.N.). 6th ed., 2017, Hanover, Ghent, Columbia, MO, Rio de Janeiro, 152.
8. **Pracy, J. P., A. White, Y. Mustafa, D. Smith, M. E. Perry**. The comparative anatomy of the pig middle ear cavity : a model for middle ear inflammation in the human? – *J. Anat*. **192**, 1998, 359-368.
9. **Runager J., C. Bonnefont, M., O. Hesselager, S. R. Bislev, J. Borch-Jensen, E. Bedixen**. Pig as a model system for biomedical research. From the journal: EuPA 2013 – Scientific meeting. 2013; 7. EuPA Congress, Saint Malo, FRA, 2013-10-14-2013-10-17, 248-248.

Institute of Experimental Morphology, Pathology and Anthropology with Museum
Bulgarian Anatomical Society

Acta morphologica et anthropologica, 27 (1-2)
Sofia ● 2020

Occupational Stress among Welders in Bulgaria

Vlayko Vodenicharov[1], Irena Ivanova[2], Konstantin Mitov[3]*

[1] *Department of Hygiene, Medical University, Sofia, Bulgaria*
[2] *Department of Organization and Economics of Pharmacy, Medical University, Sofia, Bulgaria*
[3] *Department of Clinical Laboratory, St. Ivan Rilski University Hospital, Sofia, Bulgaria*

* Corresponding author e-mail: vlayko_vodenicharov@abv.bg

The main goal of this study is to assess salivary cortisol levels a mong Bulgarian welders. Totally 39 healthy volunteers working as welders have been investigated – 31 males and 8 females; age 37±9 yr. Two saliva samples were collected for each participant in specialized containers – Salivette (Sarstedt, Rommelsdorf, Germany). First sample (Cortisol 1) between 9 and 11am and second between (Cortisol 2) 15 – 17 pm. Cortisol reference values are 0,2-4,4 ng/ml. Increased cortisol levels above the reference range were found only in Cortisol 1. Mean Cortisol 1 salivary levels are 3,47 ± 2,47 ng/ml for all studied individuals with higher levels in males (3,67 ± 2,35 ng/ml) than females (2,71 ± 2,95 ng/ml). The present quantitative study evaluates the use of salivary cortisol concentration as a biomarker of stress among welders in Bulgaria.

Key words: salivary cortisol, occupational stress, welders

Introduction

Occupational stress is a major factor of the work environment which unmanaged can lead to serious health and personal issues. Working as a welder in a metallurgical company is a job that could attract a lot of stress. There could be different reasons for the presence of occupational stress. Noise, vibration, air pollutants, bad thermal comfort, non-ionizing radiation are affecting the employees every work day [8]. Conflicts at work, emotional demands, workload, time pressure are possible stressors. Static physical activities and forced work postures are part of the working process [4]. The combined effect of different stressors in the work environment could lead to poor work performance, acute and chronic health problems.

Occupational stress is associated with high levels of cortisol [5,6]. Cortisol, also known as “the stress hormone” is a steroid hormone produced by the adrenal glands. It has a circadian rhythm with highest levels in the morning that decline throughout the day and reach lowest point at night [1, 2, 3]. It is widely used in medical studies as an indicator for the stress response of the organism. The human body reacts to stressful situations with increase in cortisol secretion. Disturbances in cortisol secretion may

lead to fatigue, depression, obesity and immune dysfunction [6,7]. The aim of our study is to assess cortisol levels among healthy Bulgarian welders during their workday.

Materials and Methods

A total of 39 healthy volunteers (31 men and 8 women), with an average age of 37 ± 9 years were included in the study. Inclusion criteria for all participants was a minimum of one year's experience as a welder. Two saliva samples during one workday were collected for each participant in specialized containers – Salivette (Sarstedt, Rommelsdorf, Germany). First sample between 9 and 11am and second between 15-17 pm. All participants were instructed beforehand to abstain from eating, smoking, brushing their teeth or drinking any kind of liquid except water for at least 30 minutes before giving their samples. Each sample was assessed for cortisol levels. The concentration of cortisol in saliva was determined by the enzyme-linked immunosorbent assay (ELISA). Cortisol reference values are 0.2 – 4.4 ng/ml. MED CALC 16.4.3. was used for statistical analysis of the data.

Results and Discussion

Results from three of the participants were excluded due to corrupted samples or missing data. Increased cortisol levels above the reference range were found only in the first cortisol measurement (Cortisol 1). Based on the data from Cortisol 1, we constructed a new variable EV (extreme value) which indicates whether or not the cortisol value is normal or increased above the reference range. A value of 0 for the EV variable indicates that cortisol is normal and code 1 is for the opposite. Twelve employees (30.77%) showed increased cortisol levels above the reference values. Results for EV variable are shown in **Table 1.**

Table 1. Frequency analysis for EV variable.

Classification variable	EV
Sample size	39
EV = 1	12 (30.77%)
EV = 0	27 (69.23%)

Cortisol levels followed their normal direction of rise and fall during day. Highest values of the hormone were present in the Cortisol 1 and they declined throughout the end of the workday. The data from the descriptive statistics of salivary cortisol levels is shown in **Table 2**.

The following values were reported as mean ± SD (min-man): Cortisol 1 - 3.47 ± 2.47 ng / ml (0.50 - 8.48) and Cortisol 2 - 1.58 ± 1.01 ng/ml (0.3 - 4.3). A significant difference in the concentrations of cortisol in saliva was not found among sexes. A significant difference was found in the levels of cortisol in saliva between the first and the second samples ($p = 0.003$), with higher values being measured in the morning. A weak positive correlation was found between the levels of cortisol between the two saliva samples ($r = 0.38$).

Table 2. Descriptive statistics for cortisol levels

	N	Mean	95% CI	SD	Median	Minimum	Maximum	Normal Distr.
Age	39	36,872	33,633 to 40,110	9,9899	37,000	22,000	66,000	0,1285
Avg_Cortisol	39	2,885	2,224 to 3,546	2,0385	2,359	0,476	9,051	0,0008
Cortisol 1	38	3,472	2,657 to 4,287	2,4794	2,653	0,501	8,485	0,0522
Cortisol 2	36	1,586	1,241 to 1,930	1,0178	1,320	0,293	4,311	0,0054

Based on the obtained results, we construct a new classification variable AGD (age group dichotomy), which has a value of 0 for people with age≤ 38 and 1 for people with age> 38. Cross tabulation analysis of EV and AGD was performed. Results are shown in **Table 3.**

Table 3. Cross tabulation analysis of EV and AGD

	Classification EV		
Classification AGD	0 Cortisol 1 normal	1 Cortisol 1 Increased	
0 /age≤38/	21 95,5% RT 77,8% CT 53,8% GT	1 4,5% RT 8,3% CT 2,6% GT	22
1 /age>38/	6 35,3% RT 22,2% CT 15,4% GT	11 64,7% RT 91,7% CT 28,2% GT	17
	27	12	39 (32 true and 7 wrong)

Table 3 shows that out of 39 classifications of welders by age group (with age≤ 38 or age> 38) and cortisol status (normal or increased above reference range) 32 are true and 7 are wrong. Based on the age classification (age≤ 38 or age> 38), it can be predicted whether a person will have abnormal or normal levels of cortisol from the first measurement.

Our data of salivary cortisol levels during welders work showed elevated values in twelve of thirty-nine participants in Cortisol 1. These results raise doubts about occupational stress in almost one-third of the study group (30.77%). A significant difference in salivary cortisol levels was not found among sexes. Older age in the studied group (age> 38) is a risk factor for the development of occupational stress. Further research about the causes of stress among these employees is needed. All samples in Cortisol 2 showed values in the reference range.

Conclusion

Salivary cortisol levels of all participants showed normal dynamics throughout the workday. Cortisol levels had highest values in the morning and lowest in the end of the workday. The higher number of employees with increased cortisol levels in saliva from the morning sample is probably the result of the factors of the work environment. Further research is needed in order to clarify main work environment factors and their role for developing occupational stress among welders.

References

1. **Baba, M., M. Ohkura, K. Koga, K. Nishiuchi, L. R. Herrersa, R. Matsuse, T. Inoue.** Analysis of salivary cortisol levels to determine the association between depression level and differences in circadian rhythms of shift-working nurses. – *J. Occup. Health*, **57**, 2015, 3, 37-44.
2. **Bozovic, D., M. Racic, N. Ivkovic.** Salivary cortisol levels as a biological marker of stress reaction. – *Med. Arch*., **67**, 2013, 374-377.
3. **Garsez, A., E. Weiderpass, R. Canuto, S. B. Lecke, P. M. Spritzer, M. P. Pattussi, M. T. A. Olinto.** Salivary cortisol, perceived stress, and metabolic syndrome: A matched case-control study in female shift workers. – *Horm. Metab. Res.,* **49**, 2017, 7, 510-519.
4. **Horvat, J., I. Polajnar, M. Čudina, R. Dahmane.** Ergonomic stresses of welders. – Strojarstvo, **49**(5), 2007, 377-382.
5. **Lindholm, H., J. Ahlberg, J. Sinisalo, C. Hublin, A. Hirvonen, M. Partinen, S. Sarna, A. Savolainen.** Morning cortisol levels and perceived stress in irregular shift workers compared with regular daytime workers. – *Sleep Disord.,* 2012, 1-5. doi: 10.1155/2012/789274
6. **Moro, A., P. Reis, I. Santos, A. Pinto, D. Reis.** Salivary cortisol analysis in shift workers. In: *Advances in safety management and human factors. Advances in intelligent systems and computing* (Ed. P. Arezes), Springer, Cham, **491**, 2016, 525-532.
7. **Niu, S. F., M .H. Chung, C. H. Chen, D. Hegney, A. O'Brien, K. R. Chou.** The effect of shift rotation on employee cortisol profile, sleep quality, fatigue, and attention level: a systematic review. – *J. Nurs Res.,* **19**, 2011, 1, 68-81.
8. **Nwafor, A.** Occupational hazards and safety practices among welders in Port Harcourt Metropolis, Nigeria. – *Int. J. Innovative Research and Development*, **8**, 2019, 119-124.

Author Guidelines

Acta morphologica et anthropologica is an open access peer review journal published by Bulgarian Academy of Sciences, Prof. Marin Drinov Publishing House.
Corporate contributors are Bulgarian Academy of Sciences, Institute of Experimental Morphology, Pathology with Museum and Bulgarian Anatomical Society.

Acta morphologica et anthropologica is published in English, 4 issues per year.
The journal accepts manuscripts in the following **fields**: experimental morphology, cell biology and pathology, anatomy and anthropology.

Publication types: original articles, short communications, case reports, reviews, Editorial, letters to the Editors.

Acta morphologica et anthropologica is a continuer of Acta cytobiologica et morphologica

The **aim** of the Journal is to disseminate current interdisciplinary biomedical research and to provide a forum for sharing new scientific knowledge and methodology. The general editorial policy is to optimize the process of issuing and distribution of *Acta morphologica et anthropologica* in line with modern standards for scientific periodicals focusing on content, form, and function.

Scope – experimental morphology, cell biology and pathology (neurobiology, immunobiology, tumor biology, environmental biology, reproductive biology, etc.), new methods, anatomy and pathological anatomy, anthropology and paleoanthropology, medical anthropology and physical development.

Acta morphologica et anthropologica is published twice a year as one volume with 4 issues. For the first two issues (1-2) the deadline for manuscript submission is March 15th and for the next two issues (3-4), the deadline is September 15th. Electronic version for issues 1-2 is uploaded on the website till June 30th and for issues 3-4 – till December 30th.

Contact details and submission

Manuscript submission is electronical only. The manuscripts should be sent to the Managing Editor's e-mail address ygluhcheva@hotmail.com with copy to iempam@bas.bg
All correspondence, including notification for Editor's decision, requests for revision, is sent by e-mail.

Article structure

Manuscripts should be in English with total length not exceeding 10 standard pages, line-spacing 1.5, justified with 2.5 cm margins. The authors are advised to use Microsoft Word 97-2003, Times New Roman, 12 pt throughout the text. Pages should be numbered at the bottom right corner of the page.

The article should be arranged under the following headings: Introduction, Material and Methods, Results, Discussion, Conclusion, Acknowledgements and References.

Title page – includes:

- **Title** – concise and informative;
- **Author(s)' names and affiliations** – indicate the given name(s) and family name(s) of all authors. Present the authors' affiliation addresses below the names. Indicate all affiliations with a lower-case superscript after the author's name and in front of the appropriate address. Provide the full postal address information for each affiliation, including the country name.
- **Corresponding author** – clearly indicate who will handle the correspondence for refereeing, publication and post-publication. An e-mail should be provided.
- **Abstract** – state briefly the aim of the work, the principal results and major conclusions and should not exceed 150 words. References and uncommon, or non-standard abbreviations should be avoided.
- **Key words** – provide up to 5 key words. Avoid general, plural and multiple concepts. The key words will be used for indexing purposes.

Introduction – state the objectives of the work and provide an adequate background, avoiding a detailed literature survey or summary of the results.

Material and Methods – provide sufficient detail to allow the work to be reproduced. Methods already published should be indicated as a reference: only relevant modifications should be described.

Results – results should be clear and concise.

Discussion – should explore the significance of the results in the work, not repeat them. A combined *Results and Discussion* section is often appropriate. Avoid extensive citation and discussion of published literature.

Conclusions – the main conclusions of the study should be presented in a short section.

Acknowledgements – list here those individuals who provided help during the research and the funding sources.

Units – please use the International System of Units (SI).

Math formulae – please submit math equations as editable text, not as images.

Electronic artwork – number the tables and illustrations according to their sequence in the text. Provide captions for them on a separate page at the end of the manuscript. The proper place of each figure in the text should be indicated in the left margin of the corresponding page. **All illustrations (photos, graphs and diagrams)** should be referred to as "figures" and given in abbreviation "Fig.", and numbered in Arabic numerals in order of its mentioning in the manuscript. They should be provided in grayscale as JPEG or TIFF format, minimum 300 dpi. The illustrations should be submitted as separate files.

References – they should be listed in alphabetical order, indicated in the text by giving the corresponding numbers in parentheses. The "References" should be typed on a

separate sheet. The names of authors should be arranged alphabetically according to family names. In the reference list titles of works, published in languages other than English, should be translated, original language must be indicated at the end of reference (e.g., [in Bulgarian]). Articles should include the name(s) of author(s), followed by the full title of the article or book cited, the standard abbreviation of the journal (according to British Union Catalogue), the volume number, the year of publication and the pages cited, for books - the city of publication and publisher. In case of more than one author, the initials of the second, third, etc. authors precede their family names.

For articles: **Davidoff, M. S., R. Middendorff, G. Enikolopov, D. Riethmacher, A. F. Holstein, D. Muller**. Progenitor cells of the testosterone-producing Leydig cells revealed. – *J. Cell Biol.,* **167**, 2004, 935-944.

Book article or chapter: **Rodriguez, C. M., J. L. Kirby, B. T. Hinton. The development of the epididymis. -** In: *The Epididymis - from molecules to clinical practice* (Eds. B. Robaire, B. T. Hinton), New York, Kluwer Academic Plenum Publisher, 2002, 251-269.

Electronic books: **Gray, H.** *Anatomy of the human body* (Ed. W.H.Lewis), 20th edition, NY, 2000. Available at http://www.Bartleby.com.

PhD thesis: **Padberg, G**. Facioscapulohumeral diseases. *PhD thesis*, Leiden University, 1982, 130 p.
Website: National survey schoolchildren report. National Centre of Public Health and Analyses, 2014. Available at http://ncphp.government.bg/files

Page charges

Manuscript publication is free of charges.

Ethics in publishing

Before sending the manuscript the authors must make sure that it meets the Ethical guidelines for journal publication of Acta morphologica et anthropologica.

Human and animal rights

If the work involves the use of human subjects, the authors should ensure that work has been carried out in accordance with *The Code of Ethics of the World Medical Association* (Declaration of Helsinski). The authors should include a statement in the manuscript that informed consent was obtained for experimentation with human subjects. The privacy rights of human subjects must always be observed.
All animal experiments should comply with the *ARRIVE guidelines* and should be carried out in accordance with the U.K. Animals (Scientific procedures) Act, 1986 and the associated guidelines *EU Directive 2010/63/EU* for animal experiments, or the National Institutes of Health guide for the care and use of Laboratory animals (NIH Publications No. 8023, revised 1978) and the authors should clearly indicate in the manuscript that such guidelines have been followed.

Submission Details

Acta morphologica et anthropologica is published twice a year as one volume with 4 issues. For
the first two issues (1-2) the deadline for manuscript submission is March 15th and for the next two issues (3-4), the deadline is September 15th. Electronic version for issues

1-2 is uploaded on the website till June 30th and for issues 3-4 – till December 30th.
Manuscript submission is electronical only.

The manuscripts should be sent to the Managing Editor email address ygluhcheva@hotmail.com with copy to iempam@bas.bg
All correspondence, including notification for Editor's decision, requests for revision, is sent by e-mail.

Submission declaration

Submission of the manuscript implies that the work described has not been published previously, is not considered under publication elsewhere, that its publication is approved by all authors, and that if accepted, it will not be published elsewhere in the same form, in English or in any other language, including electronically, without the informed consent of the copyright-holder.

Contributors

The statement that all authors approve the final article should be included in the disclosure.

Copyright

http://www.iempam.bas.bg/journals/acta/Author%20Copyright%20Agreement_last.pdf

Upon acceptance of an article, the authors will be asked to complete a "**Copyright Transfer Agreement**".
http://www.iempam.bas.bg/journals/acta/Copyright_Transfer_Agreement_Form_AMA.doc

Peer review

Once a manuscript is submitted, the Managing Editor (or the Editor-in-Chief) briefly checks the manuscript for conformance with the journal's Focus, Scope, Policies and style requirements and decide whether it is potentially suitable for publication and can be processed for review, or rejected immediately, or returned to the author for improvement and re-submission.
Manuscripts are peer-reviewed by the Editors, Editorial Board members, and/or external experts before final decisions regarding publication are made. The entire editorial workflow is performed in the following steps:

1. The submitted manuscript is checked in the editorial office whether it is suitable to go through the normal peer review process.
2. If deemed suitable, the manuscript is sent to 2 reviewers for peer-review. The choice of reviewers depends on the subject of the manuscript, the areas of expertise of the reviewers, and their availability.
3. Each reviewer will have 2 weeks to provide evaluation of the manuscript. The Editor may recommend publication, request minor, moderate or major revision, or provide a written critique of why the manuscript should not be published (rejected).
4. In case only one reviewer suggests rejection of the manuscript, the latter is subjected to additional evaluation by a third reviewer.

5. The manuscript will be published in a revised form provided that the authors successfully answer the critics received. The Editor-in-Chief is the final authority on all editorial decisions.

Open Access

This journal provides immediate open access to its content on the principle that making research freely available to the public supports a greater global exchange of knowledge.

After acceptance

Proof correction

The corresponding author will receive proofs by e-mail in PDF format and will be requested to return it with any corrections within two weeks.

ISSN 1311-8773 (print)
ISSN 2535-0811 (online)